The effects of forelands on embankment breaching in coastal and river regions

MSc thesis
Jord Smid
TU-Delft

TU Delft

The effects of forelands on embankment breaching in coastal and river regions

by

Jord Pieter Johan Smid

MSc thesis for Delft University of Technology

Committee members

Prof. dr. ir. S.G.J. Aarninkhof – TU-Delft, chairman

Prof. dr. P.M.J. Herman – TU-Delft & Deltares

Dr. ir. P.J. Visser – TU-Delft (emeritus associate professor)

Dr. ir. J.A.A. Antolinez – TU-Delft

Ir. M. v.d. Berg – TU-Delft

October 2021

Acknowledgements

I would like to thank all the committee members for their great help during the completion of this thesis. Writing a thesis was the first time I had to perform my own research and it was a large step from listening to lectures and reading study books. Fortunately I had the privilege to work with these great academics to aid me in the subject of the thesis, but also guide me in the process of the research itself. One of the greatest assets of this committee was that all members came from a different professional backgrounds, allowing for very diverse perspectives to come together, culminating into a thesis that has roots in each of these fields. I have experienced this time as a wonderful journey and I am very grateful to all you, Stefan Aarninkhof, Paul Visser, Peter Herman, José Antolinez and Mario v.d. Berg.

I would also like to extend my thanks to Ken Schoutens from the University of Antwerp and the people from the WaterLab of TU Delft. These people have made it possible to perform my experiments for this thesis and also greatly helped out with the setup and planning.

Lastly I would like to thank my family, girlfriend and friends for their support during this year. My father, Tjabe, who has supported me tremendously during this time with his expertise in the academic world and has been a great help during the writing of the thesis. My mom, Els, who was a great help during the time I had a broken shoulder and was working from home during the summer holidays. My brother Victor, who has been a great help with both writing my thesis, as well as making sure I also make time for other activities. My girlfriend Enxhi, who supported me through the stressful days and relaxed with me during the peaceful days. And finally my best friends, Jim, Gwenn, Jaap, Maurice and Alex who have all supported me greatly over the past year, be it in person or over the phone due to the pandemic. Again, I am thankful to all of you.

Finally, I would like to dedicate this thesis to my late grandfather Gerrit Scheringa, who finished his studies in civil engineering at the TU Delft many, many years ago. He would often proudly tell me how he had to go to exams in a cutaway tuxedo. These days are long gone, and in a sense it seems like we have experienced a very different journey during our time at the TU Delft. However, the friends we made, the long evenings we studied and the good times we had, I'm sure these are timeless attributes that everyone at the TU Delft shares.

It has been a pleasure.

Jord Smid

Abstract

Embankments are one of the key aspects of flood protection programs. As the sea levels are expected to rise the coming decades coastal protection is becoming increasingly important. To better prepare for the future, increased understanding of embankment breaching is desired. An area of embankment breaching that has been relatively left untouched is the impact of a foreland during a breaching event. This study examines the different effects caused by the presence of a foreland, namely reduced flow rate through the breach, limited breach growth and an elliptical erosion pattern in the foreland.

Embankments are generally more erodible than forelands, and erosion of the foreland occurs after the adjacent embankment has been breached to its base level. As water continuous to flow over the foreland, a plunging jet will form, falling from the high foreland into the breach bottom. This causes undermining in the foreland and subsequent headcut erosion. A distinction is made between cohesive and non-cohesive forelands. Cohesive soil layers experience rotational failure and non-cohesive layers experience sliding failure.

A model is presented that calculates headcut erosion in a foreland, flow characteristics over the foreland and erosion shape of the foreland. The erosion shape of the foreland affects the discharge through the breach and is captured in the non-dimensional constant m. The presented model is implemented as a module into the existing breaching model BRES. The added functionality will increase the accuracy BRES model results.

Two experiments were performed to verify the model. The first experiment examined soil failure of a foreland in dry conditions by pushing an extracted foreland soil layer from a table to observe the failure type and the effects of vegetation on the strength of the soil. The second experiment was performed in collaboration with the University of Antwerp. A soil layer was extracted from a foreland and placed in a large flume. The foreland was subjected to a plunging jet to simulate a breaching event. The outcomes of the model were in line with observations made during both experiments.

The presented model serves as a significant first step towards implementing forelands in flood protection programs, but further research is suggested. The uncertainties stemming from assumptions in the model and the underlying sediment transport relations are significant. Most importantly uniformity of the soil is assumed, whereas in reality root systems in fertile forelands can lead to significant local strengthening. The assumptions in this model are conservative, but additional studies can further increase the accuracy of the foreland- and BRES model.

Table of contents

List of figures

List of tables

List of Symbols

Symbol	Description	SI-Unit
A	Cross-sectional breach flow area	m^2
A_{lat}	Area of lateral surface of headcut failure block	m^2
b	Width of breach at breach bottom	m
B	Depth-averaged breach width	m
B_{br}	Breach width	m
B_t	Breach width at top of dike	m
B_w	Breach width at water line	m
C	Chezy coefficient	$m^{0.5}/s$
C_d	Diffusion coefficient	$-$
C_f	Friction coefficient of the soil	$-$
C_s	Soil cohesion parameter	$-$
c_u	Undrained shear strength of soil	N/m^2
d	Water depth	m
d_b	Backwater height	m
dt / Δ_t	Timestep	s
D_{10}	Particle size for which the portion of particles with diameters smaller than this value is 10%	m
D_{50}	Particle size for which the portion of particles with diameters smaller than this value is 50%	m
D_{90}	Particle size for which the portion of particles with diameters smaller than this value is 90%	m
D_a	Approach	m
d_c	Critical depth	m
d_f	Water depth undisturbed foreland	m
d_G	Force arm of G	m
d_{P1}	Force arm of P_1	m
d_{P2}	Force arm of P_2	m
d_{P3}	Force arm of P_3	m
d_N	Force arm of N	m
e	Eccentricity	$-$
E_v	Erosion on vertical face	m
$F_{c,f}$	Soil interaction force	N
F_r	Froude number	$-$

g	gravitational constant	m^2/s
G	Weight of headcut failure block	N
H_p	water level in the polder above Z=0 where Z=0 is the reference line	m
H_s	Depth of scour hole	m
H_{pc}	Depth of the potential core	m
H_w	Outside water level above Z=0	m
H_{ww}	outside water level above Z=0 in time, requires water level for different timestamps	m
J	Jet centerline length from entry point	m
J_p	Length of the jet potential core along jet centreline	m
k_d	Erodibility coefficient	$M^3/N \cdot s$
k_f	Von Karman constant	$-$
l_n	Adaptation length	m
L_{spill}	Spillway length	m
m	Discharge coefficient	$-$
M_{ef}	Material dependent erodibility factor	$s \cdot m^2/kg$
N	Soil interaction fore	N
p	Bed porosity	$-$
P_1	Water weight force	N
P_2	Flow shear force	N
P_3	Seepage force	N
q	Unit discharge	m^2/s
Q_{br}	Discharge through breach	m^3/s
Q_f	Discharge over foreland	m^3/s
R_e	Reynold's number	$-$
S	Impact distance from foreland edge	m
t	Time	s
T	Failure block width for sliding failure	m
T_0	Nappe width	m
t_f	Failure time	s
T_h	Horizontal force component backwater	N
T_v	Vertical force component backwater	N
u	Flow velocity (in BRES model)	m/s
U	Flow velocity	m/s
U_*	Bed shear velocity	m/s

U_0	Flow velocity of jet upon impact backwater	m/s
U_{br}	Flow velocity through breach	m/s
W_f	Failure block width for rotational failure	m
w_s	Settling velocity	m/s
W_s	Weight of the soil failure block	N
W_w	Weight of water on top of foreland	N
X_p	Location of maximum stagnation pressure	m
Z	Reference level vertical elevation	m
Z_{br}	Breach height above Z=0, requires initial value	m
Z_f	Height of foreland above Z=0	m
Z_p	Polder level above Z=0	m
Z_w	Height of the watercourse bottom above Z=0	m
α	Inclination angle of out stope	°
β_0	Inclination angle of inner slip	°
β_1	Critical value inclination angle of inner slip	°
γ	Inclination angle of the side slopes	°
γ_s	Unit weight of soil	kg/m^3
γ_w	Unit weight of water	kg/m^3
$\ni$	Porosity of sheared layer	$-$
ε	Undermining rate	m/s
θ	Angle of slip failure plane	°
ξ	Exponent for soil erosion	$s \cdot m/kg$ $or\ s^2m^{2.5}/kg^{1.5}$
ρ	Density of the water	kg/m^3
ρ_s	Sediment density	kg/m^3
τ_c	Critical shear stress	N/m^2
τ_e	Effective shear stress	N/m^2
τ_s	Soil shear strength	N/m^2
τ_t	Soil tensile strength	N/m^2
v	Kinematic viscousity	m^2/s
ϕ	Internal friction angle of the soil	°
ϕ_d	Angle of repose of the bed layer	°
χ	Impact angle	°

Chapter 1. Introduction

This chapter introduces the MSc topic. Firstly, the relevance of the research and some background information are provided. This is followed by the problem description and finally the research objectives and research questions are presented.

1.1 Background

Flood risk

One of the most relevant problems facing the world today is climate change. Not only are sea levels expected to rise globally, peak rainfall intensity, peak river flow and more extreme winds affecting both wave height and storm surges are also likely to become more prevalent (Masson-Delmotte, et al., 2021). These changes call for new and revised measures around the world within the field of flood risk.

A key factor in being prepared for the future is to understand and be able to accurately predict the effects of both the changing climate, and our adaptation to these changes. This will be the framework for this thesis, a safer future by increased understanding.

Dike and levee failure

Dikes (embankments that protect land which would otherwise be underwater) and levees (embankments protecting land that is normally dry but can flood during peak water levels) are two of the most crucial elements of coastal protection and river management. It has allowed countries to protect their people and land from the dangers posed by the seas and rivers as well as enabling them to claim land from these waters. Both levees and dikes fall under the category of embankments.

In the Netherlands specifically adequate coastal protection is of vital importance because a large part of the population and economic centers are below mean sea water level (Mulder et al, 2009). In the history of the Netherlands multiple disastrous floods have occurred, most notably the North Sea floods of 1717 and 1953, killing approximately 14000 and 2500 respectively (Dutch ministry of traffic and water management, 2004). Also, in recent times large floods have occurred around the world such as the New Orleans flooding in 2008 related to hurricane Katrina. As the climate changes, the probability and associated destruction level of floods is forecasted to grow in the foreseeable future due to a rising sea level and more extreme weather conditions (Vermeer&Rahmstorf, 2009; Hinkel et al, 2013).

Breach development in embankments

It is of vital importance to understand when a dike or levee fails and how a breach will develop over time. This knowledge makes it possible to create more accurate predictions of the involved risk and consequently intervene more effectively and efficiently in case of a real breach event. An extensive amount of research has been done into what causes dikes and levees to fail. The failure mechanisms, acting forces, the effects of material use, and composition of the embankment structure are all well documented, see for example 'Introduction to bed, bank and shore protection (Schiereck, 2003).

A less well documented phenomenon is the development of the breach itself. This can be understood by the fact that in coastal defense programs the focus lies on prevention of breach events as opposed to mitigation. Subsequently the emphasis in research and documentation has also been on failure mechanisms.

When considering the development of a breach a few key phases can be distinguished. After the initial breaching of an embankment, the breach will develop both vertically and horizontally. Visser (1998) reasons that this process can be split into five distinct phases from initiation of the breach until the end of breach development. The first two phases are related to the initial breaching process where the flow rate and flow velocities are limited. The last three phases entail the breach growth where flow rate and velocities become very high and substantial inundation occurs. These phases will be discussed in greater detail in chapter 3.

Effects of a foreland on breach development

A foreland is an area of land above mean water level that is situated between an embankment and the body of water the embankment was built for, see also Figure 1. It is dry during low tide and regular water levels but becomes inundated during high and spring tide or storm conditions. There is evidence that shows having a foreland will slow down the breaching process (Zhu et al, 2020). The relatively high foreland causes a reduction in discharge and subsequent flow velocity through the breach, as well as wave energy dissipation from limited water depth on the foreland. Another effect of a foreland is preventing continued inundation after the storm subsides. Since the foreland is usually situated around mean high water level (Zedler, Bonin, Larkin, & Varty, 2008), even for the case of complete failure of a dike, the strong foreland will prevent water flowing into the polder when the water level drops below the mean high water level. This is expanded upon in paragraph 2.2.1.

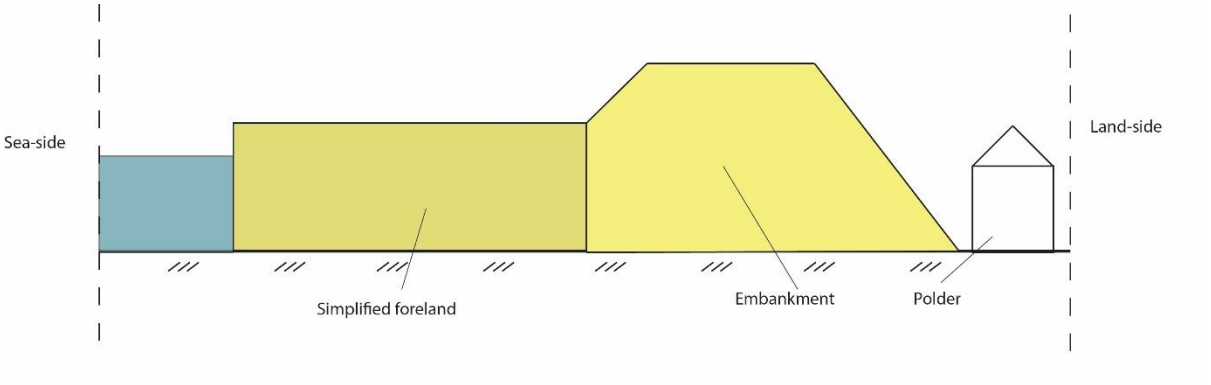

Figure 1: Simplified scenario for an embankment with an adjacent foreland, side view

1.2 Problem Description.

Although forelands are proven to have several significant effects on dike breaches (Zhu et al, 2020), current breach development models do not include these effects, or parametrize them in a single constant (see for example Breach growth in Sand-Dikes by Visser, 1998).

To more realistically model the breaching process of an embankment when a foreland is present, it is necessary to expand breach models with a method to include the effects of forelands on the breaching process.

1.3 Research objective

The aim of this study is to quantify the effects of a foreland on breach development and implement these into an existing breach development model to more accurately predict embankments breaches.

The first goal is to find the underlying relations and interactions between a foreland and the breach process. Secondly these relations and interactions will be implemented into a model and will be added to an existing breaching model. After this step a sensitivity analysis will be performed. This analysis is performed because there is an abundance of parameters involved in sediment dynamics as well as an abundance of empirically derived relations. The uncertainties arising from the relations, combined with the fact that nature-based solutions by themselves often bring an inherent amount of uncertainty (Möller, 2019), lead to the conclusion that insight in the sensitivity of the different parameters can add a lot of value. Unfortunately, historical and experimental data on embankment breaches with the presence of a foreland is limited and more qualitative in nature than quantitative. Visser (2021) has documented the 1953 North Sea floods extensively and a significant number of dike breaches during these floods had a foreland. In the cases where a foreland was present, significant reductions in inundation and breach size was observed, supporting the hypothesis that forelands can have a positive impact on coastal protection plans. The data does not include erosion in the foreland over time but presents the final result. Nevertheless, this data can be used as a basis to validate and calibrate the created foreland model. To avoid using data from just one source, the last step in the research will be to test the final model against data obtained from two experiments conducted for this thesis.

1.3.1 Research questions

Presented below are the research questions for this study. Additionally, five sub-questions have been formulated.

Main research question:

How can we incorporate the effects of forelands on embankment breaching in an existing breach development model?

Research sub-questions:

- What processes related to a breaching event are affected by the presence of a foreland?
- How can the relevant effects of a foreland on the breaching process be modelled?
- Which existing breaching model is best suited for the incorporation of a foreland erosion module?
- What is the sensitivity of the developed model to uncertainties in input?
- How can the proposed model be used in a flood defense framework?

Chapter 2. Literature study

This chapter presents an overview of the existing knowledge regarding the subject of this thesis. The first paragraph discusses embankment characteristics and failure types. Paragraph two examines forelands and their effects on embankment breaching and breach growth. Finally, paragraph three presents a review of breach development models.

2.1 Dikes and levees

Dikes and levees are flood protection measures. These embankments are situated either parallel to a river or perpendicular to a sea or lake. On one side of the embankment water is present, the other side is dry land. The difference between dikes and levees is related to the height of the dry side compared to the side at which the water is present. If the average water level is lower than the ground level on the dry side, the embankment prevents rivers or seas from overflowing. This is called a levee. Levees can be formed either naturally or artificially. If the mean water level is higher than the ground level on the dry side, it is called a dike. If a dike would fail, the land side would be flooded. Additionally, if the mean water level is higher than the level of the land, this land called a polder.

Dike failure

Dikes can experience failure; this occurs when acting forces on the dike become larger than the resistive forces. The acting forces are mainly related to hydraulic parameters, such as the water level, wave properties and difference in head over the dike. More incidental failure is also possible, for example ship collisions can cause a dike to fail. The resistive forces come from the properties of the embankment. Height, width and material use are the most relevant parameters.

There are many different failure modes associated with dike failure. Vrijling (Vrijling, Schweckendiek, & Kanning, 2011) distinguishes twelve of them.

- Overflow
- Sliding outer slope
- Erosion of first bank
- Wave overtopping
- Micro-instability
- Settlement
- Sliding inner slope
- Piping
- Drifting ice
- Shearing
- Erosion outer slope
- Collision

It is important to take all failure mechanisms into account when designing an embankment. Dike failure will be discussed in more detail in chapter 3 and 4.

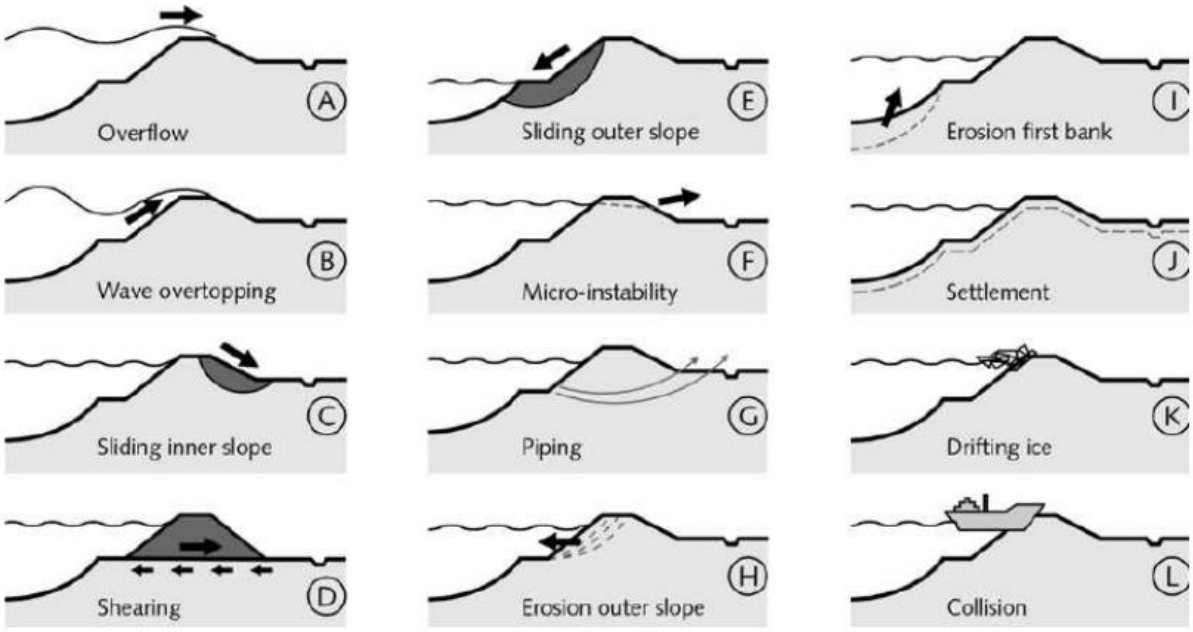

Figure 2: Dike failure types, side view
Note: Reprinted from: *Safety standerds of flood defences, Vrijling, Schweckendiek & Kanninig, 2011*

2.2 Forelands

A foreland is an area of land between a dike and a body of water, located around mean high water level. Situated just above mean water level means that although it is strictly speaking land, a foreland is frequently inundated by tides or storm surges. A foreland located in a coastal area consists of the tidal flats and saltmarsh regions, with the saltmarsh being at a slightly higher elevation than the tidal flats.

Figure 3: Salt marshes in the Westerschelde, Paree, E.(2020). Westerschelde.

This paragraph describes the basic properties of a foreland and its relation to the adjacent dike. The focus will lie on the macro-scale, namely the shape, sediment type and the hydraulic effects it has on breach development. There is evidence that forelands located next to a body of salt or brackish water (commonly known as saltmarshes) have positive effects on reducing inundation during a breach event (Zhu, et al., 2020) as well as on the environment (Taylor, Paterson, & Baxter,

2019). These effects are very important from an ecological point of view but are only discussed in a framework of their contribution to embankment breaching in this thesis.

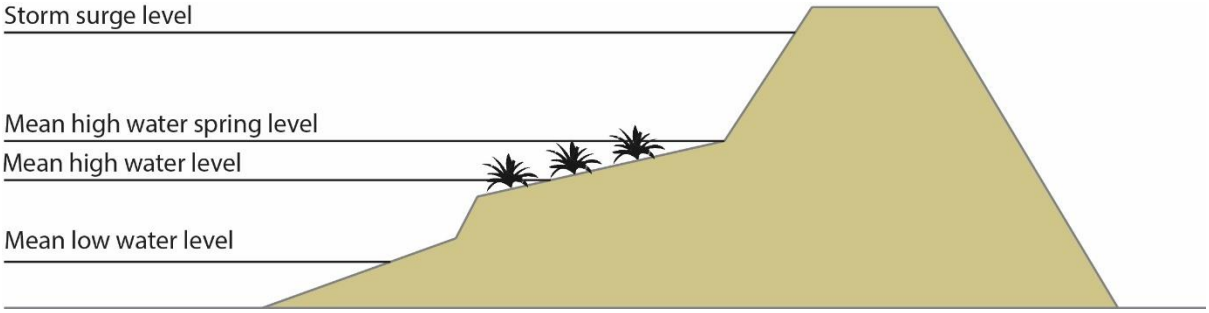

Figure 4: Water levels for different tides and storms, side view

Forelands are formed by deposition of sediment from the body of water. During slack tide sediment can settle in the shallow foreland and the vegetation found in this area also contributes to the sedimentation and entrapment of sediment. Forelands often consist of finer sediments such as clay, silt, and fine sand (Zedler, Bonin, Larkin, & Varty, 2008). During inundation of the foreland, this sediment is brought in by tides or surges. The larger sediment has already settled in the deeper regions because of their higher weight and under regular circumstances is not transported to the foreland. Forelands are said to be self-sustaining for the case of long-term changing mean water levels as long as the change is not too abrupt. This self-sustaining property is also highly related to the ecosystem present in the foreland (Fagherazzi, et al., 2020).

2.2.1 Foreland properties and effects of on embankment failure

There are two main benefits of a foreland, the ecological function, and flood protection. It is known that saltmarshes and tidal flats, both examples of forelands, can provide highly valuable ecosystem functions. Primary production takes place in these areas which form the basis of a food chain ranging from microbenthic communities all the way to larger species like birds and fish (Morris, Sundberg, & Hopkinson, 2013).These ecosystem functions are very important, however they do not directly relate to breaching process of an embankment and will therefore not be discussed further in this thesis.

The general effects and benefits of a foreland on flood protection have been understood for a long time. In the 1200's coastal engineers built dikes further inland if a foreland was present (personal communications P.J. Visser, TU-Delft). However proof and scientific documentation of these effects is much more recent, dating back to the 1990's (King & Lester, 1995).

There are two main benefits of a foreland in terms of coastal protection. These are both present during the later stages of the breaching event. The first effect is that a high foreland influences the flow rate through the breach, in most cases reducing the erosion rate on the embankment, this is expended upon in more detail in the next paragraph. The second effect is the reduction of the inundation depth in the hinterland. Since forelands are usually stronger than sand dikes, they will erode slower and can resist storms better than the dikes (Zedler, Bonin, Larkin, & Varty, 2008). This means that when a dike is completely breached during a storm, the foreland will effectively act as a new embankment. Once the storm has subsided, and the sea level falls below the level of the top of the foreland, the discharge through the breach becomes zero. See also the figure below.

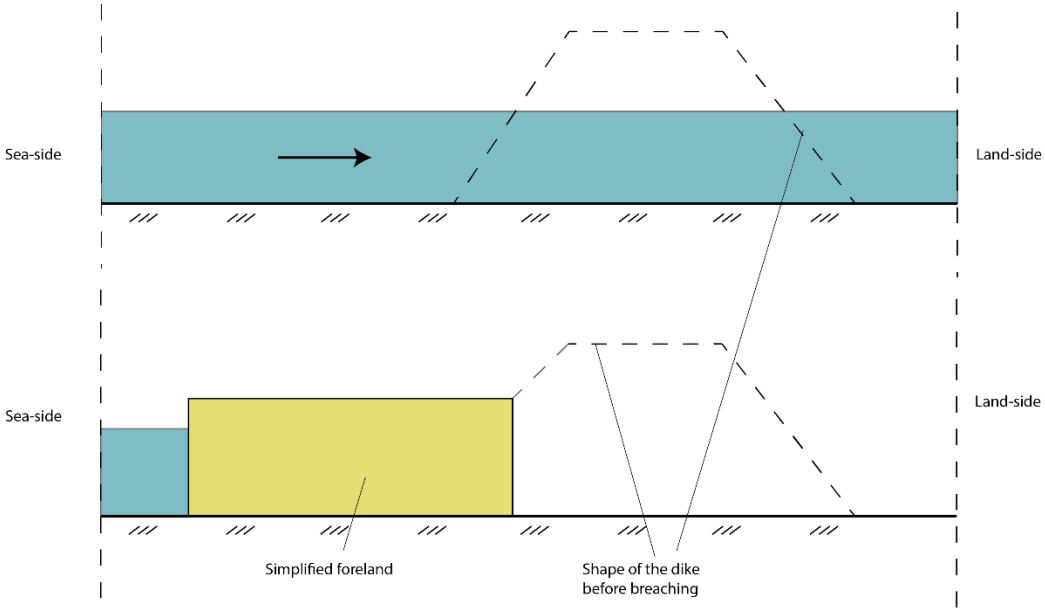

Figure 5: Inundation limited by foreland side view, top: no foreland present, bottom: foreland present

Another effect of a foreland is a reduction in wave height caused by decreased water depths. This effect depends heavily on the length of the foreland and the water depth. The reducing effect becomes more prominent the longer and shallower the foreland is (Vuik, Borsje, Willemsen, & Jonkman, 2019).

The effect of a foreland on wave behavior falls outside of the scope of this research. See also paragraph 7.2.3 on limitations of the presented model for the implications of this decision.

2.2.2 Effects on breaching process

As mentioned in the previous paragraph, a foreland influences the flow rate through the breach during the later stages of the breaching event. During this time, the flow through the breach can be considered critical (Visser, 1998). The critical flow through the breach implies that the Froude number is equal to one, giving for a roughly prismatic breach:

$$Fr = \frac{v}{\sqrt{g\frac{A}{B}}} \approx \frac{v}{\sqrt{gd}} = 1$$

Where Fr is the Froude number, v the kinematic viscosity, g is the gravitational constant, A and B are the area and the width of the prismatic channel and d is the water depth in the channel.

A foreland generally lays on a higher elevation than the bottom of the embankment. This means that the critical flow state is instead determined by the water depth over the foreland, see Figure 6. Using the assumption of critical flow $(Fr = 1)$, both water depth and therefore flow velocity are reduced when a foreland is present. Since discharge per unit width is equal to the flow velocity multiplied by the water depth, it is clear that when both the flow velocity and depth decrease, the flow rate over the foreland and the breach will also decrease.

$$q = ud \quad \left[\frac{m^2}{s}\right]$$

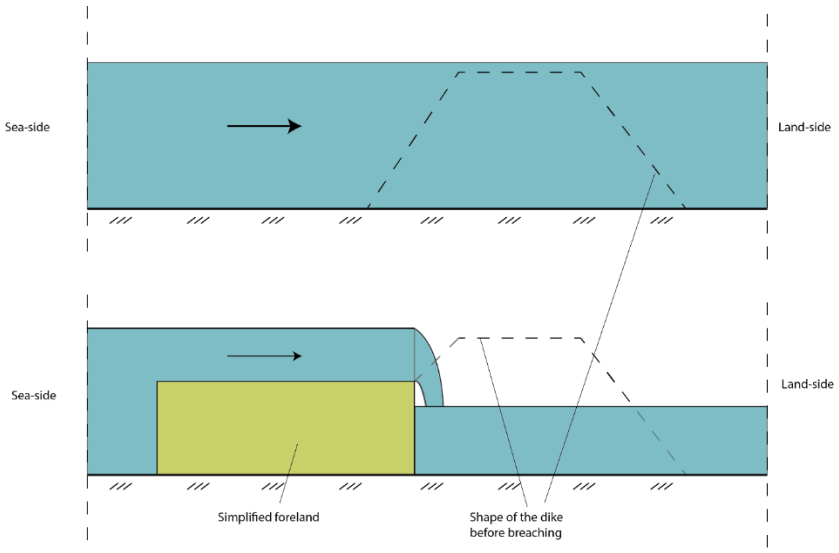

Figure 6: reduced flow rate over breach due to presence of a foreland, side view

Another phenomenon caused by the presence of a foreland is an increased discharge over the spillway caused by an increased spillway length. The increased discharge over the spillway is caused by a headcut erosion that takes place on the foreland. A storm can cause overtopping on an embankment and it local breaching initiates in the embankment. Once the breach reaches the level of the foreland, the foreland will experience seaward headcut erosion. The headcut erosion follows the width of the breach, when a new part of the embankment is eroded, headcut can start to appear in the adjacent foreland, see Figure 7. This headcut erosion, limited by breach width creates an erosion pattern in the shape of half of an ellipse (Figure 8). The circumference of this half ellipse is longer than the width of the breach, effectively increasing the length of the spillway compared to the situation where no foreland is present ((left) Figure 9).

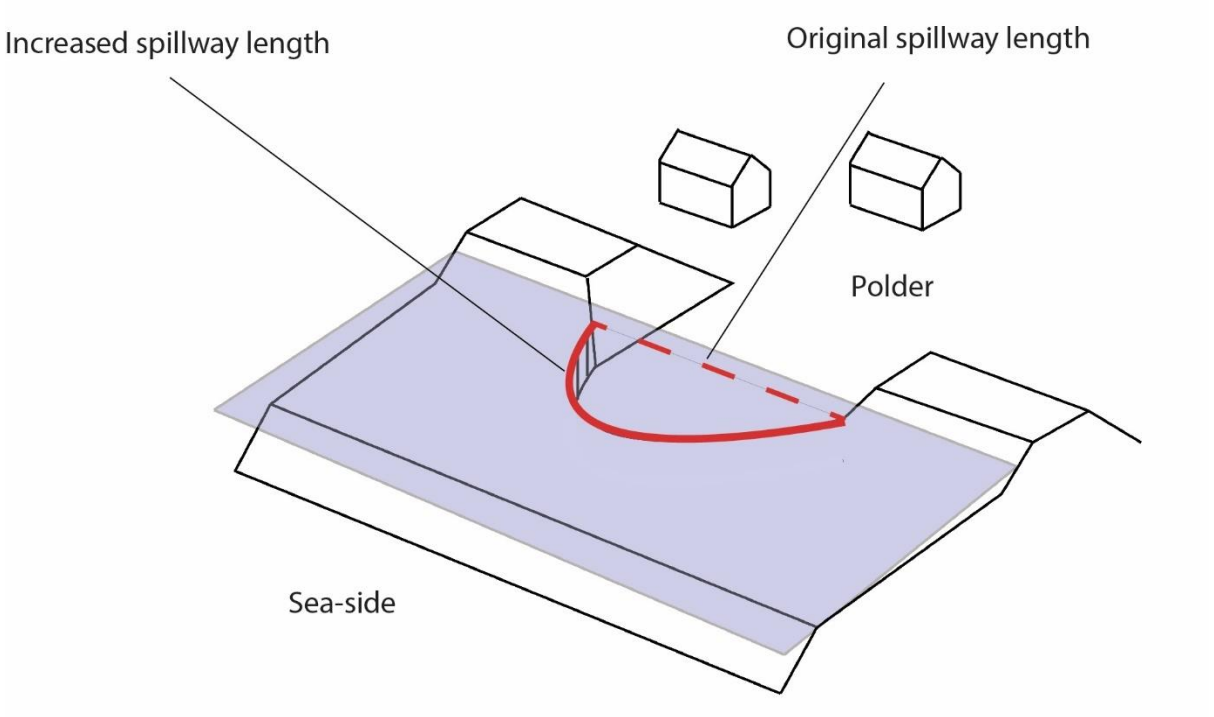

Figure 7: Increased spillway length caused by foreland

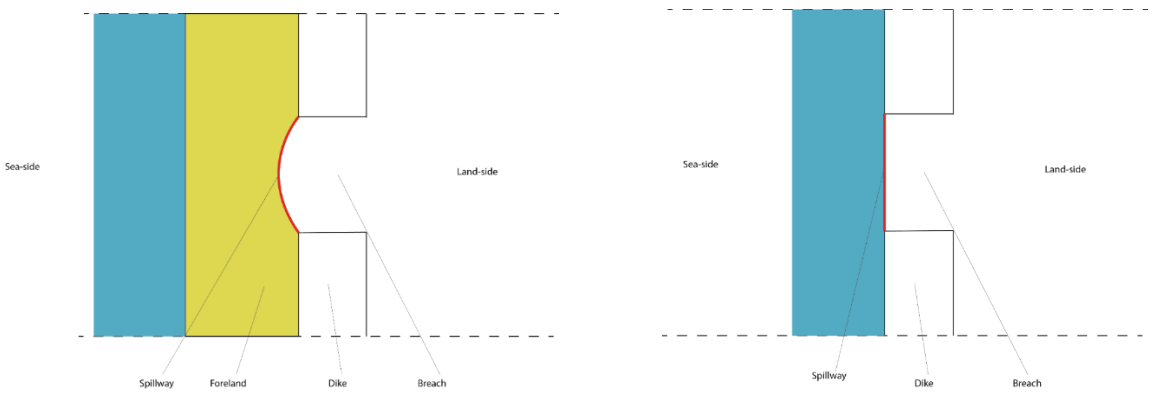

Figure 8:Top view of increased spillway due to elliptical foreland erosion (left) Figure 9: Top view of spillway length in absence of a foreland (right)

From the combination of these two phenomena, it can be seen that the effect of the foreland on the breach growth can go in two different directions. One reduces total discharge while the other increases total discharge. It is important to note that many forelands contain fine sediment and experience very little headcut erosion (personal communications P.J. Visser, TU-Delft). This means that the increased spillway length is hardly visible, leaving only the discharge reducing effect to be relevant.

2.2.3 Sediment types in forelands

Forelands can consist of different sediment types. These sediments range from coarser material (sandy) to very fine sediment (clayey). Furthermore, organic material can be found both in and on top of the foreland (Zedler, Bonin, Larkin, & Varty, 2008).

The critical shear stress of fine sediments can be much higher than that of coarser sediments. This can be explained by the fact that fines can experience a strong cohesion and coarser materials cannot (van Prooijen, 2019). In addition, organic layers that contain fibrous materials such as root systems are extremely difficult to erode and will can also trap sediment (Marin-Diaz, Bouma, & Infantes, 2020).

Forelands consisting of fine sediments and organic material will therefore be very resistant to erosion. As a result, these types of forelands are the most effective in reducing breach development in embankments. The different sediment types play a key role in the required approach for modelling the erosion patterns, this will be discussed further in chapter 4 and 5.

Figure 10: Foreland erosion restricted by system of roots
Note: adapted from: "Resistance of salt marsh substrates to near-instantaneous hydrodynamic forcing", Brooks et al., 2020.

2.3 Breach development models

Studies into the causes of breach events have been conducted for hundreds of years, but studies into how the breach develops in time is a relatively new topic with the earliest works stemming from the 1960's (Zhu, Visser, & Vrijling, 2004). Models used to simulate breach development calculate how the height and width of the breach develop over time and how the flow rate and velocity through the breach are impacted by this deformation.
According to Wurbs (Wurbs, 1987) breach size predictions (width and height) are the most uncertain parts of breach development modelling. The uncertainty in these models combined with involved potential damages that embankment breaches cause, asks for caution when applying these models, and might require significant safety factors in order to be used.

2.3.1 Types of breach development models

There are multiple breach development models currently available with varying degrees of functionality and accuracy. The earliest known breach model was made by Cristofano in 1965 (Cristofano, 1965).This relatively simple model used a trapezoidal breach geometry and an empirical sediment transport formula. In the past fifty years significant progress has been made in these mathematical models. This progress stems from increased understanding of the processes as well as the advancements in computational power available to run these models. In paragraph 2.3.3 an overview of the different available models is presented.

In general, two types of breaching models can be distinguished. The first type is those using a parametric approach, the second comprises physically based models.

The basis of parametric models is using a set of parameters that simplify the breaching process (Zhu Y. , 2006). These parameters usually entail the ultimate breach dimensions, the total duration of the breaching event as well as sediment properties. The values of these parameters are derived using historical data of breaches and sediment samples. A review of parametric breach development models by Zhu (2004). shows varying levels of complexity in the models. Where the first model by Cristofano uses constant breach width and an empirical sediment transport formula, by 1988 the BREACH model (Fread, 1988) was able to use different breach shapes and allowed for different levels of saturation in the embankment.

One of the largest drawbacks of many models is that they are based on instantaneous breaching. Although this is generally how concrete structures are breached, this does not hold true for soils where breach growth happens more gradually (Zhu Y. , 2006). Fortunately, using instantaneous breaching for soil embankments is a conservative approach.

The basis of the physically based models lies in combining multiple physical equations to simulate the breach development and the ultimate state of the breach. Hydrodynamics, sediment transport and soil mechanics are all used in these models. A key difference between physically based models and parametric models are that where parametric models have a predetermined end-state, the physically based models do not, and instead calculate an end-state themselves.

A further distinction can be made within the physically based models into empirical and theoretical models, where the empirical models use empirically derived relations in their calculation as opposed to theoretically derived equations. An example of an empirical physically based model is SIMBA (Temple, Hanson, Neilsen, & Cook, 2005). An example of a full physical model is BRES (Visser, 1998).

When comparing the type of models, it can be concluded that empirically based models are relatively simple, fast, and conservative. However, due to the lack of physical relations and the usage of assigned key parameters, these models are likely less accurate than their physically based counterparts. The physically based models are more complex and give more accurate and detailed results. These models are still limited by the understanding of the underlying relations, as well as by available computational power (Robinson, Hanson, & Hassan, 2008).

2.3.2 Incorporation of forelands

As stated in chapter 1, the aim of this research is to implement the effects of a foreland in a breach growth model. These effects include the final shape and dimensions of the breach. It is therefore preferred to make use of a model that does not have a preset ultimate shape and size. Most parametrically based models do require this information and are therefore not suitable for this thesis. In contrast, physically based models derive the final dimensions of the breach through the underlying equations and balances. Furthermore, as mentioned in 2.3.1, physically based models have shown to give more accurate results than parametrically based.

For this research it is also preferred to use a light model in terms of computational power required. Since complex natural relationships are used in the modelling of foreland behavior (see also paragraph 2.3.4), a sensitivity analysis is highly advised. This requires many repeated runs of the model and would be cumbersome with a highly complex model. Additionally, lighter models often require less input parameters due to simplifications used. This is especially relevant since the amount of experimental and historical data on breach development is limited (Nagy, 2006). It is also easier to both implement and determine the effects of a new functionality in a simpler model.

Lastly, the number of available models is limited, and several models, such as EMBREA, are commercially distributed and the source code is not accessible.

In conclusion the optimal breach model to implement a foreland functionality in is computationally light, physically based and one for which the source code is readily available.

2.3.3 Overview of breach development models

Multiple studies have been done into the different types of breach growth models (see for example (Zhu, Visser, & Vrijling, 2004). These studies look at the flow equations, sediment transport type, breach geometry and required input parameters. They also distinguish the parametrically and physically based models. One of the more recent studies looks at the then state-of-the-art breaching models (Peeters, Heredia Gómez, Van Damme, & Visser, 2016). This review only examines five models which Peeters et al. attribute to the "availability of the code, experience and expertise with the model".

For this thesis, a selection of breach growth models will be presented. This selection is based on the preferred model type as discussed in paragraph 2.3.2. This selection will be examined on formula use, involved simplifications and approximation (e.g., breach geometry), complexity, sediment transport and flow type, required input parameters and if foreland (parametric) functionality is included. The presented list is based on a selection of studies (Zhu, Visser, & Vrijling, 2004), (Wahl, 2010), (Peeters, Heredia Gómez, Van Damme, & Visser, 2016).

Model name (year)	Flow type	Sediment transport type	Breach geometry/ morphology	Complexity	Foreland parametrically included	Required input parameters (only most important are presented)
NWS BREACH(1988)	Broad crested weir flow	Meyer-Peter Mullër	Rectangular and trapezoidal	Low	No	Soil properties, embankment geometry, more
SITES (1997)	Spillway stage-discharge curve	Detachment model for stages 1&2, energy dissipation for stage 3	Three stages of failure in XZ direction. Grass cover erosion, headcut formation, headcut erosion.	Medium	No	Soil and grass layer properties, embankment geometry, more
BRES (1998)	Broad crested weir flow & Bélanger	Multiple available sediment transport formulae: Wilson, Engelund & Hansen, Van Rijn and more	Five stages of failure. YZ direction: trapezoidal XZ direction: Global Exner with variable b	Medium	Yes	Soil properties, geometry of embankment, embankment, and foundation, sediment transport type, more
HR Breach (1999)	Broad crested weir flow & 1D steady non-uniform flow equation	Multiple available sediment transport formulae: Bagnold-Visser, Yang and more.	Effective shear stress dependent & Exner equation	High	No	Soil properties, initial breach dimensions, embankment geometry, sediment transport type more
Zhu (branching out from BRES model) (2006)	Broad crested weir flow & Bélanger	Multiple available sediment transport formulae: Wilson, Engelund & Hansen, Van Rijn and more	Five stages of failure. YZ direction: trapezoidal XZ direction: Global Exner with variable b	Medium	Yes	Soil properties, geometry of embankment, embankment, and foundation, sediment transport type, more
FIREBIRD (2006)	St. Venant and Exner equations	Exner equation	Trapezoidal	Medium	No	Soil properties, embankment geometry, more
SIMBA (2006)	Broad crested weir flow	Parametric equations for headcut advance	Rectangular & trapezoidal	Low	No	Soil properties, embankment geometry, more
EMBREA (continuation of HR BREACH) (2011)	Variable weir flow & 1D steady non-uniform flow equation	Two different erosion equations: Chen & Anderson and Hanson	Variable erodibility & YZ direction: effective shear stress XZ direction: Erosion	Very high	No	Soil properties, initial breach dimensions, embankment geometry, structure type (layered, homogeneous etc.), sediment transport type, more

Table 1: Comparison of selection of breach models

2.3.4 Uncertainties in breach development models

Breach growth is heavily dependent on sediment erosion rates and the associated critical shear stress. Unfortunately, the critical stress for soils is difficult to predict, especially for soils or structures involving fine sediments. The difference in expected critical shear stress for identical soils can be up to two orders of magnitude (Zhu, 2006). It is therefore essential to consider that even though these mathematical models can give very specific results, the underlying physical relations are still not perfectly understood, allowing for considerable errors. This can give the outcomes of these models a false sense of precision. Therefore, a sensitivity analysis will be performed to better understand the relative impact of each parameter and their accuracy.

Another uncertainty arises from the calibration of the models. Nature based (soft) coastal protection measures are often much more complex and less well understood than their 'hard' counterparts. This means that breach growth models frequently rely on experimental data to calibrate parts of the models. However, breach growth is a complex process, and one must be careful when using a model that has been calibrated for a specific case for a different scenario. For example, the presence of tree roots in a clayey soil can greatly impact the shear strength of said soil. This will be discussed in more detail in chapter 3.

2.4 Model choice: BRES

The final breaching model choice for the foreland model to be added into is the BRES model. The source code for this model is available, the model is relatively simple and already has a functionality for relatively high forelands. This functionality is limited to forelands with a height equal to the top of the dike foundation. Furthermore, initially a circular erosion pattern in the foreland is assumed, which can be calibrated to specific cases. The calibrated erosion pattern can be anywhere from a circular shape to a straight line. The proposed foreland model for this thesis instead calculates and predicts the erosion pattern mathematically and does not limit the height of the foreland. However, the BRES model does serve a foundation to build upon the proposed foreland model.

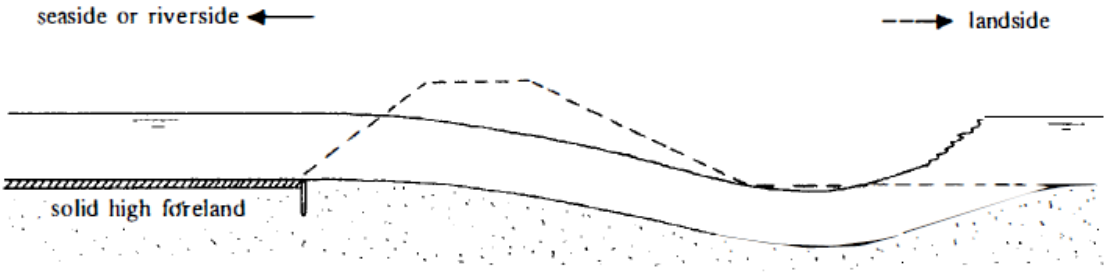

Figure 11: Height of a solid high foreland limited to foundation level of the embankment
Note: reprinted from: "Breach-growth in sand dikes", Visser, P.J., 1998

Chapter 3. BRES model overview

This chapter introduces the BRES model (Visser, 1998), the model of choice to implement the foreland effects module in. It is a physically based model using five distinct steps in the breaching process.

In the first paragraph a basic overview is given of the functionalities of BRES. The second paragraph presents the five different stages the model uses to compute the breaching process. The following paragraphs will present the flow types, the multitude of sediment transport formula and breach geometry. Lastly the applicability and recommendations for the foreland erosion effects are discussed.

3.1 General overview of BRES model

BRES is a 1-D mathematical model that describes the growth process of a breach during embankment failure. The assumed failure types are a combination of overtopping and instability of the slope. It also describes the flow rates through the breach during the simulated breaching process. In the model it is assumed that the dike is made up of sand and, if present, clay layers do not decelerate the erosion process. The model is based on breach erosion observed in laboratory tests, as well as field tests. A similar model for clay dikes has been developed as well (Zhu Y. , 2006).

The dike is highly schematized and takes the form of a trapezoid in the model, greatly reducing the complexity of the model. This schematization is discussed in paragraph 3.3 alongside a multitude of figures.

Lastly three different foundation types are present in the model for the user to choose from. The first case relates to the situation where a toe construction is present. The second relates to the case where a relatively high foreland is present and lastly the third case entails the situation where there is unlimited foundation erosion. This is discussed in more detail in paragraph 3.4.

3.2 Embankment failure stages

The model assumes a small initial breach on the top of the dike caused by overtopping. This is the starting point for the BRES model. After this initial breach, five separate phases in the breach process are distinguished. The first two phases relate to steepening of the dike slope and a decrease in width of the dike. An important characteristic of these first phases is that the breach depth has not increased substantially compared to the initial breach. Therefore, flow rates through the breach are still low and hardly increased compared to the initial breach.

During stage three and four the width of the breach grows rapidly both in height and width. This growth is accompanied by a large increase in discharge through the breach. An important characteristic of the flow during stage three and four is that the flow is assumed critical. During the fifth and final stage, the backwater in the polder decreases the flow velocity through the breach causing the growth of the breach width to reduce. The rising backwater level causes an eventual stop of flow through the breach, this happens when the backwater and sea level are equal. During the fifth phase in the breaching process the flow is no longer assumed critical. The five stages serve as a central principle for the rest of the chapter will get expanded on further in the following paragraphs.

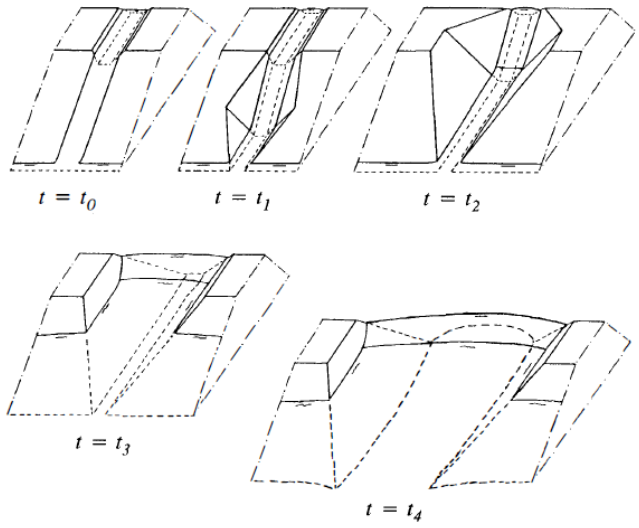

Figure 12: Failure stages during the breaching event
Note: reprinted from: "Breach-growth in sand dikes", Visser, P.J., 1998

3.3 Breach schematization

This paragraph will describe the schematizations used by BRES to reduce a complex 3D problem into a workable model. The schematizations are mostly related to the shape of the dike and breach, which in turn also reduce the complexity of the flow properties. An additional schematization is related to the different types of breaches observed in nature.

3.3.1 Schematization of the dike

A dike is a 3D structure, and a breach also erodes the dike in all three directions. The breaching process and failure stages have been described in 3.2, see also Figure 12. Unfortunately, a 3D flow model is too complex for the time and spatial domains of the breaching event. Full 3D models are usually reserved for events that happens on a much smaller timescale and size (Pietrzak, 2020). Visser has therefore taken the approach of reducing the 3D nature of a dike to a cross-section of the dike and a cross section of the breach. In this paragraph the cross-section of the dike is examined.The assumed shape of the dike is trapezoidal. The embankments are assumed to be straight lines and the crest of the dike is assumed to be horizontal, see the figure below.

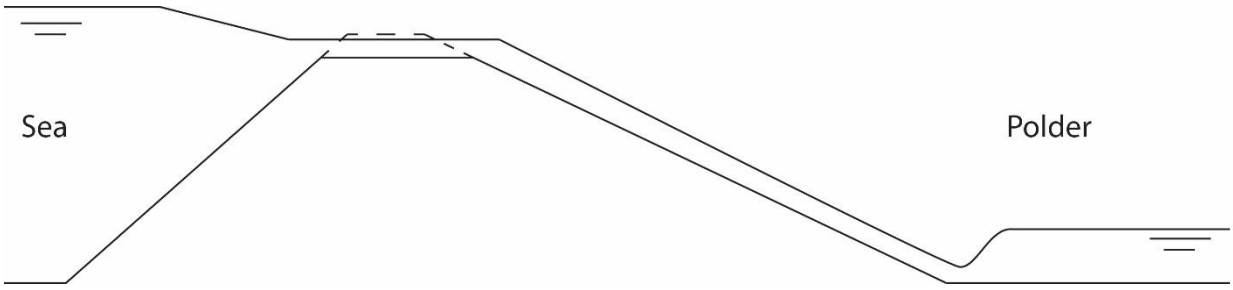

Figure 13: Erosion of embankment crown, side view

Erosion of dike is initiated by a small breach on the crest of the dike. This initial breach causes water to flow into the polder and starts eroding the inner slope of the dike. This first erosion of the inner dike is the beginning of phase one in the erosion process.

As the inner slope of the dike erodes, the slope is assumed to remain constant. However, the slope angle β, (angle between the slope and the base level) becomes larger. This steepening of the inner slope is caused by the water picking up sediment as it flows down the slope. From a hydraulic perspective, the embankment slope is very steep, causing the water to accelerate sharply as it flows down. As flow velocity positively relates to the amount of sediment entrainment, this acceleration in flow causes more sediment to be picked up towards lower part of the slope. This entrainment and transfer of sediment is what we observe as erosion of the dike, with the largest erosion occurring at the inner toe. The steepening of the inner slope can be seen from Figure 14.

As the inner slope erodes, the slope angle eventually will reach a maximum steepness, defined as β_1. At this angle, erosion at the toe of the dike will cause the sediment above it to slide down as well, leading to erosion of a slab of soil. In BRES this is not modelled as period slab failure, instead the erosion is of the slope is modelled as being continuous.

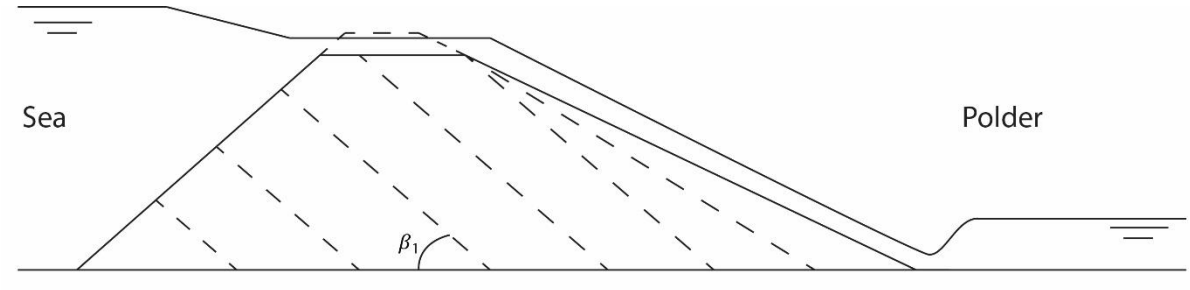

Figure 14: Erosion of inner slope in slabs, side view

During the first two phases in the breaching process, erosion is assumed to only take place at the inner slope of the dike (the initial crown erosion is not considered part of the five phases). The outer slope stays intact, and the crest of the dike remains horizontal and at the same height. The length of the crest reduces as the soil slabs erode, see Figure 14.

As the slabs continue to be eroded from the inner slope, the horizontal crest gradually becomes shorter and will eventually disappear, see Figure 15. This is also the start of the third phase in the erosion process. From this moment the dike is schematized to a triangle, as opposed to a trapezium. The erosion of the inner slope continues, and the breach depth increases rapidly. The triangular form of the dike is maintained throughout the remainder of the erosion process until the dike has completely disappeared.

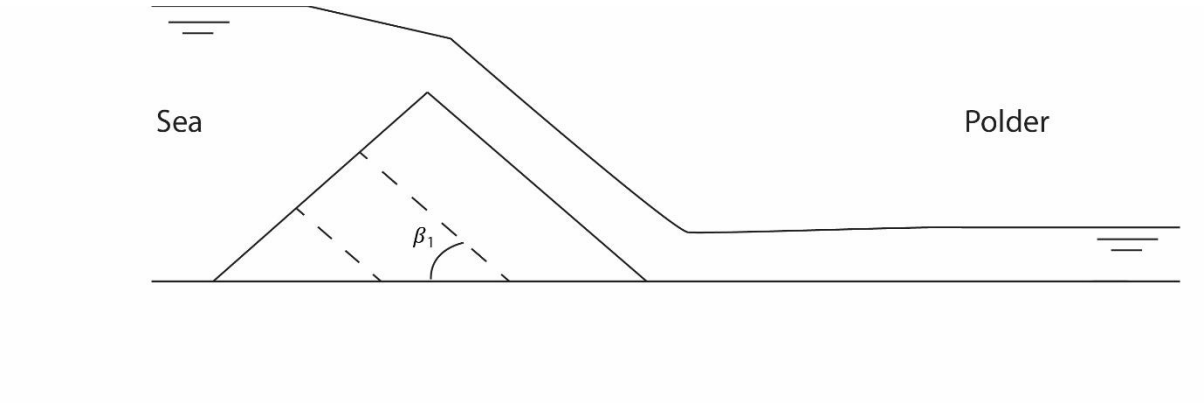

Figure 15: Decreasing embankment height, side view

3.3.2 Breach geometry

Similar to the dike, the breach geometry is also schematized as a trapezoid. The assumption made by Visser is that the process of initial breach formation has created slope angles equal to the angle of repose,ϕ, the maximum angle a soil layer of granular material can have with the horizontal before failure occurs, see the figure below. A newer study by suggests that this angle is actually much larger (Foortse, Visser, Bisschop, & van Rhee, 2019). The weight of the water acts as a force on the breach slopes, causing them to be more stable with angles up to $80°$ thought possible.

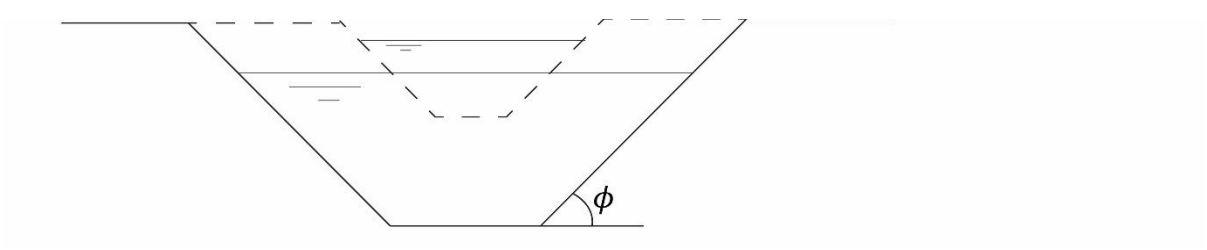

Figure 16: Increasing breach width and height, side view

As the dike erosion continues the trapezoidal breach grows both in height and width. The slope angle remains equal to the angle of repose. Erosion occurs similar to the behavior observed when examining the inner slope of the dike in the previous paragraph, with unstable slabs of sediment experiencing sliding failure. The sides of the breach are at the angle of repose and additional erosion on the lower parts of the slope cause failure of the entire slab, see also Figure 14. In BRES however this is simplified to a continuous process.

During phase four and five the breach depth has reached the polder level, causing breach growth within the dike to be restricted to mainly lateral growth in these phases. Depending on the sediment type of the dike base, some erosion can continue below the polder level. The different types of breaches will be discussed in detail in paragraph 3.3.3.

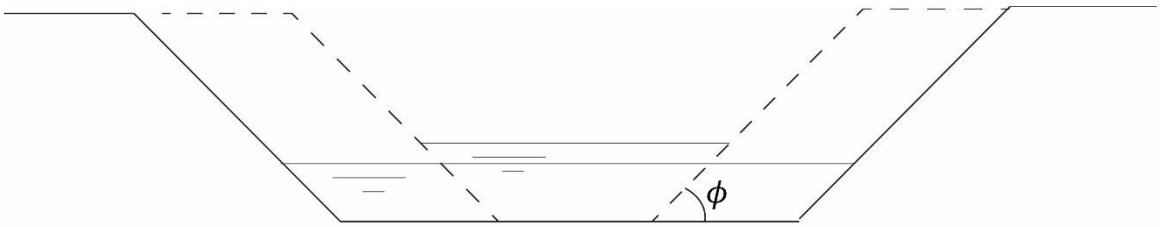

Figure 17: Breach reached non-erodible base, only lateral growth, side view

3.3.3 Breach types

The model distinguishes three different classes of breach types related to the sediment type in the bed as well as toe constructions and forelands, of which one has two sub-classes. It is important to note that these breach types only start affecting the model in phase four, when the bottom of the breach has reached the bed level.

Breach type A

Breach type A describes a situation where a toe construction is present. Two situations are considered for breach type A, in the first the base of the dike consist of a solid non-erodible clay

layer and in the second the base material is similar to the rest of the dike and erosion can not be considered negligible.

Type A.1: base consists of a solid clay layer

For this situation the breach acts as a broad-crested spillway. The flow is effectively uniform along the breach, causing the water depth to be constant and equal to the critical water depth. The toe structure stabilizes the sea-side base of the dike and prevents erosion below the base. For this case the erosion is limited to the dike and the polder, the base and seaside bed stay fully intact.

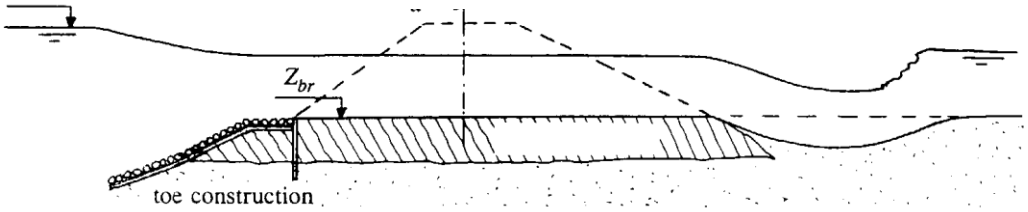

Figure 18: Stable base and toe construction, side view
Note: reprinted from: "Breach-growth in sand dikes", Visser, P.J., 1998

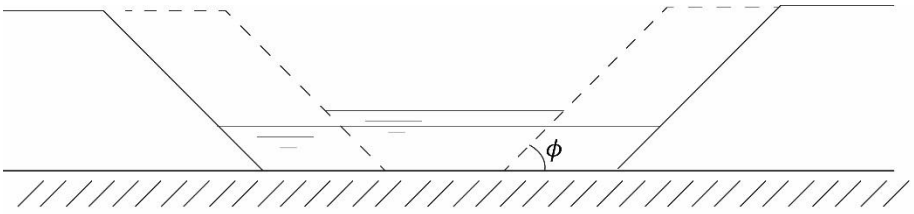

Figure 19: Breach growth limited to lateral plane, side view

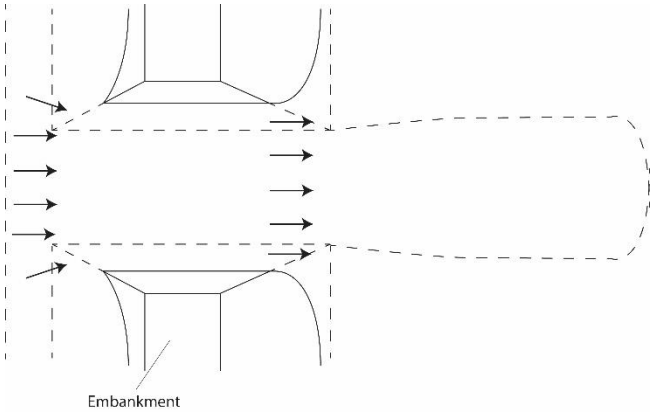

Figure 20: Erosion shape for stable base and toe construction, top view

Type A.2: Erodible base

For this breach type again a toe structure is considered, this time the dike base is not solid and can experience significant erosion. In this case the toe construction effectively acts as a spillway, which can be either broad- or sharp-crested.

After passing the toe construction, the flow experiences acceleration followed by deceleration. The acceleration at the toe construction causes the flow to become critical. The deceleration further downstream causes a hydraulic jump when the flow velocity falls below the critical flow velocity. This jump occurs downstream of the breach itself, meaning flow through the entire breach is critical. As the adaptation length, l_n of the flow is much larger than the length of the breach, the flow through the breach can be assumed to be uniform and critical, which is the same as observed in type A.1. For the determination of the adaptation length, see Appendix A.

Breach type B

Breach type B relates to a situation in which a relatively high foreland is present. This means that from the sea side toe of the dike there is an almost horizontal bed in seawards direction. As the breach reaches the base of the dike the foreland will start to experience retrograde erosion. This erosion causes an elliptical erosion pattern in the foreland. The edge of this ellipse effectively becomes the spillway over which flow is directed through the breach, see Figure 7 and Figure 22.

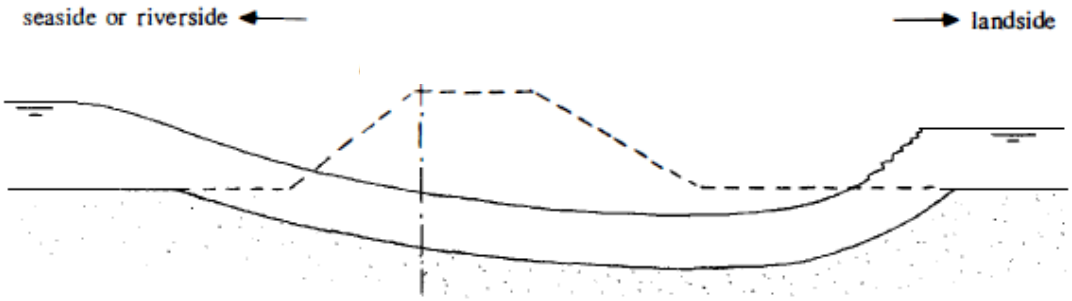

Figure 21: Erosion pattern for a relatively high foreland, erodible base and no toe construction, side view
Note: reprinted from: "Breach-growth in sand dikes", Visser, P.J., 1998

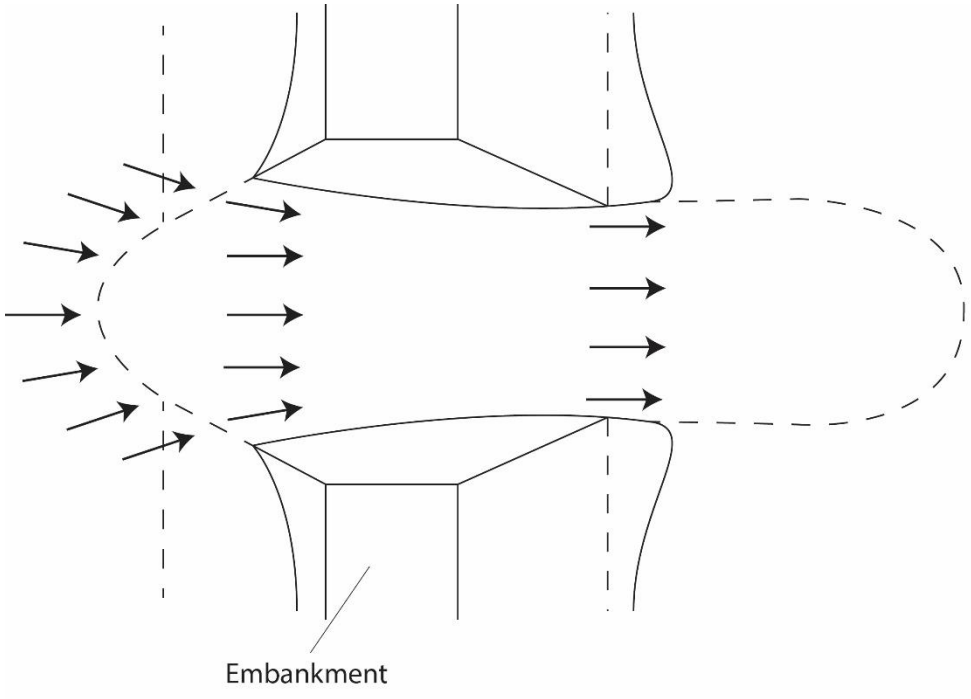

Figure 22: Erosion patter for a relatively high foreland, erodible base and no toe construction, top view

It is important to note that the erosion of the foreland does not start until stage four and five in the breaching process. During phase four the dike has been locally breached to the level of the hinterland. As the top of the foreland generally lies higher than the hinterland, a jet flow from the foreland onto the breach bottom takes place. The impact of this jet causes the foreland to erode seawards. At the start of phase four in the BRES model, the breach also starts to develop laterally, allowing for the foreland to follow this growth. As more parts of the foreland become exposed due to the erosion of the dike, the foreland will also start eroding in these areas. The result is a growing spillway in the shape of a half ellipse, with its width being limited by the growth of the breach.

This spillway is significantly larger than for type A.1 and A.2 where the spillway is equal to the breach width. The increased spillway dimension influences the discharge through the breach, where the length of the spillway is linearly proportional to the discharge through the breach. This means that when looking at for example a semi-circular erosion pattern in the foreland with length $\frac{\pi}{2}b$, the discharge is increased by a factor $\frac{\pi}{2}$.

This effect is captured in the constant discharge coefficient m. Discharge through the breach is defined as:

$$Q_{br} = m\left(\frac{2}{3}\right)^{\frac{3}{2}}\sqrt{g}B(H_w - Z_{br})^{\frac{3}{2}}$$

This discharge coefficient is the length of the semi-circular shape, L_{spill} (the length of the spillway in the foreland) divided by the diameter of the semi-circular shape (or breach width). This breach width, B_{br}, is also the length the spillway would have been in the absence from a foreland, see also Figure 7. From this definition of m, it can be understood that m is a form-factor that represents the factor at which the spillway is larger than the spillway would have been in the absence of a foreland:

$$Discharge\ coefficient:\ m = \frac{L_{spill}}{B_{br}}$$

For the case of a semi-circular erosion pattern m is equal to $\frac{\pi}{2}$. In absence of a relatively high foreland m is equal to one.

The BRES model was calibrated using a large-scale experiment conducted in 1994 in Het Zwin near Cadzand in the Netherlands (Visser, Smit, & Snip, 1996). From this experiment the discharge coefficient was observed to be around 1.3. However, the shape of the foreland erosion is very dependent on the sediment type it consist of and can range from semi-circular to an almost straight line linear to the dike. Depending on sediment type a type B breach can behave anywhere between the semi-circular spillway case and a type A breach.

Breach type C

Type C breaches refer to the situation of unobstructed breach growth. There is no toe construction or high foreland preventing erosion of the outer slope, and the base of the dike is erodible. The spillway for this breach type is approximately straight, causing the discharge coefficient m to be equal to one in the discharge equation.

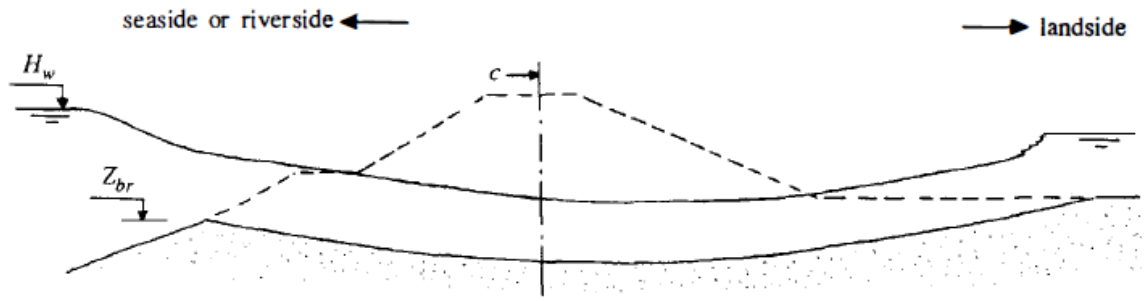

Figure 23: Unobstructed breach growth, side view
Note: reprinted from: "Breach-growth in sand dikes", Visser, P.J., 1998

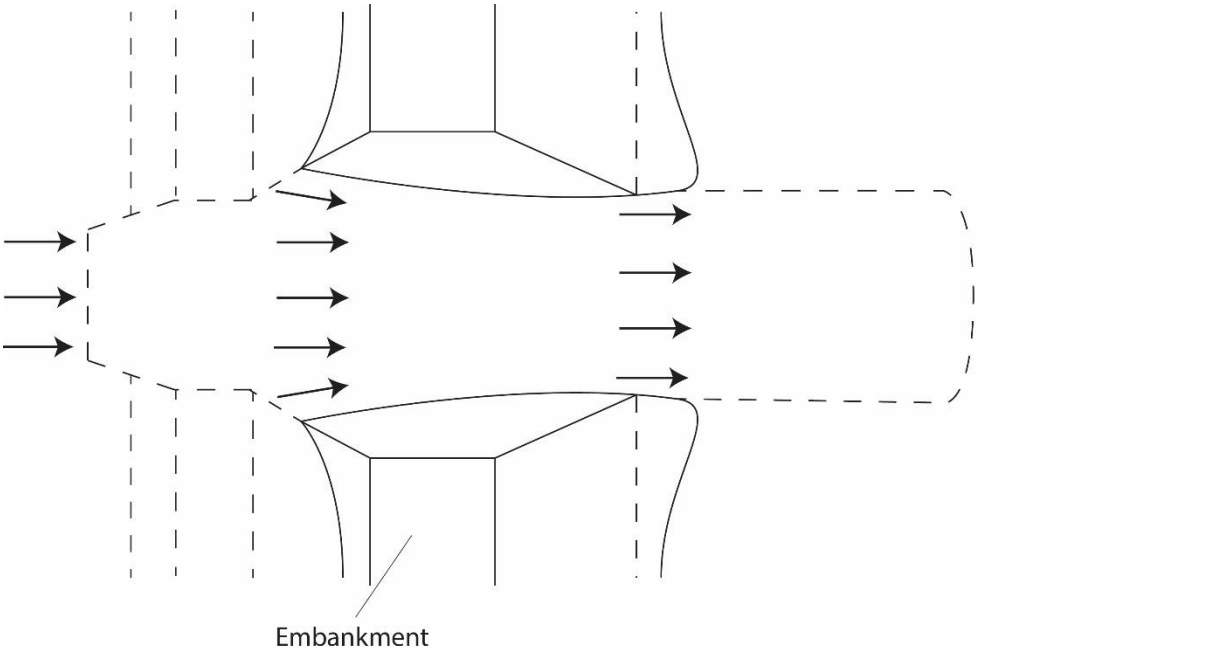

Figure 24: Unobstructed breach growth, top view

In this situation the dike base is erodible, meaning the breach depth is not limited by the base of the dike. Due to the 1-D approach of the BRES, the model is unable to predict the reduction of erosion rates past the base of the dike. It is up to the user to input the final depth of the breach. The one 1-D approach will be discussed in more detail in paragraph 3.4.

3.4 Erosion process

As mentioned in paragraph 3.4.2, in order to model the 3-D breaching event with a 1-D flow model, the BRES model uses sediment pick-up equations to calculate the erosion speed in the dike. For this the hydrodynamics of the flow are required and the sediment transport equations used by the model. This paragraph introduces these concepts and how they are utilized in the BRES mode.

3.4.1 Hydrodynamics

The BRES model uses a 1-D approach to model the breaching process of a dike or levee. A sediment transport formula, in combination with a sediment fall velocity equation, is used to calculate the erosion rate in the breach. The "select sediment transport formulae" function in the "input" module of BRES lets the user choose between multiple sediment transport formula's, listed below.

- Bagnold-Visser (1989)
- Engelund-Hansen (1967)
- Van Rijn (1984a,b)
- Wilson (1987)

As discussed in paragraph 3.2, the discharge and subsequent erosion rate in phase one and two is low. In these first two phases the erosion is limited to eating away of the landward side of the dike, but the crest of the dike maintains it is original height. See also Figure 14.

During phase three through five the discharge through the breach and the erosion rate increases dramatically. During these phases the crest of the dike is lowered, and the breach also grows laterally. This erosion is direct result of the 1-D sediment transport formula. BRES assumes continuous erosion of the dike slopes, relating the breach width and depth directly to the results of the transport formula. In reality slope erosion will not be continuous. Undermining of the slope causes instability, causing more incremental failure. Given the inherent uncertainty of the complete model, the error caused by this approximation is deemed insignificant.

Due to the 1-D nature of the BRES model, a boundary condition is required for the maximum depth of the breach. For breach type A and B this is determined by the dike base level and the height of the foreland respectively. For breach type C manual input by the user is required. A maximum width for the breach is not required. As the flow rate through the breach decreases and eventually stops during phase five, erosion will cease and the final width of the breach is given as an output parameter.

3.4.2 Sediment transport

A sediment transport formula describes the behavior of a flow eroding and picking up sediment from the bed or, if present, the slopes of a breach or riverbanks. Historically it has proven to be difficult to accurately predict these sediment fluxes due to the complexity of the hydrodynamics involved. Some examples of the involved hydrodynamics are the combination of steady flows and oscillatory flows (waves), strong turbulence caused by wave breaking, and flow adjustments to the bathymetry.

Due to the inherent complexity of the sediment fluxes, most sediment transport equations have been developed and calibrated for specific data sets (Cristofano, 1965). Therefore, depending on the situation different equations can be preferred. Most transport equations relate the sediment transport to bed shear stress caused by a flow. This relatively simple approach is then calibrated for specific situations and can give a relatively accurate prediction of the sediment transport.

Special caution should be given when examining transport and erosion in beds consisting of fine (cohesive) sediment. The expected erosion and transport using different equations may vary by two orders of magnitude.

As discussed in paragraph 3.4.1, different sediment transport formulae are available in the BRES model. For each of the stages a separate formula can be selected. The default selection in BRES is Bagnold-Visser for stages one through three, and van Rijn for stages four and five. The selection of transport equations in the model and the default selection is based on testing of a large amount of transport equations against experimental data of breach erosion experiments (Visser, 1998).

During the first two stages of breach development initiation of motion plays a significant role. The initiation of motion is defined as the threshold at which sediment particles start to move in an open channel flow. Because the flow rate and velocity through the breach is low during the first two stages, sediment transport is limited by the initiation of motion. For example, during phase one the water flows over the crest of the dike without eroding it, but erosion does occur and the landside toe of the dike after the flow has accelerated over the slope. During later stages of the breach development the flow rate and velocity are high enough so that initiation of motion does not play a significant role anymore. This lasts until the very end of phase five when erosion ceases due to reduced flow velocity.

Initiation of motion is taken into account within the sediment transport formulas. However, the sediment type of a dike or dike base greatly influences the erosion rate, and one should take care to select the applicable sediment transport formulas. BRES is limited to non-cohesive material and is therefore unable to compute sediment transports of fine sediment typically found in forelands.

A final important parameter when computing sediment fluxes is the fall velocity in the sediment. A sediment flux is a function of sediment being picked up as well as it settling on the bed again. The total sediment transport is a combination of bed load and suspended load. The equation to determine whether the transport is dominated by bed or suspended load is as follows:

$$\frac{u_*}{w_s} = \frac{\sqrt{C_f}u}{w_s}$$

And the criterion is:

$$\frac{u_*}{w_s} \gg 1, suspended\ load\ dominates$$

$$\frac{u_*}{w_s} \ll 1, bed\ load\ dominates$$

Where u_* is the bed shear velocity, w_s is the sediment fall velocity, C_f is the friction coefficient and u is the flow velocity.

Visser found that throughout all the five stages of the breaching process the bed shear velocity was much larger than the fall velocity, meaning suspended load dominates during the entire breaching process. Since the flow is roughly uniform through the breach and suspended load dominates, we can expect sediment to settle only after passing the breach. Therefore, fall velocity plays a limited role in the breach.

3.5 Model input and output

The BRES model uses a plethora of input and output parameters. This chapter paragraph will give an overview of the parameters and a brief explanation on what they are and how they affect the model results. The parameters will be presented categorically.

3.5.1 Input parameters and model functions

Below is a list of the most important input parameters and selectable functionalities used in the BRES model, for a more extensive list, see Appendix B.

Model functions

- Erosion functions: allows the user to choose an erosion function per stage of the breaching process.
- Breach type: requires the user to select the breach type to be modelled. In case of breach type B a value for discharge coefficient m is also required. The discharge coefficient is dimensionless.
- Inclusion of a flow slope: calculates the quantities that determine the erosion of the inner slope, u, d and C_f during phase one through three. Can be toggled on or off.

Water parameters

- H_p, water level in the polder above Z=0 where Z=0 is the reference line$[m]$
- H_w, outside water level above Z=0 $[m]$
- H_{ww}, outside water level above Z=0 in time, requires water level for different timestamps $[m]$

Dike body parameters

- Z_p, polder level above Z=0 $[m]$
- Z_{br}, breach height above Z=0, requires initial value $[m]$
- Z_w, height of the watercourse bottom above Z=0 $[m]$
- H_d, height of the dike above Z=0 $[m]$
- W_d, width of the dike crest $[m]$
- b, width of the breach at breach bottom, requires initial value $[m]$
- β_1, critical value of inclination angle of the inner slope in degrees

Sediment parameters

- D_{10}, the particle size for which the portion of particles with diameters smaller than this value is 10% $[m]$
- D_{50}, the particle size for which the portion of particles with diameters smaller than this value is 50% $[m]$
- D_{90}, the particle size for which the portion of particles with diameters smaller than this value is 90% $[m]$
- ϕ_d, angle of repose of the bed layer in degrees
- C_f, friction coefficient $[-]$

3.5.2 Output parameters

Below is a list of all the output parameters obtained after running the BRES model.

Parameters given as a function of the computed timestep

- B_t, breach width at the top of the dike $[m]$
- B_w, breach width at the water line $[m]$
- B, depth averaged breach width (over water depth d) $[m]$
- b, breach width at breach bottom $[m]$
- Q_{br}, breach inflow rate $\left[\frac{m^3}{s}\right]$
- U, depth average flow velocity $\left[\frac{m}{s}\right]$
- d, water depth above breach bottom $[m]$

Chapter 4. Foreland erosion

In this chapter the proposed foreland module is introduced. First, a basic overview of the interactions between the foreland and breach growth will be presented. In the second paragraph the erosion behavior of a foreland will be discussed, followed by a review of the two different methods to model the erosion process. Following this, the behavior of foreland and the embankments are discussed for different soil types and soil type combinations. The main distinction being made here is whether the soil is made of coarse (non-cohesive) or fine (cohesive) sediment, as those are the largest factors in different erosion behavior in a uniform soil layer (van Prooijen, 2019). Finally, in the last paragraph, a comparison between the applicability and the advantages and disadvantages of the two different erosion types is presented.

4.1 Foreland-dike interactions

The main objective of this research is to add a foreland module to the BRES model (Visser, 1998). This module will be based on physical relations and will interact with the breach growth model in a two-way relation. On the one hand, the breach growth will determine the maximum width of the foreland erosion. On the other hand, the foreland will determine the flow rate and velocity through the breach. These subjects will be discussed in more detail in chapter 5.

Currently, in the BRES-model foreland erosion is modelled as a semi-circular spillway that follows the lateral growth of the breach. It is important to note that the erosion of the foreland does not start until the last two phases in the breaching process (chapter 3). During phase four the dike has been locally breached to the level of the hinterland. As the top of the foreland generally lies higher than the hinterland, a jet flow from the foreland onto the breach bottom takes place. The impact of this jet causes the foreland to erode seawards. At the start of phase four in the BRES model, the breach also starts to develop laterally, allowing for the foreland to follow this growth. As more parts of the foreland become exposed due to the erosion of the embankment, the foreland will also start eroding in these areas. The result is a growing spillway in the shape of a half ellipse, with its width being limited by the growth of the breach. This is explained in greater detail in chapter 5.

Chapter 2 discussed the opposing effects an elevated foreland has on the flow rate through a breach. On the one hand the reduced flow rate due to a decrease in water depth, on the other an increased flow rate due to an increase in spillway length.

Even for the case of a relatively low foreland and erodible foreland the discharge reducing effect is still likely to dominate. This can be understood by a modified discharge equation from chapter 3. The original equation is presented below for convenience:

$$Q_{br} = m \left(\frac{2}{3}\right)^{\frac{3}{2}} \sqrt{g} B (H_w - Z_{br})^{\frac{3}{2}}$$

If an elevated foreland is present, the height of the spillway changes from being at the level of the breach bottom, Z_{br}, to the elevation of the foreland, Z_f, leading to the following equation.

$$Q_{br} = m \left(\frac{2}{3}\right)^{\frac{3}{2}} \sqrt{g} B \left(H_w - Z_f\right)^{\frac{3}{2}}$$

Given that discharge coefficient m is likely to fluctuate between 1.0 and 1.6 (see chapter 3), the elevation of a foreland is often around mean high water level, and the exponent $\frac{3}{2}$, it is clear that in most cases the flow rate reducing effect of the foreland is larger than the increasing effect.

For the rare cases that the discharge reducing effect is stronger, the model will still predict the erosion pattern in the foreland and the effect on the breaching process, however the user is urged to examine if the assumptions used in the model are still valid. If the foreland is extremely low, it is questionable if the plunging jet is still present in the breach and if headcut erosion is still the dominant erosion pattern. Furthermore, if the discharge coefficient m is very large, it means that the foreland is highly erodible compared to the erodibility of the embankment. The assumption used that foreland erosion follows the breach width might not be valid for that case.

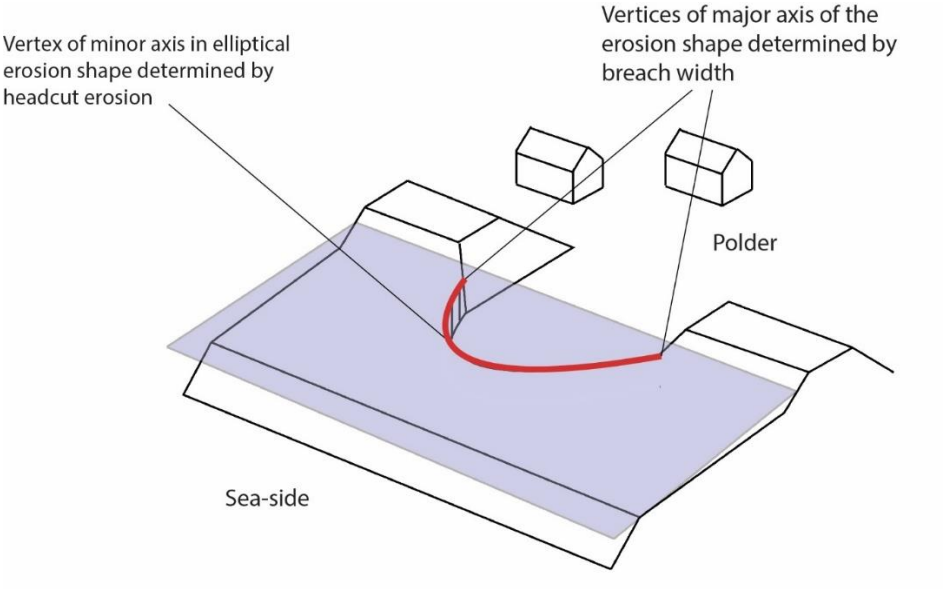

Figure 25: elliptical headcut in a foreland determined by headcut and breach width

4.2 Types of erosion

In the field of flood protection, several types of erosion can play a role. Specifically for the case of embankment breaches, three types can be distinguished: bed erosion, erosion caused by wave action and headcut erosion. This paragraph will explain each of the three types and why they are relevant for breaching events.

4.2.1 Bed erosion

Erosion of the bed takes place when a water flow passes on top of it and has enough velocity to mobilize and transport the sediment of the bed. Many equations have been introduced for this phenomenon, with one of the most famous ones being the Shields-formula. The idea behind this formula is that the bed must experience a certain threshold of shear stress depending on the sediment size for this sediment to be picked up by the flow. A related phenomenon is the fall velocity. If a flow containing sediments decelerates, sediment particles start to sink and eventually settle in the bed again. In the case of a dike breach, the sediment that is mobilized by the flow is transported out of the breach before the flow decelerates. This means the erosion takes places

within the dike and deposition of sediment occurs after the breach, all eroded material is washed out of the breach.

A distinction can be made between bed load and suspended load. Bed load relates to the transport of sediment along the bed, where the particles roll and hop over the bed but remain in direct contact with the bed. Suspended load refers to the situation where particles are picked up and brought higher into the water column by the flow, causing transport of particles without those particles being in contact with the bed anymore.

In the case of dike breaches, it was concluded in paragraph 3.4.2 that for sand dikes the transport is almost entirely of the suspended type.

4.2.2 Wave action

The presence of waves in shallow water can also cause erosion on the bed. This is because in shallow water the wave-induced velocity field reaches the bottom, the waves 'feel' the bottom. The orbital motion of the water causes friction and subsequent erosion of the bed.

In the case of a foreland, the water depth is generally considered shallow. This is because the water depth is small compared to the wavelength. The foreland lies around the mean high water level, so the water depth is very limited, even during a storm. The (ocean) waves will have a very large wavelength and thus the small wave theory holds true.

As mentioned in chapter 2, wave action is not considered in this study. The implications of this decision are discussed in the paragraph limitation of the model, 7.2.3.

4.2.3 Headcut erosion in a foreland

Forelands often contain fine (cohesive) sediment (Zedler, Bonin, Larkin, & Varty, 2008), this makes the erosion process very different from that of soil layers consisting solely of more coarse (non-cohesive) material. Soil layers with non-cohesive material subjected to lateral stress erode to a critical angle after which erosion over the entire layer takes place with a constant failure angle, similar to erosion of a sand dike, see Figure 14. This erosion can be modelled as a continuous or as a discrete process where a layer of soil fails in intervals, see also paragraph 3.3.1

In contrast, soil layers consisting of cohesive material do not exhibit a critical failure angle. Instead, they erode by a process called headcut erosion. This erosion is caused by undermining of the lower parts of the soil layer. As these lower parts are eroding, the higher parts of the soil layer become unstable and fail when the acting forces (weight and hydraulic forces) become larger than the resistive forces (soil interaction forces), see Figure 26. After this failure, the process starts anew with undermining of the lower layers of the foreland. The undermining and periodic failure is what gives a soil layer experiencing headcut erosion their distinct appearance of a sudden vertical drop with very steep failure planes (Figure 27).

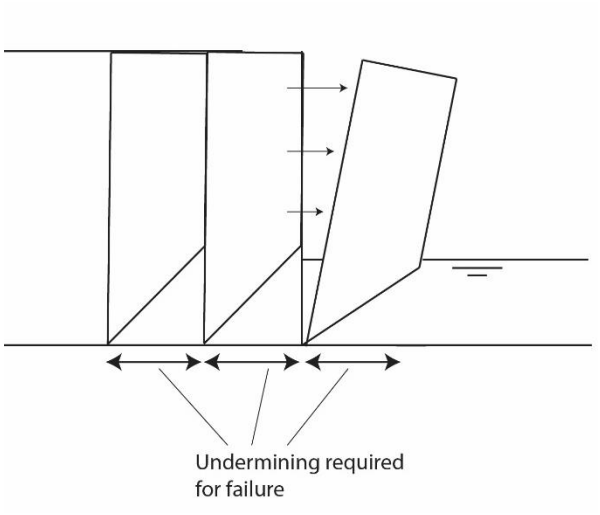

Figure 26: Periodic failure by headcut erosion, side view

Figure 27: Typical headcut erosion pattern
Note: still retrieved from: "Headcut" by A.Crim, 2015 (Video)

4.3 Headcut erosion modeling

The process of headcut erosion was explained in 4.2. However, there are multiple ways to model this erosion behavior. These methods can be classified in two categories. The first method is based on a balance of forces, the second is based on a balance of moments. In the two following subparagraphs both will be examined, in paragraph 4.4 the applicability and advantages will be discussed.

The failure type that occurs is dependent on the cohesion of the soil, which in turn is heavily dependent on the sediment type. For cohesive material, rotational failure is the assumed failure type, and for non-cohesive, the soil experiences sliding failure. From the field of sediment dynamics, we know that fine sediment such as clay behaves cohesively, whereas more coarse material is non-cohesive (van Prooijen, 2019). Combining the failure and the cohesivity of the sediment, it can be concluded that the choice of failure type depends on the size of the sediment. This paragraph is limited to a theoretical description of the failure types, the balance equations and the forces involved are discussed in chapter 5.

4.3.1 Headcut erosion based on balance of forces

The first possible failure type is based on a balance of forces. A foreland experiences headcut erosion when its vertical edge becomes exposed. This erosion occurs when the adjacent embankment has been breached to its foundation. As water continuous to flow over the foreland, it plunges down at the landward edge of the foreland. The resulting jet impacts the bed, and the kinetic energy diverges into two different directions, upstream and downstream. The upstream direction is relevant for the erosion process. As the highly turbulent flow is forced upstream, it impacts the lower layers of the foreland, causing undermining.

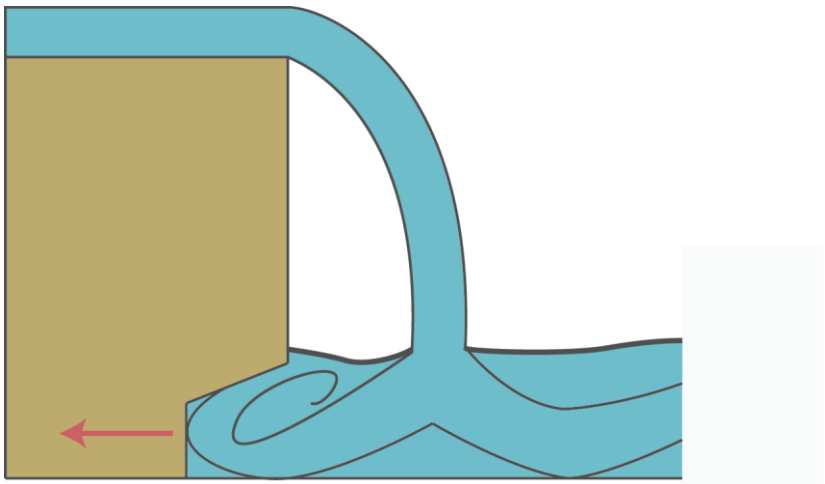

Figure 28: Jet flow causes undermining in lower layers of foreland, side view

While the process of undermining is continuous, the overhanging soil block slowly becomes unstable but does not experience continuous failure. The headcut erosion process based on a balance of forces assumes that failure occurs as a sliding phenomenon. Robinson and Hanson introduced a model to predict the amount of undercut in the lower layers of the foreland and subsequent headcut erosion (Robinson & Hanson, 1994). To simplify this complex process, some assumptions are required which Robinson and Hanson documented. These assumptions are listed below, as well as their implications for the model.

1. *"The headcut height is at its maximum and will migrate upstream at that height."*
   This assumption has two different implications. Firstly, the headcut height being at a maximum means that the embankment height is reduced to a non-erodible layer. This causes the undermining to occur at a constant level in the foreland (Figure 29). When the embankment is still descending in height, the undermining will occur at different levels, causing the location of the undermining to move downwards, restarting the undermining process at a different location (Figure 30).
   The second implication of this assumption is that as the foreland solely migrates stream upwards (seawards in the case of a foreland), the headcut height, plunge weight and soil block dimensions stay the same as long as the foreland is uniform, and the backwater height is constant. This means that these parameters can be modelled as constants, greatly reducing the complexity of the headcut erosion.

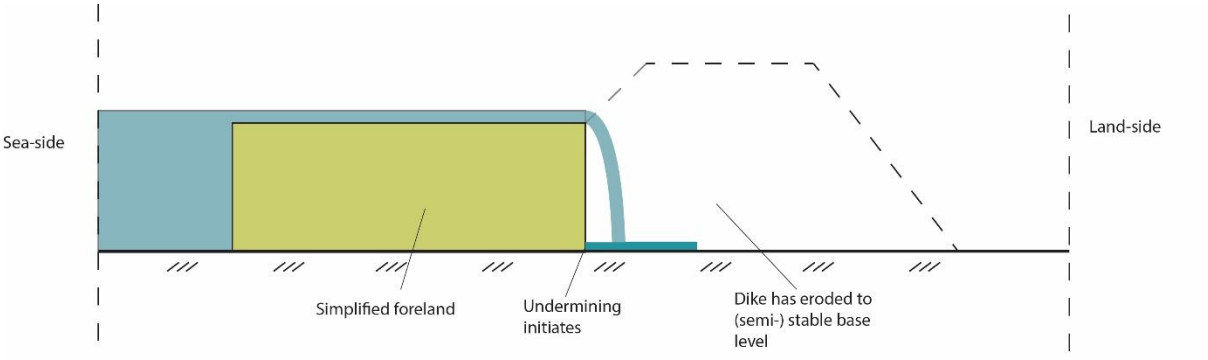

Figure 29: Breach has reached stable base of the embankment, undermining occurs at constant location, side view

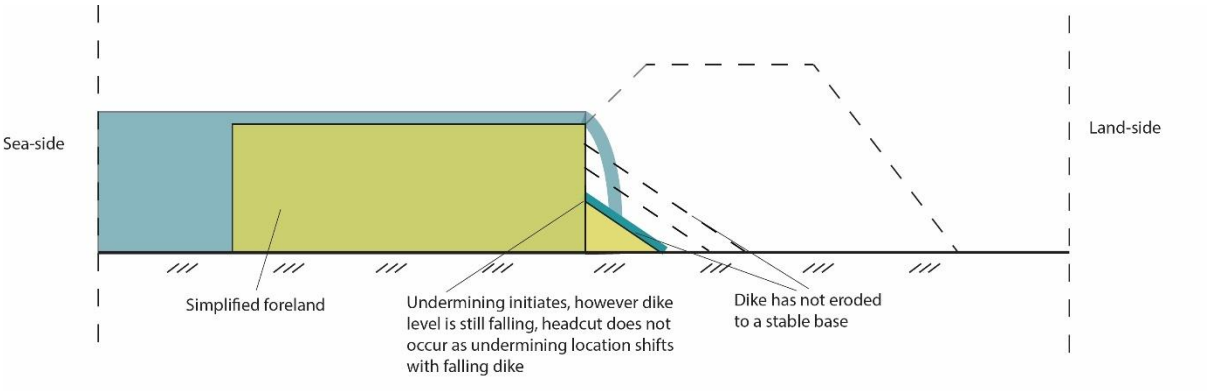

Figure 30: Breach has not yet reached stable base of the embankment, side view

2. *"The material deposited downstream of the headcut does not interfere with the migration process."*
   In the model of Robinson and Hanson the undermining is modelled as a constant continuous process and the subsequent headcut failure is a periodic process with constant intervals and soil block dimensions. In reality this is a much more irregular process. Soil properties can vary within layers, flow patterns can vary locally and many more processes can cause irregularities. However, in their approach the soil properties and flow patterns are modelled as being constant. In addition to this, failing soil blocks could cause buildup in front of the foreland, changing the erosion behavior. By assuming that this deposited material is washed away instantaneously, this buildup does not form, and in combination with the other assumptions the erosion behavior can be modelled as being constant. This assumption will be verified by an experiment of which the setup and results are presented in chapter 6.
3. *"The unconfined compressive strength may be used to represent the headcut stability."*
   This assumption implies that the headcut erosion is only caused by forces in a 2D-plane. These directions are the elevation and the direction of the flow, the Z-axis and the X-axis, respectively. In reality, there is a third direction that is relevant for headcut modelling, the Y-axes normal to the XZ-plane. This is the axis along which the breach grows in width.
   As the side of the foreland locally becomes exposed, a block in the soil becomes unstable (see also the start of this paragraph). This instability is due to several different acting and resisting forces. Due to the weight of the foreland, a compressive force is exerted on the block. This force acting on the soil block occurs in the Y-direction, applying pressure on

the soil block, causing it to become more stable. An analogy can be made to three slabs of concrete. If two of the slabs are forced against the sides of the third, this third slab will be held into place by the pressure forces of the other two, see Figure 31.

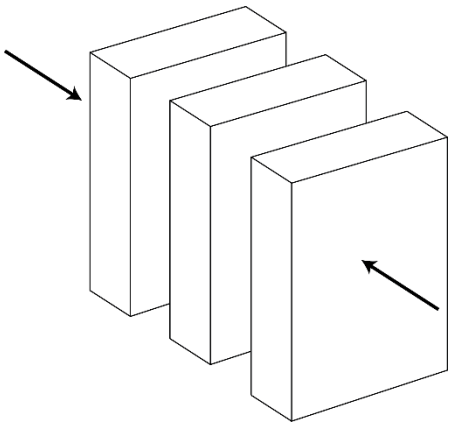

Figure 31: Two concrete blocks forcing a third block in place

This pressing behavior in the context of foreland erosion is shown in Figure 32. Fortunately, these ignored forces are resistive. In reality, the foreland is stronger than how the model predicts it to be, therefore making this a conservative assumption.

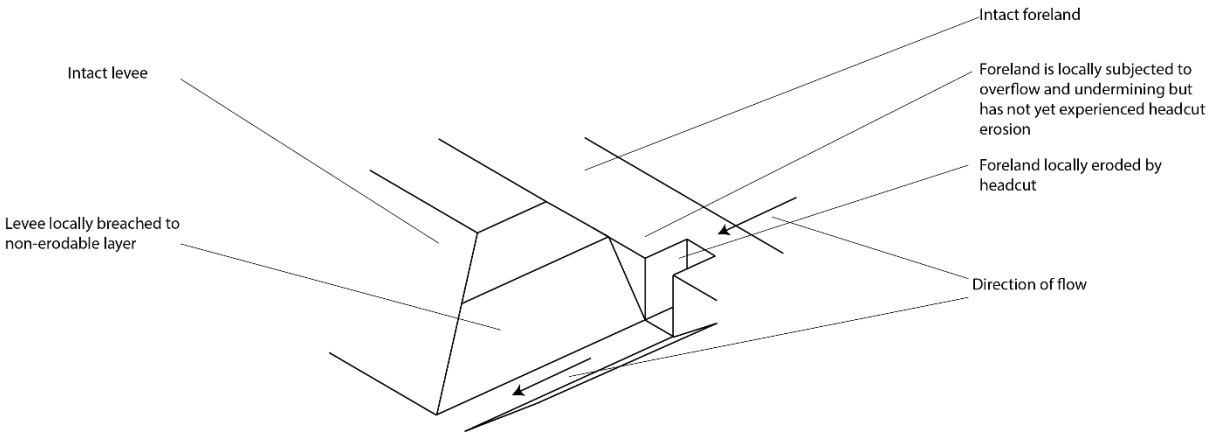

Figure 32: Foreland erosion assumption in 3D.

Using the listed assumptions, we end up with a model based on a balance of forces in a 2D-plane with constant undermining and periodical soil failure and a constant failure block size. Robinson and Hanson (1994), use a balance equation that uses the angle of the slip failure surface plane, which is based on the angle of internal friction of the soil, see Figure 33. The angle of the slip failure surface plane τ, represents the angle between the slip surface, L, and the bed level of the breach. The maximum value of this angle is defined by 45° plus half of the internal friction angle of the soil ϕ:

$$Angle\ of\ the\ slip\ failure\ surface\ plane: \theta(°) = 45 + \frac{\phi}{2}$$

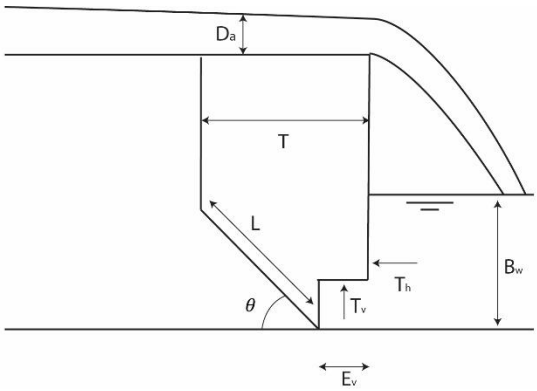

Figure 33: Forces on the soil block, side view

From the above figure it can be seen that the predefined soil block is subject to undermining caused by the hydraulic forces that result from the jet impacting the bed. As the block continues to be undermined, the angle of the slip failure surface plane grows larger, ultimately reaching the maximum value, causing the soil block to become unstable and fail.

After failure of this soil block, the entire process starts anew, with undermining of the newly exposed foreland layer. This newly exposed layer will have experience the same forces, undermining rate and the soil block will have the same dimensions. This is due to the previously discussed assumptions in combination with using a constant discharge, flow velocity and a uniform soil.

In Robinson and Hanson's model, the hydraulic conditions are set as a constant. In 2001 (Hanson, Robinson, & Cook, 2001) the authors also performed over 30 large scale flume experiments to verify the model. In all these experiments different values for flow rate and velocity were used between the separate tests but every test used a constant value for these parameters.

When modelling a breach, these parameters are not constant. Flow velocity, discharge and water depth can all vary during the breaching event. Fortunately, the headcut erosion model does allow for non-constant hydraulic conditions. This will change the value of some of forces on the soil block and impact the balance of forces. However, the underlying balance formula still holds, allowing this model to be used in our foreland erosion computations.

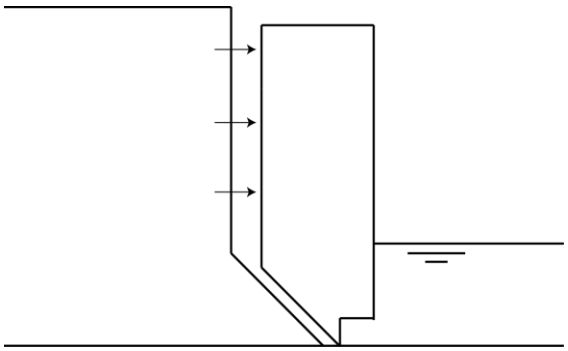

Figure 34: Sliding failure of foreland, side view

4.3.2 Headcut erosion based on balance of moments

The second possible failure type is based on a balance of moments. The erosion process is the similar to the failure type based on forces, the foreland experiences headcut erosion on the exposed edge. The flow on top of the foreland causes a downstream jet impacting the backwater. If the jet is strong enough to penetrate to the bottom of the backwater, the impact on the bed causes diversion of the jet flow. This creates a turbulent vortex upstream of the impact, causing undermining of the soil block, see Figure 28. For a more detailed explanation refer to section 4.3.1.

The key difference between the two approaches is the failure type experienced by the failing soil block. When examining the balance of forces, the underlying mechanism is a sliding failure. For the case of the balance of moments, the underlying mechanism is rotational failure.

Figure 35 shows rotational failure at the edge of a foreland. A clear difference in terms of the shape of undermining can be seen compared to the sliding failure from Figure 34. The difference is attributed to observed undermining behavior for different sediment types. For soil layers dominated by coarse sediment the erosion pattern of Figure 34 is observed, and for fine sediment dominated layers the erosion pattern of Figure 35 is observed (Hanson, Robinson, & Cook, 2001), (Zhu Y. , 2006).

The three key assumptions from paragraph 4.3.1 are applied for the case of rotational failure as well. The behavior of continuous undermining, leading to periodic failure described in paragraph 4.3.1 also applies for the rotational failure type.

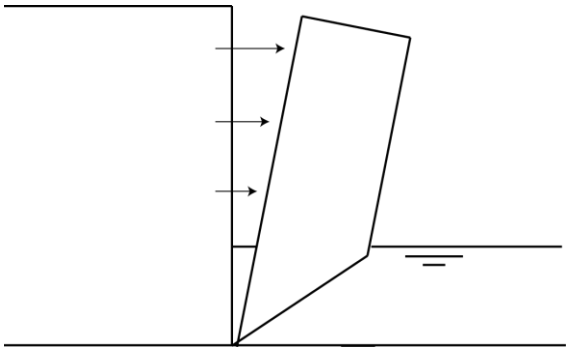

Figure 35: rotational failure of foreland, side view

4.4 Foundation type

A distinction can be made between two foundation types. The foundation is defined as the soil layer the jet from the foreland impacts during stage 4 and 5 of the breaching event. The two types considered are an erodible foundation and a non-erodible foundation. For the case of a non-erodible foundation, the impinging jet leads to turbulent motion in the backwater, which is directly responsible for the undermining of the foreland (Figure 36).

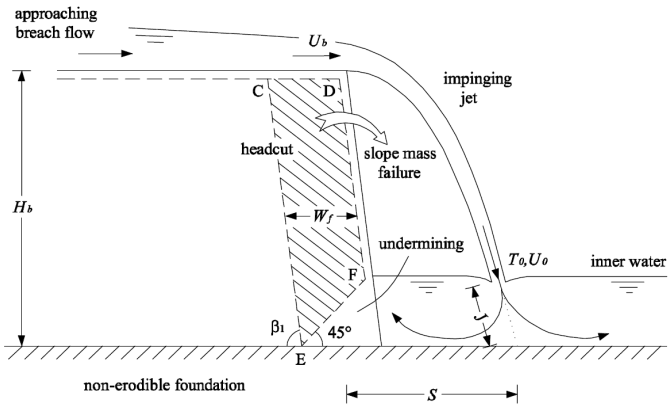

Figure 36: Undermining direct result of turbulent motions in backwater, side view
Note: reprinted from: "Breach-growth in clay dikes", Y.H. Zhu, 2006.

For the scenario of a non-erodible foundation the impinging jet causes a scour hole directly downstream of the foreland edge. As the scour hole becomes larger, it starts to undermine the foreland. The normative undermining type can be either the direct undermining caused by the turbulent motions or the growth of the scour hole, depending on the soil strength properties and the jet properties. After failure occurs for a soil block, the nappe moves with it and a new scour hole starts to form in the newly exposed foundation.

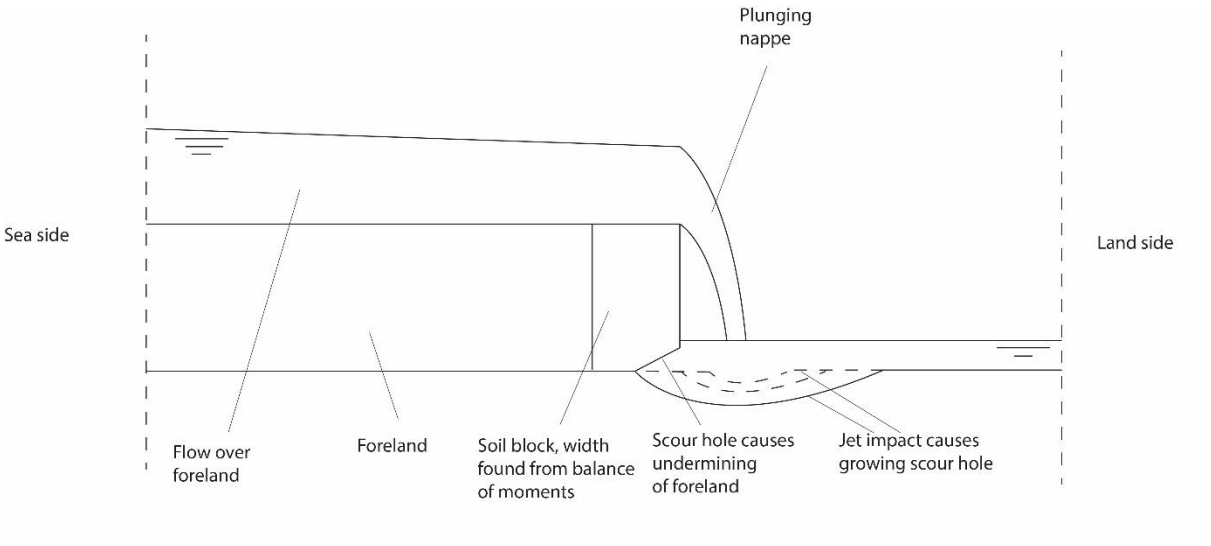

Figure 37:Undermining of foreland as a result of scour hole growth, side view

Chapter 5. Mathematical model

This chapter will introduce the mathematical model used to predict the headcut erosion experienced by a foreland during a breaching event in the adjacent embankment. This model will be created as a new functionality for the BRES model by Visser (1998). The interaction between the embankment and the foreland have been explained in chapter 4, and the BRES model has been discussed in chapter 3.

The chapter starts by introducing the functionalities of the model. In the second paragraph the mathematics behind the model are discussed. In the following paragraph, the interaction between the foreland functionality and the BRES model are examined. After this, the different possible scenarios, and the decision tree within the headcut model are presented.

5.1 Overview of foreland erosion model

The headcut functionality is a set a models added to the existing BRES-model, some changes were made to the original BRES-model as well to allow it to work with the new functions. It consists of multiple scripts that can calculate the amount of headcut erosion for different scenarios, as well as predicting the shape of the foreland spillway. These scenarios are split into two different groups with two different options within each group. The two groups are sliding failure and rotational failure of the foreland. Within these two failure types, a choice needs to be made whether the embankment is built on an erodible or a non-erodible foundation. This leads to a total of four different scenarios. The failure and foundation type is chosen by the user.

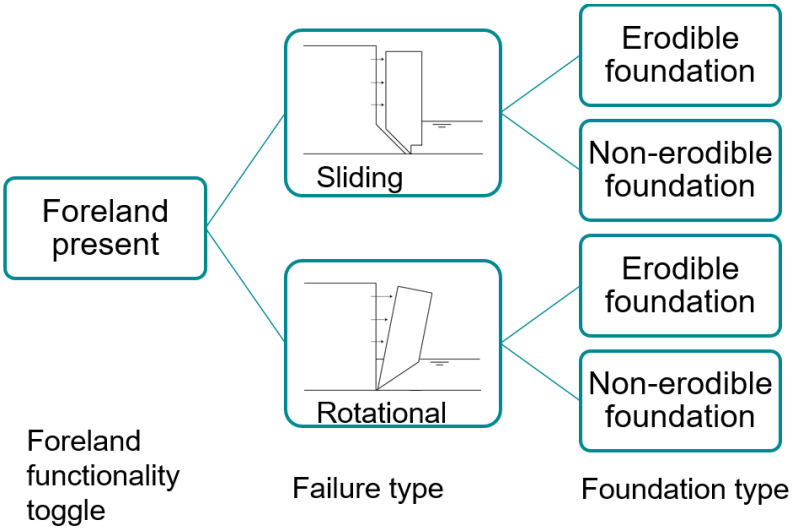

Figure 38: Decision flowchart foreland model

5.2 Modelling foreland erosion

This paragraph will discuss in detail the physical relations and mathematics used in the headcut erosion model. The interaction between this model and the BRES-model will be discussed in paragraph 5.3. A distinction will be made between the sliding failure and rotational failure. As discussed in chapter 4, these failure types use very different underlying approaches.

5.2.1 Sliding failure model, balance of forces

The theory behind the sliding failure model based on a balance of forces has been discussed in 4.3.1. In this paragraph the mathematics behind this model will be presented.

Headcut erosion by failure blocks

The erosion that takes place on a foreland during a breaching process is headcut erosion (see again 4.3.1). In the lower layer of the foreland gradual undermining takes place, which causes periodical failure with a constant failure block size and time between failures. Important hydraulic parameters for this type of erosion are flow velocity u, water depth on the foreland $D_a$and tailwater depth B_w, see also Appendix C.

The basis for headcut erosion lies in a balance of forces. When the summation of the combined acting forces surpasses the value of the combined resistive forces, the soil block will fail. Hanson et al describe this process of headcut erosion and present an equation for the balance of forces (Hanson, Robinson, & Cook, 2001). The equation is as follows:

$$\left(W_s + W_w - T_v - C_s L sin(\theta)\right)\tan(\theta - \phi) - T_h - C_s L cos(\theta) = 0$$

Where W_S is the weight of the soil block, W_w the weight of water on top of the foreland, T_v and T_h are the vertical and horizontal force components from the backwater, C_s the soil cohesion parameter, L the length of the surface failure plane and finally θ and ϕ are the angle of the failure surface plane and the angle of internal friction, respectively.

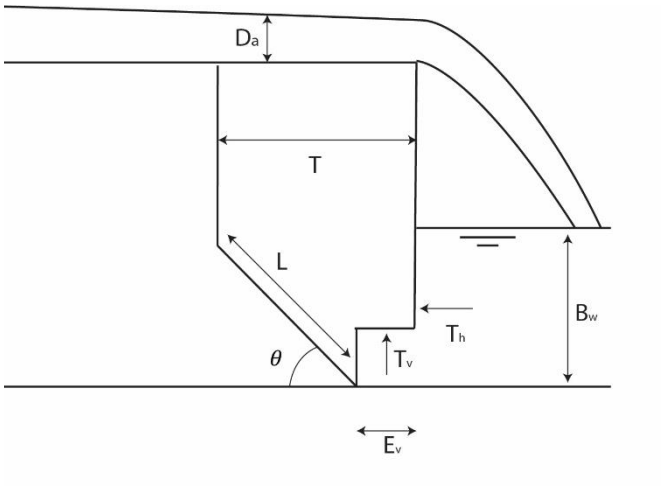

Figure 39: headcut erosion for sliding failure, side view

To be able to calculate the value of these forces we need to know the erosion on the vertical face, as $W_S, T_v$and L are all dependent on this parameter. Additionally, the erosion on the vertical face is a distance parameter and can be found by dividing the (erosion) rate of undermining by the time the undermining acts on the foreland, or

$$E_v = \frac{\varepsilon}{\Delta t}$$

The erosion rate of undermining, ε, is given by the following formula:

$$\varepsilon = k_d(\tau_e - \tau_c)^a$$

Where $k_d$is the erodibility coefficient, $\tau_e$and τ_c are the effective and critical shear stresses and a is a factor assumed to be 1 (Hanson et al, 2001).

A very important observation made by Robinson (1996) is that the effective shear stresses in headcut erosion processes are normally multiple orders of magnitude larger than the critical stress.

Combining this with the knowledge that $a = 1$, the erosion rate formula reduces to the product of the erodibility coefficient and the effective stress, or:

$$\varepsilon = k_d \tau_e$$

A key assumption in this model is that the width of the soil block, T (Figure 39) is equal to half the height of the foreland, or

$$T = \frac{H}{2}$$

The time between failure (t_f) can thus be easily calculated by dividing the width of the soil block by the undermining erosion rate, or:

$$t_f = \frac{T}{\varepsilon}$$

This, in combinations with the assumptions discussed in 4.3.1, means the total headcut erosion distance at time t can be calculated by a summation of all the failed soil blocks at time t. In the model by Hanson and Robinson (1994), it is assumed that after a soil block fails, the residual soil below the failure block's position does not influence the headcut erosion rate. After failure of a block, undermining of the next soi block immediately initiates. However, a case be made that for the first soil block, the amount of undermining required for failure is less than the subsequent blocks. This can be understood from Figure 40. It can be seen that after the first soil block failed, there is still a significant amount of soil on the foundation level that needs to be eroded in order for the foreland edge to be vertical again. Hanson and Robinson do not explicitly state the reason for this method, however, for this study, their approach is followed.

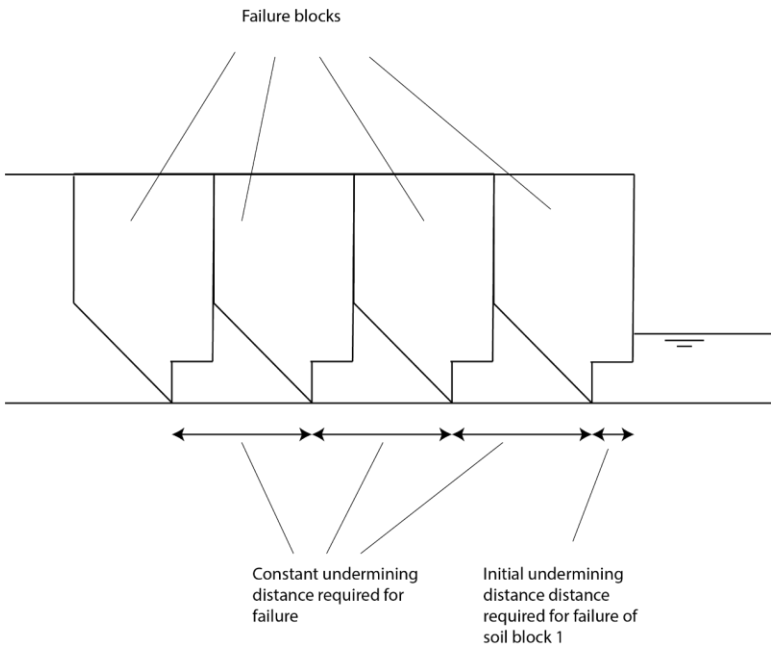

Figure 40: Undermining required for soil block failure, side view

Historical data has shown that foreland erosion can be very limited during breaches, with soil layers consisting of fine sediment and root systems experiencing almost zero erosion (Rijkswaterstaat, 1961). To find the erosion on the vertical face, E_v, at the time of failure, the balance of forces mentioned can be used:

$$\left(W_s + W_w - T_v - CLsin(\theta)\right) * \tan(\theta - \phi) - T_h - CLcos(\theta) = 0$$

Using the following parameters (Figure 39):

$$Weight\ of\ soil\ block, W_S = \gamma_s(T - E_v)\frac{2H - (T - E_v) * tan\theta}{2} + \gamma_s E_v H$$

$$Weight\ of\ water, W_w = \gamma_w D_a T$$

$$Vertical\ component\ of\ backwater\ force, T_v = \gamma_w B_w E_v$$

$$Horizontal\ component\ of\ backwater\ force, T_h = \frac{1}{2}\gamma_w B_w^2$$

$$Length\ of\ the\ soil\ surface\ failure\ plane, L = \frac{X - E_v}{cos\theta}$$

The erosion of the vertical face, E_v, can be found by using a quadratic function, as described by Hanson et al, (2001). Where:

$$E_v = \frac{-b \pm \sqrt{b^2 - 4ac}}{2a}$$

And:

$$a = \frac{\gamma_s}{2}$$

$$b = \gamma_w B_w - \frac{\gamma_s H}{2} - 2c_u$$

$$c = c_{uH} + \frac{\gamma_w}{2}B_w^2 - \frac{3}{8}\gamma_s H^2 - \frac{\gamma_w}{2}D_a H$$

Where γ_s and γ_w are the unit weights of the soil and water, H is the headcut height, D_a the approach flow depth on top of the foreland and lastly c_u represents the undrained shear strength.

Combining the required erosion of the vertical face for the soil block to fail, E_v, with the undermining erosion rate ε gives the time at which this block fails, see Figure 41.

$$time\ of\ failure\ soil\ block, t_f = \frac{E_v}{\varepsilon}$$

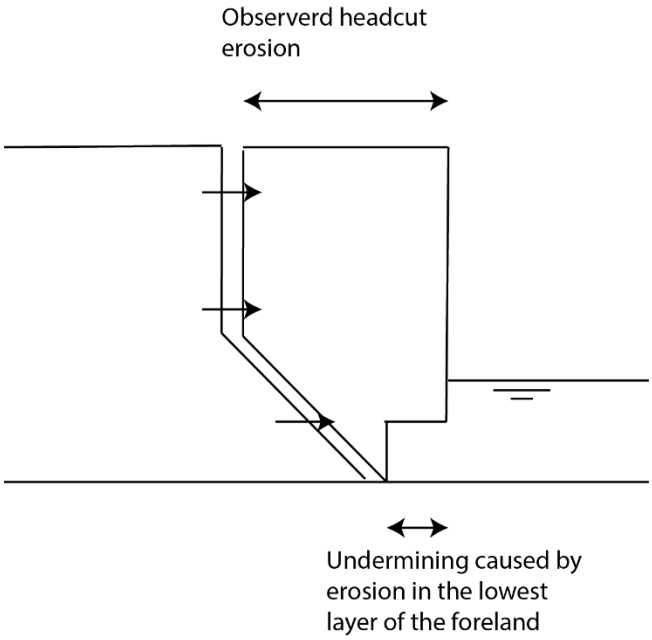

Figure 41: Observed erosion on top of the foreland versus erosion of the vertical face, side view

Undermining erosion rate

The final parameter required for the modelling of foreland erosion is the continuous erosion rate in the lowest layer of the foreland, ε. This erosion is caused by water falling from the foreland into the backwater, see also Figure 28 and Figure 29 in chapter 4. Robinson (1992) originally observed and documented the behavior of headcut erosion, as well as creating empirically derived equations to find the erosion rate. Zhu (2005 & 2006) used the same equations for his modelling of the breaching of dikes consisting of fine sediment. Both authors verified their methods with experimental data, unfortunately the documentation of these experiments is too limited to be of use for additional verification.

As mentioned earlier in this paragraph, the equation for erosion rate ε is given by:

$$\varepsilon = k_d \tau_e$$

The effective shear stress is heavily dependent on the foundation type. This can be broadly categorized into two different scenarios, the first being a non-erodible foundation type and the second being an erodible foundation type. This will be discussed in more detail in paragraph 5.2.3.

5.2.2 Rotational failure model, balance of moments

For the scenario where a foreland consists of fine sediment, cohesion plays a large role, and the sliding failure model is no longer valid. Instead, a rotational failure model is assumed. This model is based on a breach development model in clay dikes by Zhu (Zhu Y. , 2006).

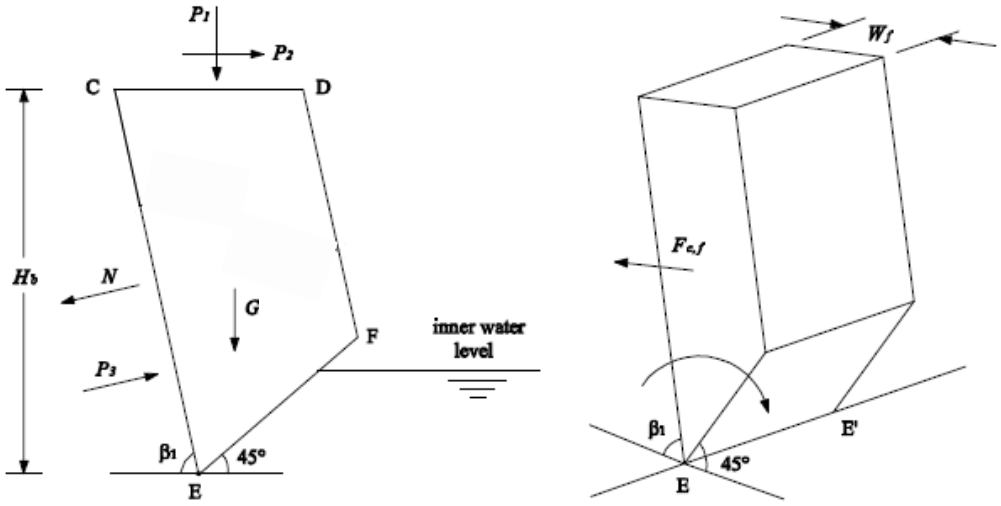

Figure 42: Forces on soil block, left: side view, right: 3D impression
Note: adapted from: "Breach-growth in clay dikes", Y.H. Zhu, 2006.

The essence of this failure type is that instead of undermining causing a slab of soil to slide down, the fine sediment causes the soil layer to behave cohesively and prevent sliding from occurring. As the undermining continuous, the soil block starts to become unstable. The moments caused by the cohesive force, combined with the other resisting forces can no longer withstand the moment caused by the gravitational force of the exposed soil block. The soil block tumbles over and falls into the backwater, exposing a new edge in the foreland and the headcut erosion process starts anew. It is important to note that more undermining is required for a cohesive soil to fail compared to a non-cohesive soil. The forces considered for the approach are presented below

Resistive forces

There are two significant resisting force, soil interactional forces $F_{c,f}$ and N. $F_{c,f}$ represents the soil interactional force acting on the two lateral surfaces of the block (see Figure 31) and N represents the soil interactional force between the failure block and the foreland, they are defined as follows:

$$F_{c,f} = A_{lat} \cdot \tau_s,$$

$$N = \frac{H}{sin\beta_1} \cdot b \cdot \tau_t$$

Where A_{lat} is the surface of the lateral side of the soil block, τ_s is the soil shear strength, H is the height of the foreland compared to the initial breach bottom, $\beta_1$is the critical inclination angle of the soil block, b is the width of the soil block and τ_t is the soil tensile strength. There are also two resistive forces caused by the backwater, one in the horizontal direction and one in the vertical, however these are not considered because they are small compared to the other forces acting on the soil block (Zhu Y. , 2006).

Acting forces

The acting forces leading to moments on the soil block are the gravitational force G, the forces caused weight and the shear caused by the flow on the foreland, P_1 and P_2, and the force from the pore pressure, P_3. They are defined as follows:

$$G = \rho g A_{lat} b$$

$$P_1 = \rho g d_b W_f b$$

$$P_2 = \tau_b W_f b$$

$$P_3 = \frac{1}{2} \rho g b l$$

Where, g is the gravitational constant, $d_b$is the water depth on the foreland, W_f is the width of the soil block, and l is length CE in Figure 42.

Width of the soil block

The approach for modelling the two scenarios is also slightly different. For the non-cohesive cases the width of the block is assumed to be half the height of the foreland, this approximation was found empirically (Robinson & Hanson, 1994). For the cohesive case, the width of the soil block is calculated directly from the balance of moments (Zhu Y. , 2006). These different approaches can be justified when the amount of erosion occurring in the foreland is considered for the two cases. From soil mechanics we know that erosion of cohesive soil is much slower (van Prooijen, 2019) and, as discussed prior, more undermining is required for a soil block to fail as well. Therefore, the expected amount of soil blocks that will fail is larger for the case of non-cohesive soil. An empirically found approximation for the width of the soil block is therefore justified, as the amount of erosion in the foreland is less dependent on an individual block if there are multiple failures.

For the cohesive case, much less erosion is expected, and far fewer soil blocks are expected to fail during a breaching event. In order to accurately predict the erosion pattern, it is therefore necessary to calculate the width of the block from the balance of moments instead of using an approximation. This is because if there are few failures in the foreland during a breach event, the width of the individual blocks becomes the dominating factor in the amount of erosion.

Balance of moments

The width of the soil block can be found using a balance of moments:

$$f(W_f) = P_1 d_{P1} + P_2 d_{P2} + P_3 d_{P3} - 2F_{c,f} d_{c,f} + G d_G - N d_N = 0$$

Where $d_{P1}, d_{P2}, d_{P3}, d_{c,f}, d_N$ and d_G are the forece arms of the three hydraulic forces, the two soil interaction forces, and the gravitational force. Combining this equation with erosion rate ε from paragraph 5.2.1, the time required for a soil block to fail can be found. Using this information and the breach width obtained with BRES, the width of the failure block can be found and the erosion pattern of the foreland is fully known. This will be discussed in paragraph 5.3.

5.2.3 Foundation type

To find the effective shear stress a choice must be made whether the bed downstream of the foreland is erodible or non-erodible, as these cause different erosion behavior and thus require different approaches.

Non-erodible foundation

The scenario of a non-erodible foundation is examined first, presented in Figure 43.

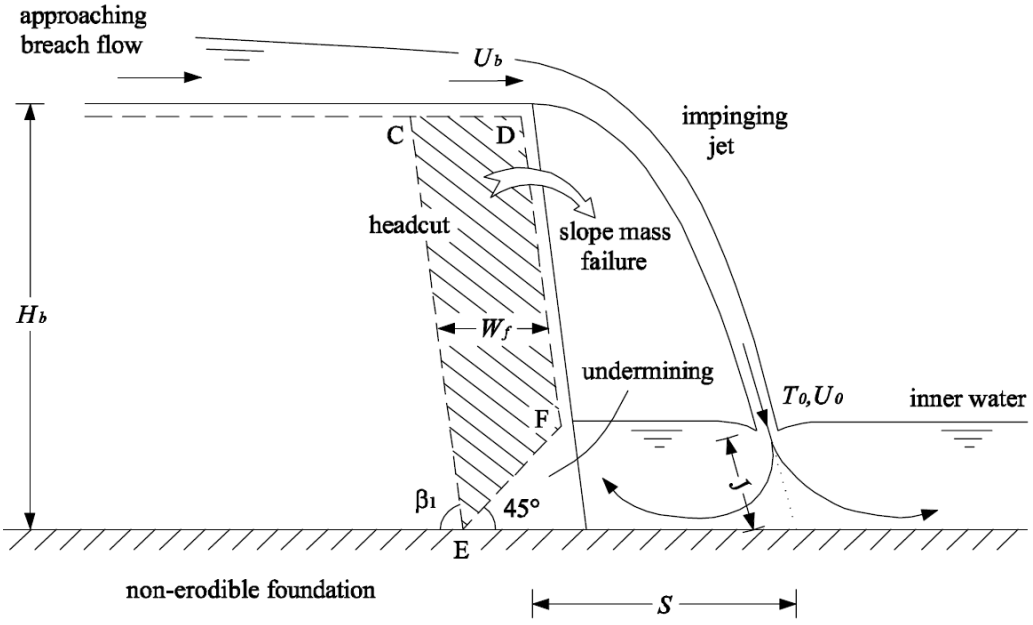

Figure 43: Undermining of foreland with a non-erodible downstream bed, side view
Note: reprinted from: "Breach-growth in clay dikes", Y.H. Zhu, 2006.

In chapter 4 undermining of the foreland was discussed. The jet falling from the foreland impacts the foundation and diverges, causing a vortex in the backwater just in front the foreland. This vortex causes a shear stress on the lower layer of the foreland and undermining starts to occur, see Figure 28. To find the effective shear stress a non-dimensional equation is introduced. This equation contains different hydraulic parameters and their influences on the shear stress, and is defined as follows below (please note π_n represent non-dimensional parameters and is not equal to 3.14):

$$\pi_1 = 0.025\pi_2^{-1.295}\pi_3^{0.026}\pi_4^{0.221}\pi_5^{-1.062}$$

Where:

$$\pi_1 = \frac{\tau_e}{\rho g D_a}$$

$$\pi_2 = \frac{q^2}{g D_a^3}$$

$$\pi_3 = \frac{H}{D_a}$$

$$\pi_4 = \frac{B_w}{D_a}$$

$$\pi_5 = \frac{X_p}{D_a}$$

In which ρ is the density of the water, q is the discharge per unit width and $X_p$is the location of maximum horizontal stagnation pressure. This is the location where the horizontal pressure in the backwater is the highest and is closely related to the distance between the top of the foreland and the location of impact by the jet onto the bed, S, see Figure 44.

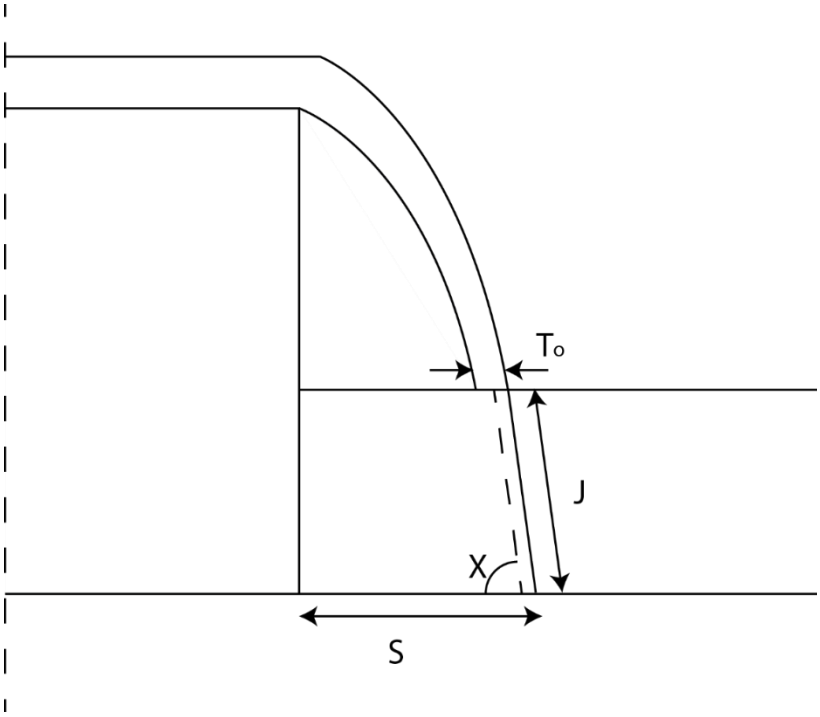

Figure 44: location of jet impact on bed, side view

The equation for the location of maximum horizontal stagnation pressure, X_p, is as follows:

$$X_p = S - 0.154\, J cot(\chi) - \frac{T_0}{2}$$

Where S, distance between the top of the foreland and the location of impact by the jet onto the bed, is reduced by half of the nappe width and by a value that is based on impact angle χ and the impact distance through the backwater, J. The reduction by half of the nappe width is to account for the fact that the impact point of the jet lies on the centerline of the jet instead of the edge of the jet, as can be seen in Figure 44. The other reduction is described by Beltaos (1976) as eccentricity, which can be physically interpreted as "the small distance upstream of the predicted tangential impact with the bed required for streamlines to impact normal to the floor".

What the non-dimensional equation for shear stress does is use empirically derived equations to relate the hydraulic parameters along with headcut height H, to the acting effective shear stress on the foreland. The location of maximum horizontal pressure X_p, impact angle χ, nappe width T_o and the impact distance through the backwater J are the means to convert the hydraulic properties to the effective stress on the foreland, τ_e.

Using the effective shear stress, together with the erodibility coefficient and balance of forces, the entire foreland erosion process can now be modelled for the scenario of a non-erodible foreland.

Erodible foundation

For the case of an erodible foundation, a different approach is required. Instead of using the turbulent motions caused by the impinging jet directly as the driver of undermining, for the erodible foundation case the undermining is caused by the formation of a scour hole. The impinging jet creates a scour hole directly downstream of the foreland edge, which leads to instability of the foreland (Figure 45).

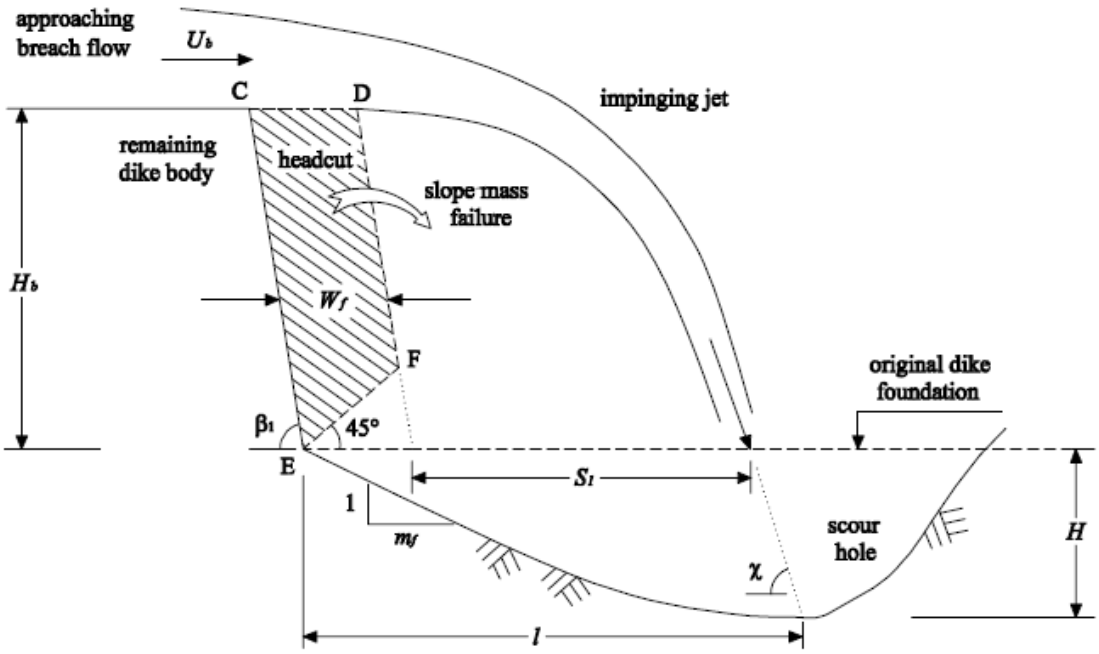

Figure 5.10 Sketch definition of scour hole dimensions.

Figure 45: Undermining of foreland with an erodible downstream bed, side view
Note: reprinted from: "Breach-growth in clay dikes", Y.H. Zhu, 2006.

A key parameter in modelling headcut erosion with erodible foundation is m, which is defined as $\frac{l}{H}$. Where length l is the distance between the scour hole bottom and the foreland edge at the original foundation, scour hole depth H_{sc} is the elevation difference between the scour hole bottom and the original dike foundation. With this ratio the undermining rate can be found from the vertical erosion rate in the scour hole. This parameter is dependent on the soil and hydraulic properties. Presently there are no equations available to predict the value of this parameter. In Bennet's experiments (2000) values between 0.9 and 2.6 were obtained (see Appendix E). Zhu suggests a value between 2.0 and 4.0 (2006).

To calculate the vertical erosion rate, two different regions in the foundation must be considered, related to the flow velocity of the jet in the plunge pool. When the jet enters the plunge pool it diffuses. To account for this length the potential core length, J_p, is introduced, defined as the distance over which the flow velocity in the in the jet is equal to the velocity of the plunge pool entrance velocity, U_0 (Figure 46). The first region is the horizontal area of the plunge pool where the potential core is still present. The second region is horizontal area where the depth of scour

hole becomes large enough for the jet to no longer have a flow velocity in the centerline equal to the entrance velocity.

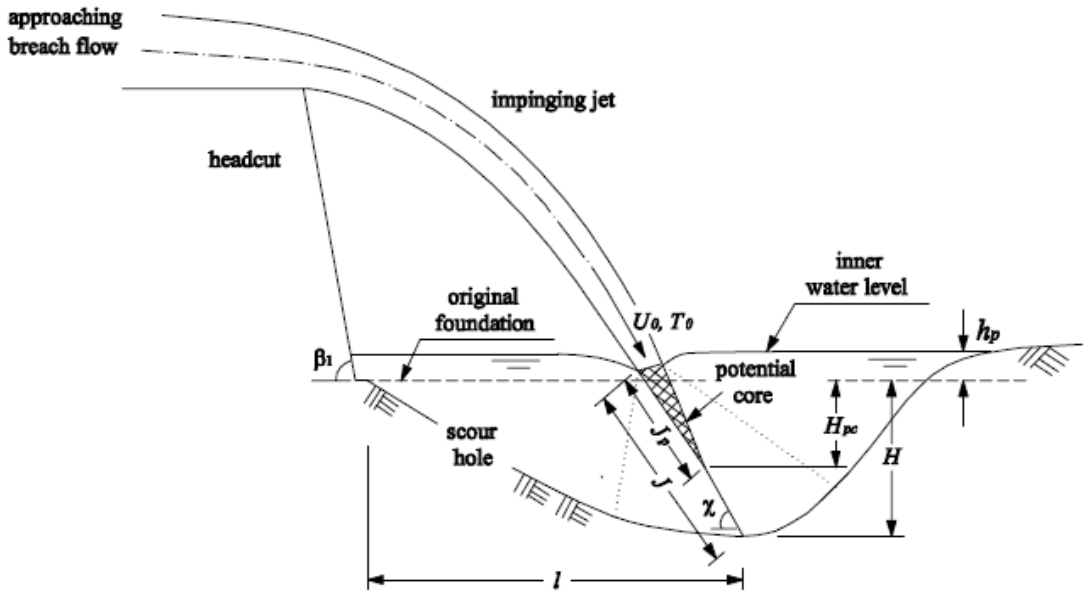

Figure 46: Potential core length in plunge pool for erodible foundation, side view
From "Breach-growth in clay dikes", Y.H. Zhu, 2006.

This leads to a criterion for the vertical erosion equation based on the depth of the scour hole, leading to two different equations. The first equation is used to calculate the erosion rate at depths where the potential core of the jet still reaches the scour hole bottom. For the second equation, the potential core no longer reaches the scour bottom. The equations are as follows (Zhu Y. , 2006):

$$E = \frac{dH}{dt} = M_{ef}\left(C_f \rho U_0^2 - \tau_c\right)^{\xi} \text{ for } H_e \leq H_{pc},$$

$$E = \frac{dH}{dt} = M_{ef}\left[\frac{C_f \rho U_0^2 (H_{pc}+H_{bw})}{H+H_{bw}} - \tau_c\right]^{\xi} \text{ for } H_e > H_{pc}$$

Where:

$$H_{pc} = C_d^2 T_0 sin\chi - H_{bw}$$

And:

$$Cf = \left(\frac{0.22}{8}\right)\left(\frac{q}{v}\right)^{-0.25} = \left(\frac{0.22}{8}\right) Re^{-0.25}$$

H_e is the depth of the scour hole below the original foundation level, H_{pc} is the depth of the potential core and C_f friction coefficient in which q is unit discharge, v the kinematic viscosity and Re the Reynold's number. E is the vertical erosion rate, M_{ef} a material dependent factor related to the erodibility of the foundation, U_0 the entrance flow velocity of the jet in the plunge pool, ξ is a constant for soil erosion (1.5 for non-cohesive and 1.0 for cohesive) and H_{bw} is the water depth in the backwater. Finally, C_d is a diffusion constant and assumed 2.60 by Zhu (2006) and χ is the angle between the horizontal and the potential core centerline.

M_{ef} is an important parameter that depends on the soil properties. It can be obtained through calibration from a set of experiments or be found from soil tests in a laboratory. The value of this factor can vary by one order of magnitude. Since the erosion rate can be seen to be linearly related, the expected erosion rate can also vary by one order of magnitude depending on the value chosen for M_{ef}.

5.3 Interaction foreland functionality and BRES model

The foreland functionality consists of four separate models that are implemented in the BRES model. In order to make the foreland models be able to communicate with the foreland model, the original foreland required some changes and additions. These are presented in this paragraph.

5.3.1 Calculating the discharge parameter for an elevated foreland

One of the most principal parameters within breach development models is the amount of discharge through the breach (Visser, 1998). The shape and length of the spillway over the foreland directly influence this discharge over the foreland and are thus very important parameters in the model.

Chapter 2 discussed the opposing effects an elevated foreland has on the flow rate through a breach. On the one hand the reduced flow rate due to a decrease in water depth, on the other an increased flow rate due to an increase in spillway length.

Even for the case of a relatively low foreland and erodible foreland the discharge reducing effect is still likely to dominate. This can be understood by a modified discharge equation from chapter 3. The original equation is presented below for convenience:

$$Q_{br} = m \left(\frac{2}{3}\right)^{\frac{3}{2}} \sqrt{g} B (H_w - Z_{br})^{\frac{3}{2}}$$

If an elevated foreland is present, the height of the spillway changes from being at the level of the breach bottom, Z_{br}, to the elevation of the foreland, Z_f, leading to the following equation.

$$Q_{br} = m \left(\frac{2}{3}\right)^{\frac{3}{2}} \sqrt{g} B \left(H_w - Z_f\right)^{\frac{3}{2}}$$

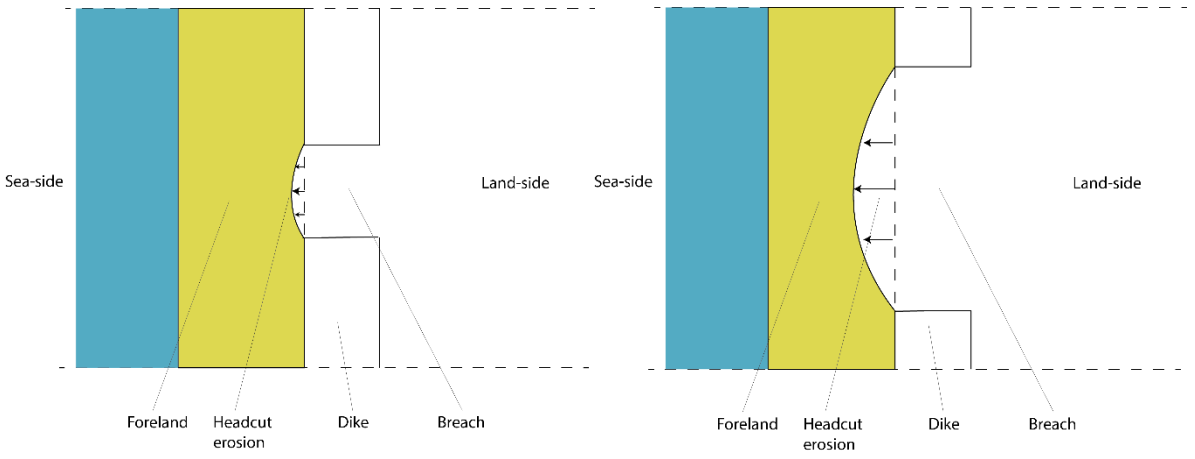

Figure 47: Foreland erosion follows lateral breach growth, left figure is at an earlier point of time, top view

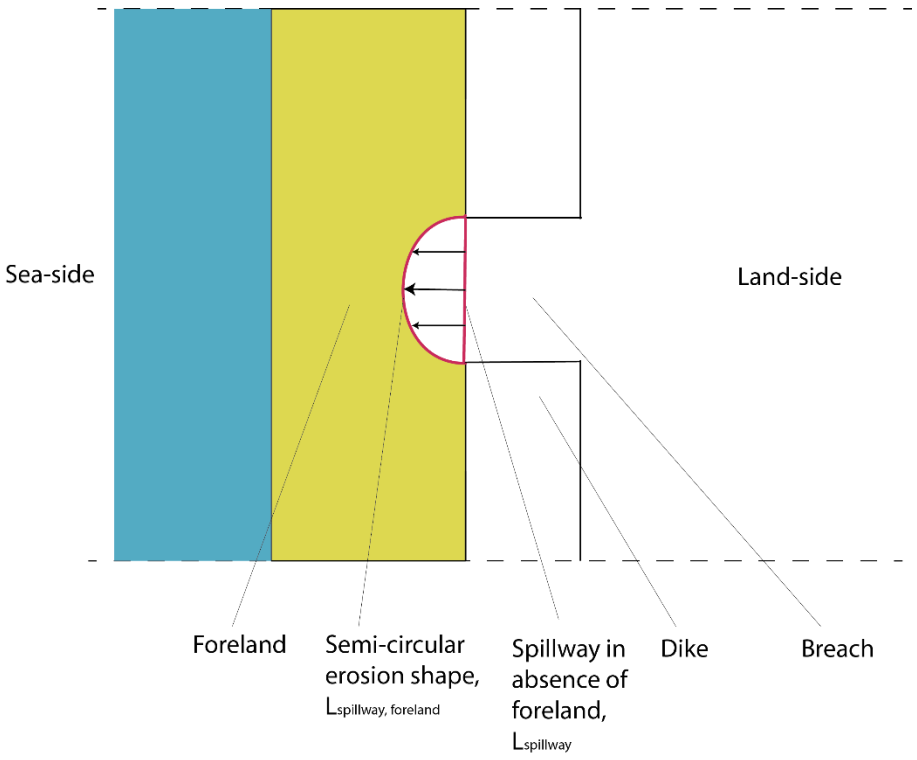

Figure 48: Semi-circular erosion shape in foreland, top view

In reality, a foreland is likely to erodes much slower than the adjacent embankment, causing the elliptical erosion shape in the foreland (Visser, 1998). Unfortunately, there is no straightforward method for calculating the circumference of an ellipse. The formula for the circumference of an ellipse is as follows:

$$p = 4a \int_0^{\frac{\pi}{2}} \sqrt{(1 - e^2 \sin^2 \theta)}\, d\theta$$

with:

$$eccentricity, e = \frac{\sqrt{a^2 - b^2}}{a}$$

Where a is the radius of the major axis of the ellipse and b the radius of the minor axis. In order to efficiently use the integral in the model, an approximation or a mathematical series is required. There are many different possibilities to calculate the circumference of an ellipse and for this research a restriction is made to five different methods. Three are approximations, and two infinite series. These can be found in Appendix C. The methods are chosen for their applicability for the model, with varying levels of accuracy and required computational power. In order to find the most appropriate method to calculate the length of the elliptical spillway and the discharge coefficient m, a short analysis is performed into the accuracy of the different methods. In this analysis a is again the radius of the major axis of the ellipse and b the radius of the minor axis. Furthermore, the radius of the major axis, a, is equal to one.

Method	a/b = 1	a/b=2	a/b=4	a/b=10	a/b=100	a/b=1000	Max Error (%)
Approximation 1	6.2831	4.9672	4.5796	4.4650	4.4431	4.4428	11
Approximation 2	6.2831	4.8442	4.2887	4.0605	3.9874	3.9837	0.5
Approximation 3	6.2831	4.8442	4.2892	4.0639	4.0001	3.9985	0.04
Series 1 (100 terms)	6.2831	4.8442	4.2892	4.0655	4.0107	4.0101	0.25
Series 2 (7 terms)	6.2831	4.8442	4.2892	4.0638	3.9990	3.9969	0.08
"Perfect" value (Series 2 with 1000 terms)	**6.2831**	**4.8442**	**4.2892**	**4.0640**	**4.0011**	**4.0000**	**-**

Table 2: Performance of methods for different values of a/b

From this analysis we can see that the greater the difference in radiuses, the greater the difference in outcome between the different methods. From comparison with a near perfect value of the ellipse circumference (calculated by using the second infinite series using 1000 terms), it can be seen that approximation one and two are too rough when $\frac{a}{b}$ becomes larger. From a computational power point of view, using approximation three is superior over using a series. Using a series to calculate the discharge coefficient takes roughly ten times longer than the approximation. As the discharge coefficient is repeatedly calculated during the running of BRES, using a series becomes the largest component in the model in terms of required computational power. Running the model a single time takes a very short time but doing Monte Carlo simulations for a sensitivity analysis or calibration of the model takes a long time. Since approximation three is both more accurate and takes less computational power than both methods involving a series, this formula will be used to calculate the discharge coefficient m in the foreland erosion model.

5.3.2 Modelling discharge over foreland and through breach

In the original BRES model, the water surface is continuous, and the water depth is constant across the breach. For the case of an elevated foreland this is not the case. As long as the water level in the polder is below the foreland level, the water surface is discontinuous over the edge of the foreland leading to a water jet falling from the foreland into the polder backwater. This leads to changes in flow rate and flow velocity during stage three, four and five of the breaching event, compared to the situation without an elevated foreland.

5.3.3.1 Flow rate and flow velocity during stage three

In the original BRES model, the flow rate and subsequent flow velocity are governed by the water depth on the embankment top, see Figure 49. For the case of an embankment with an elevated foreland, the limited factor during stage three becomes the water depth over the foreland (Figure 50). In the figure H_w is the outside water level, Z_w the height of the watercourse bottom above $Z = 0$ and Z_f the height of the foreland above $Z = 0$.

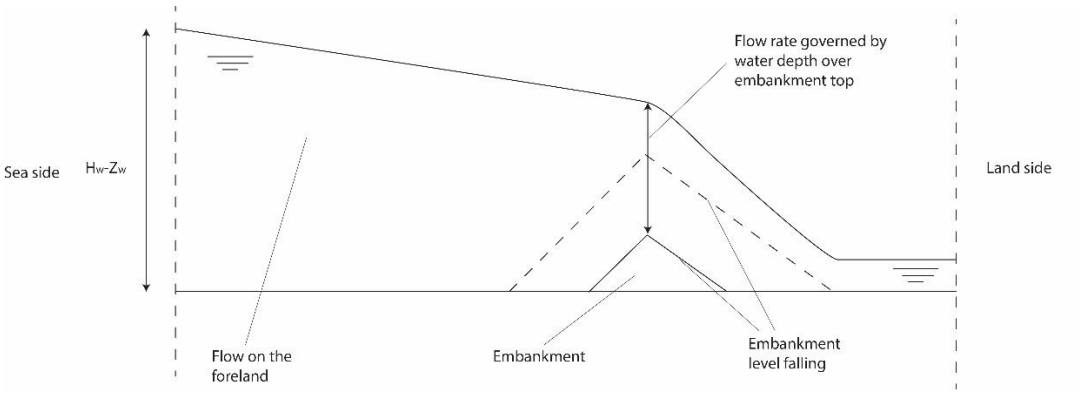

Figure 49: Flow rate during stage three in the original BRES model, side view

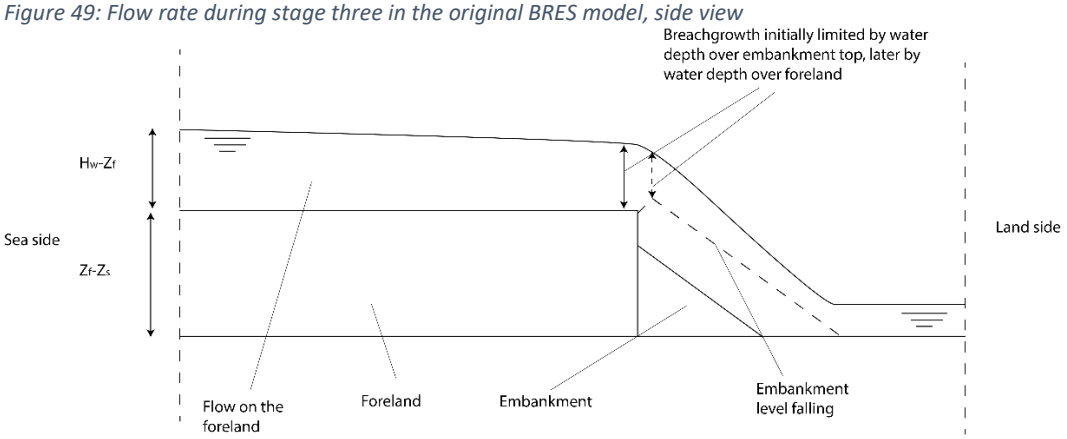

Figure 50: Flow rate during stage three in the adjusted BRES model, side view

5.3.3.2 Flow rate and flow velocity during stage four

Stage four of the original BRES initiates when the embankment locally has fully eroded to its foundation, the flow rate through the breach is critical and breach growth is limited to the lateral direction.

If an elevated foreland is present, this scenario changes. The embankment has been locally eroded to its foundation, however the foreland has not experienced any erosion. This causes a jet falling from the foreland into the backwater of the polder (Figure 51). The approach depth, the water depth immediately stream upwards of the nappe, is critical. The approach depth is equal to 0.7 times the water depth on the foreland a distance three times the approach depth upstream of the nappe, or:

$$d_f = d_c = 0.7(H_w - Z_f)$$

Where d_f is the approach depth on the foreland and d_c is the critical depth. Using the fac that the discharge over the foreland is equal to the discharge in the breach, the flow velocity in the breach can be found. This flow velocity calculated by using the discharge, combined with the width of the breach and the water depth. In this equation the water depth in the breach is assumed equal to the water level in the polder, giving:

$$U_{br} = \frac{Q_{br}}{B(H_p - Z_p)} = \frac{Q_f}{B(H_p - Z_p)}$$

Where U_{br} and Q_{br} are the flow velocity and discharge through the breach, $H_p - Z_p$ is the water depth in the breach and Q_f is the discharge over the foreland. U_{br} is subsequently used to calculate the erosion on the embankment in lateral direction.

The flow state of the water in the breach depends on the relative depth compared to the approach depth. If the water depth in the breach is lower than the approach depth, the flow is super-critical, for an equal depth the flow is critical, and for a depth larger than the approach depth the flow in the breach is sub-critical. As discharge into the polder continuous, the water level in the breach continuous to rise, eventually become larger than the critical depth. That moment marks the end of stage four and the initiation of stage five.

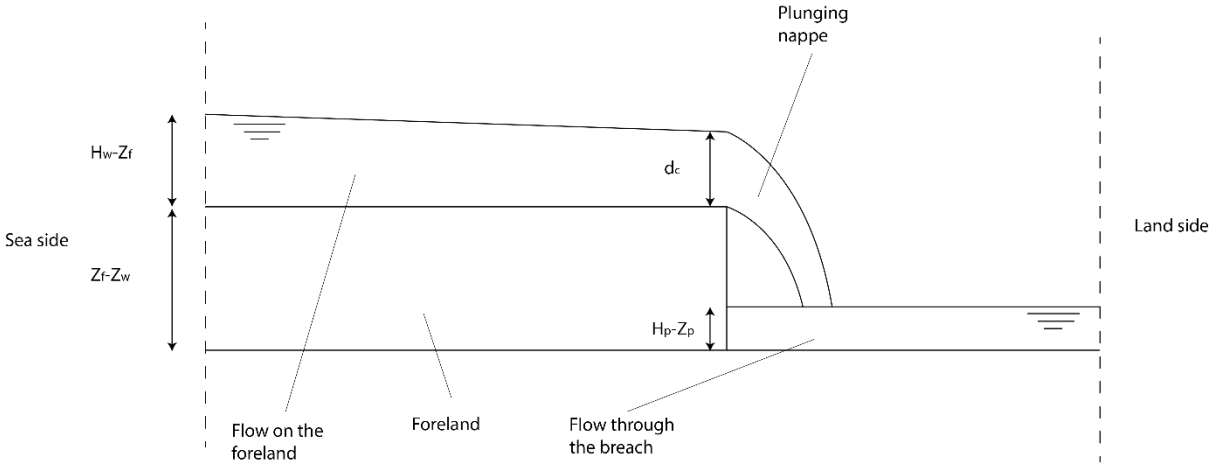

Figure 51: Plunging nappe from foreland into backwater of the polder, side view

5.3.3.3 Flow rate and flow velocity during stage five

The initiation moment of stage five is when the water depth in the breach becomes larger than the critical depth, causing the flow rate to become sub-critical. In the original BRES model this accompanied by a change in the velocity equation. In the adjusted BRES model however, stage five is split into three different parts, determined by the water level in the breach.

The first case is when the water depth in the breach is higher than the critical depth, but low enough for the jet from the foreland to cause headcut erosion, see Figure 52. The subsequent flowrate over the foreland is critical and the flow rate over the breach is subcritical. Using the same approach as for stage four, the discharge through the breach can be found using the critical flow state at the edge of the foreland:

$$U_{br} = \frac{Q_f}{B(H_p - Z_p)}$$

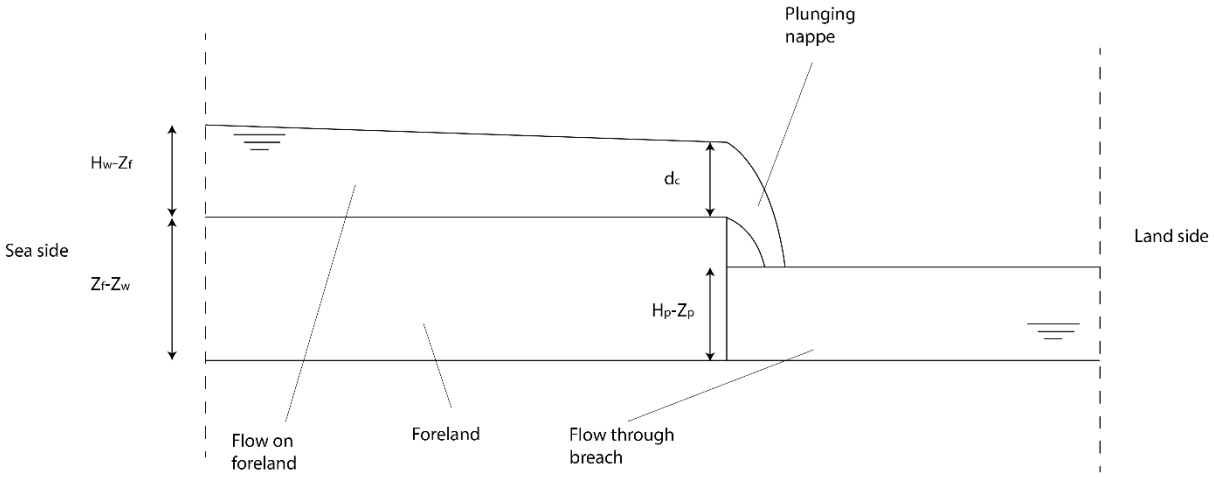

Figure 52: Side view, critical flow on foreland, sub-critical flow overbreach, plunging nappe causes headcut erosion

The second case is when the water level in the breach is too high for headcut erosion occur, but below the water level on the edge of the foreland, see Figure 53. The jet from the foreland into the backwater of the polder is now too short compared to the water level in the breach to impact the bottom and cause headcut erosion. This is the case when the water depth in the breach becomes larger than 0.9 times the foreland height and there is no longer a plunging nappe profile.

$$H_p - Z_p > 0.9(Z_f - Zp)$$

At that moment, headcut erosion in the foreland stops. As the breach continuous to grow laterally, the discharge coefficient m only becomes smaller.

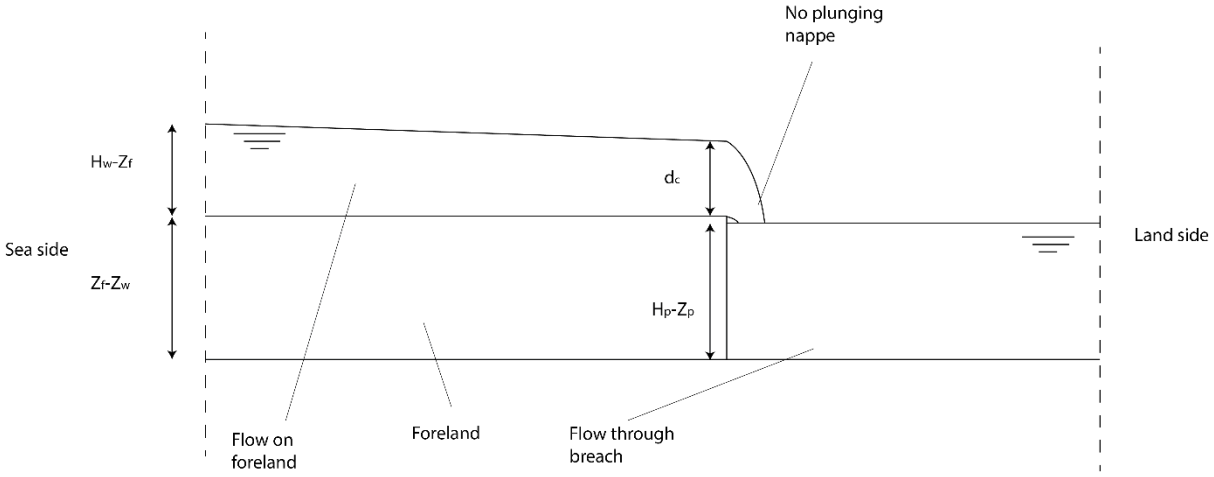

Figure 53: Jet impact no longer reaches breach bottom, headcut erosion stops, side view

As the water level continuous to rise in the polder, the water level in the polder eventually surpasses the elevation of the foreland. If the water level in the breach is below the water level at the edge of the foreland, the flow at the edge of the foreland is still critical. Because the approach depth is critical for both cases, the flow velocity in the breach can again be calculated using the formula:

$$U_{br} = \frac{Q_f}{B(H_p - Z_p)}$$

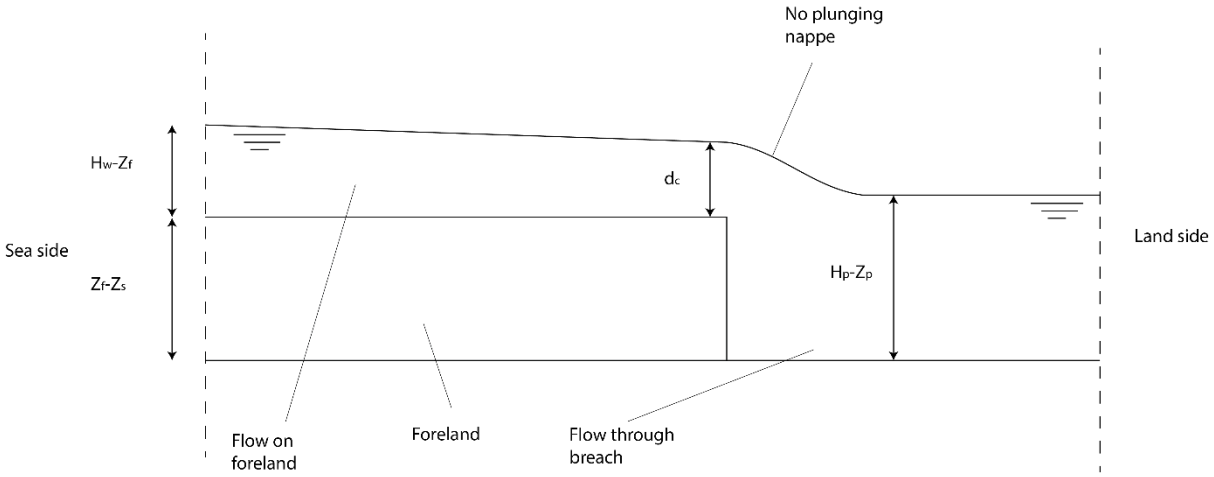

Figure 54: Backwater risen above foreland elevation, flow state on edge of foreland still critical, side view

The final case initiates when the water level in the breach becomes higher than the water level on the edge of the foreland, see Figure 54. This means the flow state is no longer critical and the approach depth can longer be used to calculate the discharge through the foreland. For this case the flow velocity through the breach can instead be calculated using the difference in water levels in the polder and the outside water level,

$$U = \sqrt{2g(H_w - H_{p)}}$$

As the water level in the polder continuous to rise, the flow rate and velocity reduce, eventually becoming zero when the outside water level is equal to the water level in the polder, total inundation. This is also the endpoint for the BRES model.

Chapter 6. Model validation

This chapter discusses the validation and calibration of the proposed model. This is an important step in the research as there are many inherent uncertainties involved in this building with nature approach to coastal defenses. These uncertainties come from simplifications of processes and soil layers, empirical relations, assumptions and approximations used in the model.

This chapter will start by introducing the validation data available. Since the available data on breach growth with forelands is limited, flume experiments have been performed in a controlled setup for this research. These experiments and their results will be presented in the second and third paragraph. The last paragraphs of this chapter will present the interpretation of the model results and a sensitivity analysis.

6.1 Validation

This paragraph will present the validation of the model. Given the fact that little detailed data is available for foreland erosion during a breaching event, an alternative solution had to be found. This approach discussed in the first sub-paragraph, the following paragraphs present the results of the validation.

6.1.1 Validation approach

Very little data is available of headcut erosion in a foreland during or after a breaching event. This is likely caused by a combination of factors. First and foremost, breaching of an embankment is usually unexpected and a dangerous events, and the priority does not lie with documenting erosion patterns. Secondly, forelands have only recently began appearing in scientific documents as potential flood protection measures. From history we know that around the 1400's in the Netherlands dikes were constructed further land inward where a foreland was present. The engineers of that time knew of some of the benefits of a foreland, mainly the wave reduction. Up until around ten years ago, this information seemed to be largely forgotten and forelands were not taking into account in flood defense programs.

Given the lack of validation data available for the complete breaching process, a different approach is taken. By validating separate events for which data is available and combining these validated processes, the complete validation of the model can be approached. The validation is split into three distinct parts.

- Validation of the foreland erosion width, the width of the breach is the limiting factor for foreland erosion in lateral direction
- Verificationof the different headcut models
- Validation of the erosion shape in the foreland

These three separate events combined give the full picture and will be discussed separately in the following paragraphs.

6.1.2 Validation of foreland erosion width

An assumption was made for this model that the erosion of the foreland is limited by the breach width. This is based on the idea that the foreland does not experience erosion until the breach has reached a (semi-)stable level. From that moment onwards, undermining can start to occur in the foreland, leading to periodic headcut erosion. This is not possible when the breach level is still dropping, compare also Figure 29 and Figure 30. In reality the foreland and the breach might have

a more two-way relation, where the erosion of the foreland also effects the breach width. This assumption will be addressed further in the recommendations of chapter 9.

Given that breach size is leading for the width of the foreland erosion, this width can be found directly from the BRES model. Some additional constraints need to be in place to make sure the model functions. An example would be that when the sea level drops below the height of the foreland, inundation ceases. The BRES model has already been validated by Visser (Visser, 1998), therefore, as long as the aforementioned assumption holds, this validation holds for the foreland erosion width. Additional research into this assumption is recommended and a planned large-scale experiment into foreland erosion by Ir. v.d. Berg, TU Delft, is also expected to produce valuable data into the interaction between foreland erosion and the breach growth.

6.1.3 Validation of different headcut models

For this research two different headcut models were examined, the rotational failure model and the sliding failure model. They are examined separately in the next sub-paragraphs.

6.1.3.1 Validation of sliding failure model

The sliding failure model is largely based on the model by Robinson (Robinson K. , 1996). Robinson, Hanson and Cook (2001) performed many large-scale flume test to observe headcut erosion which were used to verify the model by Robinson. This model was not available in code and therefore has been built from the ground up into MATLAB for this research. The results from the flume experiments were then used to calibrate and validate the model.

Unfortunatelly the full datasets of the experiments were not available, most notably the value of the effective shear stress on the foreland. This value is required to calculate the headcut erosion. The documentation of the experiments included several figures presenting results of their models(Figure 55), in these figures the effective shear stress is not presented, but the headcut erosion is.

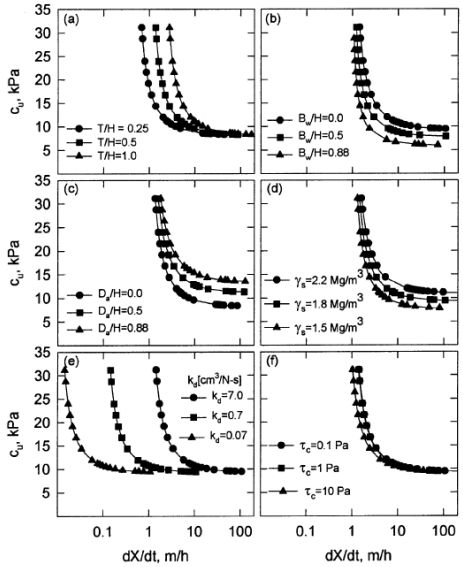

Figure 55: Model results by Hanson, Robinson and Cook, migration rate dX/dt versus undrained shear strength.
Note: reprinted from: "Prediction of Headcut Migration using a deterministic approach", Hanson, Robinson &Cook, 2001

Using these figures, the effective shear stress can be found. This is done by taking a single line in one of the figures (for example 55(a)), representing a constant condition and calculating the

effective shear stress for the different values of undrained strenght c_u using the sliding failure model. The rationale for using a single line is that the changing variable is the undrained strength and the effective shear stress does not depend on this parameter. This can be understood when looking at the shear stress equation for headcut erosion by Robinson(1996) from chapter 5, repeated below for convenience.

$$\pi_1 = 0.025\pi_2^{-1.295}\pi_3^{0.026}\pi_4^{0.221}\pi_5^{-1.062}$$

Where:

$$\pi_1 = \frac{\tau_e}{\rho g D_a}$$

$$\pi_2 = \frac{q^2}{g D_a^3}$$

$$\pi_3 = \frac{H}{D_a}$$

$$\pi_4 = \frac{B_w}{D_a}$$

$$\pi_5 = \frac{X_p}{D_a}$$

This equation can then also be used to calculate the expected erosion rate and compare it to the value obtained from the figures using the sliding failure model. Using this approach, the shape of the graphs obtained from the sliding failure model are almost identical to the graphs from the results found by Hanson, Robinson and Cook (Figure 55). Furthermore the effective shear stress obtained from the figures and the equation by Robinson were also roughly equal in vaule. This concludes that the model is valid given the circumstances used in the experiments by Hanson, Robinson and Cook. The documentation of these results can be found in Appendix D.

6.1.3.2 Validation of rotational failure model

The sliding failure model is based on the headcut advance model in clay dikes created by Zhu (Zhu Y. , 2006). This model was created for dikes but given the assumptions from paragraph 4.3.1, is also valid as a headcut model in forelands. If the crest length of the dike is assumed to be infinite, the case of a foreland is created, see Figure 56.

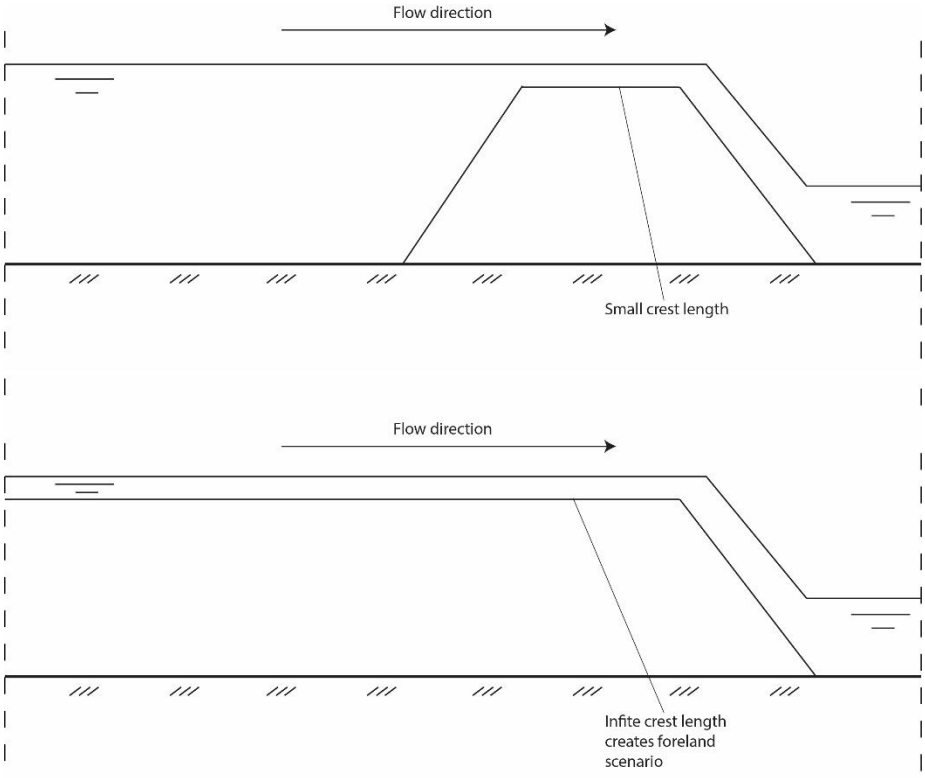

Figure 56: Infinite crest length creates foreland scenario, side view

The code for this model was not available and had to be constructed from the ground up for this research, which means validation of the model was required to make sure it functioned as intended. Zhu verified his model with his own experiments, however these experiments were conducted for the case of a dike, not a foreland, therefore the validation results are not directly applicable to the rotational failure model presented in this study. Instead a set of experiments by Bennet et al (2000) was used to verify the model. These experiments consisted of a thin layer of water flowing over cohesive soil bed with a small initial step in the bed layer (Figure 57). The flow over the bed was caused by a head level difference between the up- and downstream part of the flame, as well as by a rainfall simulator, showering the bed with water. The rainfall simulator was necessary for the study by Bennet et al., however in this study it plays no role and does no influence the headcut erosion behavior. The step in the bed causes a nappe and a scour hole will start to form downstream of the step. As the scour hole becomes wider, it starts to undermine the initial step in the bed, eventually leading to headcut failure, see Figure 58. As discussed in chapter 5, the undermining rate can then be found using the ratio between the depth and length of the scour hole. The rotational failure model was tested for the undermining rate using the values used in the experiments as input for the model. The results were generally within the range of 5 to 10 percent, and are presented in table 3. The value of material dependent coefficient in the rotational failure, M_{ef}, was calibrated using the results of the first three test runs and was subsequently used to verify the other runs. The calibrated value was $M_{ef} = 1.06 \frac{\mathrm{sm}^2}{\mathrm{kg}}$. For a more detailed description of the experimental setup and the values of used parameters, see Appendix E.

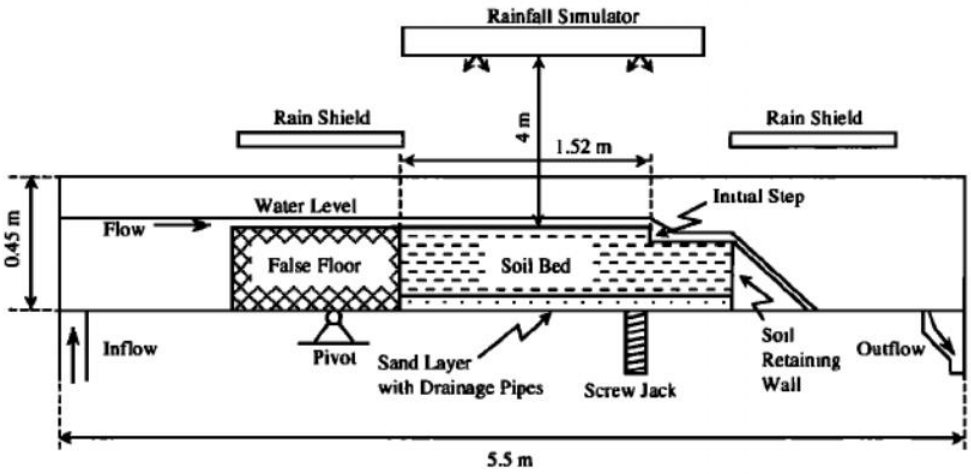

Figure 57: Experimental setup for headcut erosion tests, side view
Note: reprinted from "Experiments on headcut growth and migration in concentrated flows typical of upland areas.", Bennet et al., 2000.

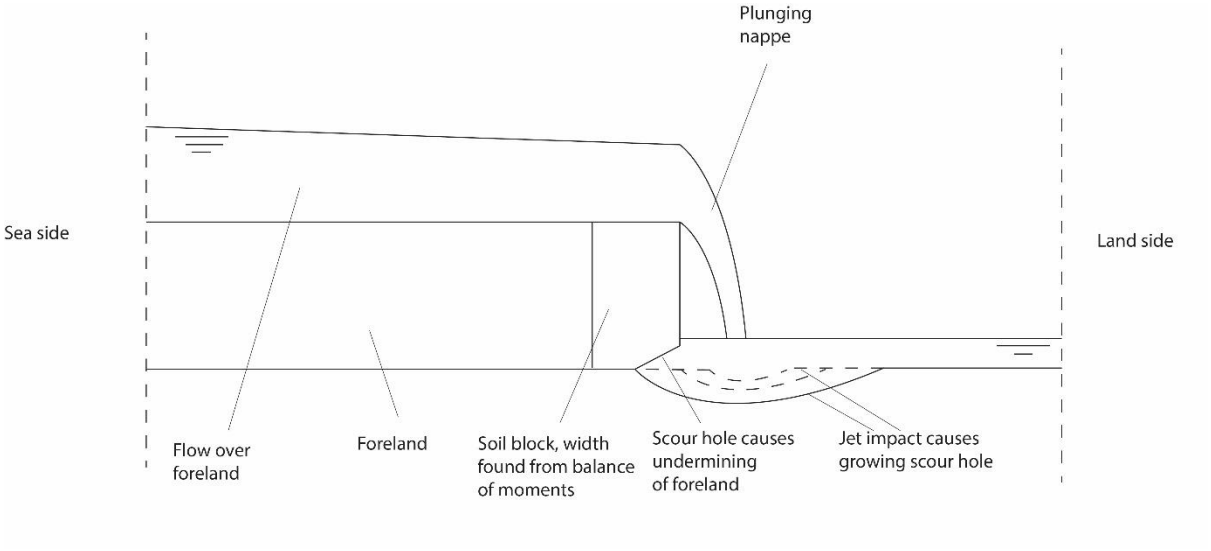

Figure 58: Scour hole created by plunging nappe causes undermining of foreland, side view

Test run number	Calculated migration rate(mm/s)	Migration rate from experiments(mm/s)	Error (%)
1	1.7	1.8	5.8
2	1.9	1.7	10.5
3	1.9	2.0	5.3
4	1.6	1.4	12.6
5	1.6	1.6	0.0
6	1.7	1.9	11.7

Table 3: Rotational model results versus experimental results

6.1.4 Validation of the erosion shape in the foreland

The shape of the foreland is the most difficult to validate. There is no quantitative data available and even qualitative data is sparse. The foreland module follows the one-dimensional flow approach of BRES to compute the elliptical shape of the foreland. The foreland erosion in the centerline of the breach is taken as the normative erosion. From here half of an ellipse is drawn, with two of the vertices being the sides of the breach, see Figure 59 below. The normative erosion is taken at the centerline because the initial undermining of the foreland started on this line, therefore this is the line upon which the foreland has experienced the most erosion.

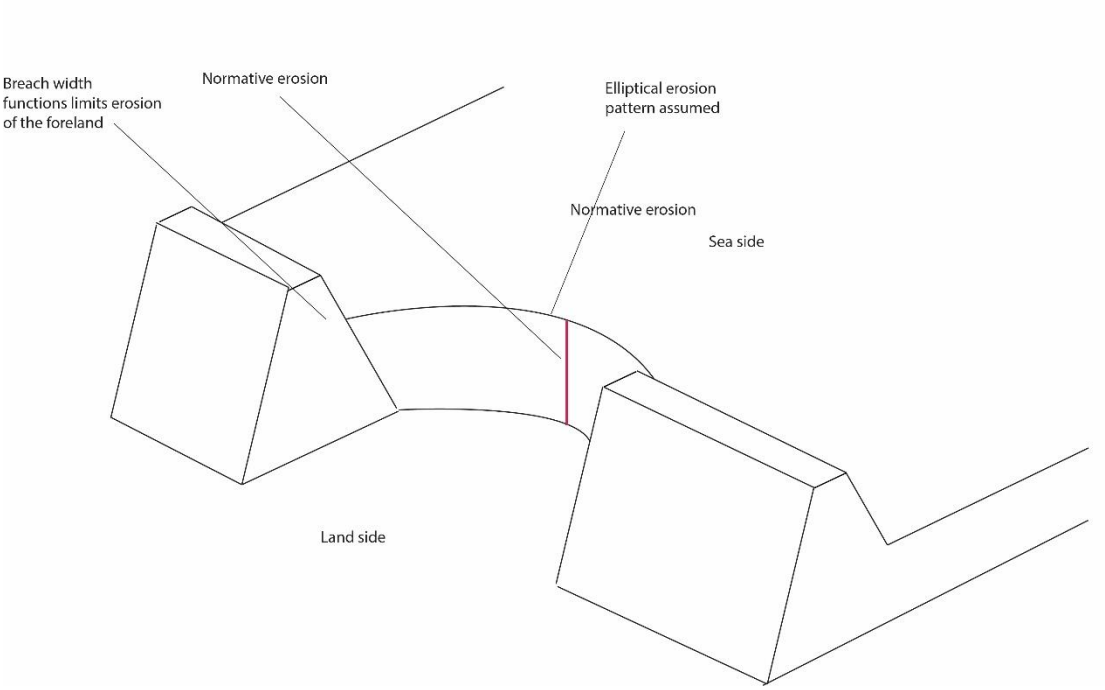

Figure 59: Elliptical foreland erosion

An alternative approach would be to model the headcut erosion process for separate vertical layers within the foreland with a specified width, see Figure 60. The erosion pattern would still approach an elliptical erosion shape, however the ellipse would not have a smooth edge but rather a saw tooth pattern, see Figure 61.

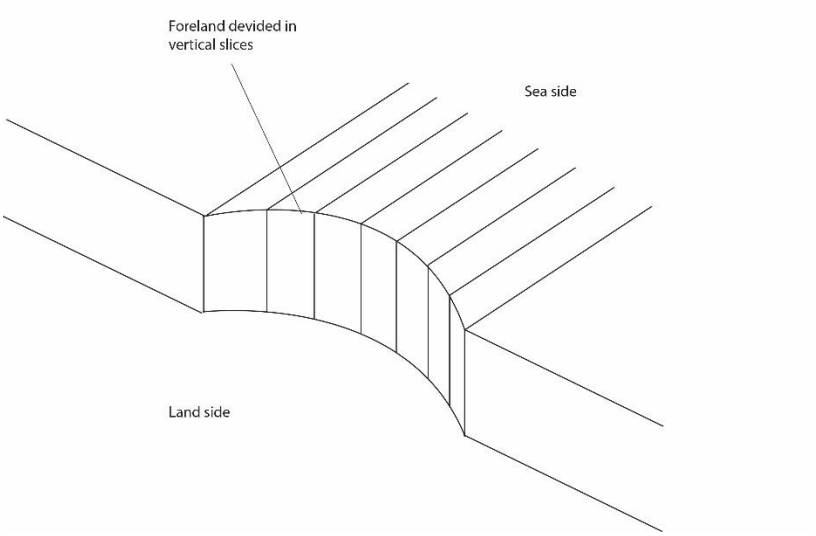

Figure 60: Foreland divided in vertical slices

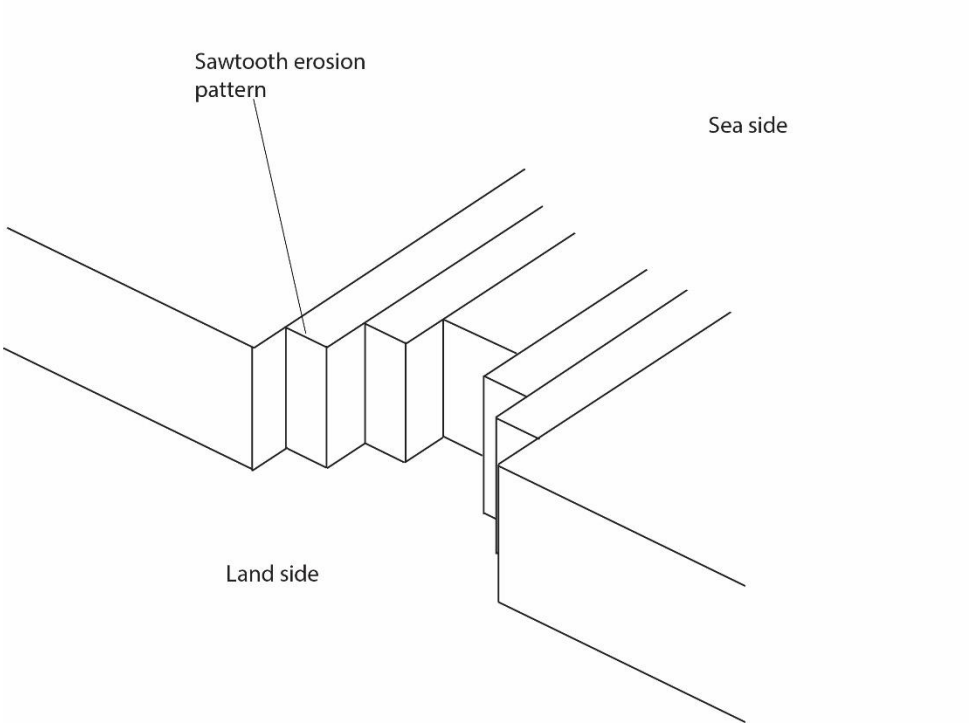

Figure 61: Sawtooth erosion pattern in foreland

On first glance the second approach might seem more physically sound because it models the erosion pattern from a multitude of location as opposed to a singular dot. However, when historical breaches with a foreland are examined, the smooth, elliptical shape from the first approach is observed. This is because the foreland is not a set of individual vertical slices, but must be seen as a more continuous entity. If enough undermining takes places locally to cause headcut erosion, this will cause adjacent parts of the foreland to fail as well. This is caused by both the cohesion of the failing soilblock taking nearby sediment with it, as well as a sudden disappearance of a resistive force. This lateral force is caused by the soil exerting horizontal pressure caused by gravity on adjacent sediment, see also Figure 31.

Another difficulty in the prediction of the erosion shape in the foreland is the non-uniformity of the sediment layer. Local strength or weakness within the soil can cause failure at locations

different than predicted. Therefore, a purely elliptical erosion shape can never occur in a non-uniform foreland.

Given the above discussed limitations, it is important to understand the uncertainties in the model and take care when examining the results. Nevertheless, a case is made for the elliptical erosion pattern in the foreland. The 1953 flooding in the Netherlands has been well documented (Rijkswaterstaat, 1961) and there are several images of dike breaches that had a high foreland. In these photographs elliptical erosion patterns can be observed. Additionally, small embankments were created on the foreland that surrounded the erosion locations. These embankments are also elliptical in shape and are further evidence that the erosion pattern was indeed elliptical. One is presented below; additional figures can be found in Appendix F. The elliptical shape can be observed, however it is far from a perfect ellipse. This can be attributed to local differences in soil strength, which is expected in a natural soil layer.

Figure 62: Elliptical erosion pattern in foreland after dike breach
Note: reprinted from: "Verslag over de stormvloed", Rijkswaterstaat, 1961.

6.2 Soil failure experiment

One of the most critical parameters in the foreland module is the undermining distance required for headcut erosion to occur. Chapter 4 and 5 describe the different headcut erosion patterns in the foreland for cohesive and non-cohesive sediment. For both cases an assumption is made that the bed material is uniform. In reality this is not the case, not only can there be variance in sediment size, there can also be undermining or strengthening of the soil by benthic organisms and plants or roots.

As stated, many forelands consist of fine sediment and they are generally located around mean high water levels. This makes them ideal locations for flora and fauna to grow. A prime example of this would be salt marshes, one of the most important actors in the aquatic food web and nutrient source in the coastal region. Due to the high level of benthic activity and plants present in forelands, it is probable that the headcut erosion is considerably different from the expected headcut erosion for fine sediment. Therefore, an experiment has been conducted into the failure behavior in a soil layer taken from a foreland. The focus of the experiment is to qualitatively analyze the failure behavior. The experiment was done in dry conditions, in absence of any flow related forces and there was no soil data available for this soil layer. Therefore, it was impossible to quantify the expected behavior.

There were two goals for this experiment

- Observe if the failure type of the soil matches the expected failure type of fine sediment (rotational failure)
- Observe if roots or other clear indicators play a significant role in the failure behavior of the soil block

6.2.1 Experimental setup

This experiment was conducted outside, at a facility of the TU-Delft. The experimental setup for this experiment was relatively simple. A soil block extracted from a foreland in the Scheldt near Antwerp was placed on a table with large plastic foil covering the table. This foil was necessary for the soil block to be moved without sticking to the table surface. The soil block was then slowly pushed over the edge of the table, the plastic foil moved along with the block. As the block was pushed further over the edge, deformation of the soil block was observed. The final stage of the experiment was complete failure of the soil block, the point at which the overhanging part broke off. The dimensions of the block were around 100x40x14cm.

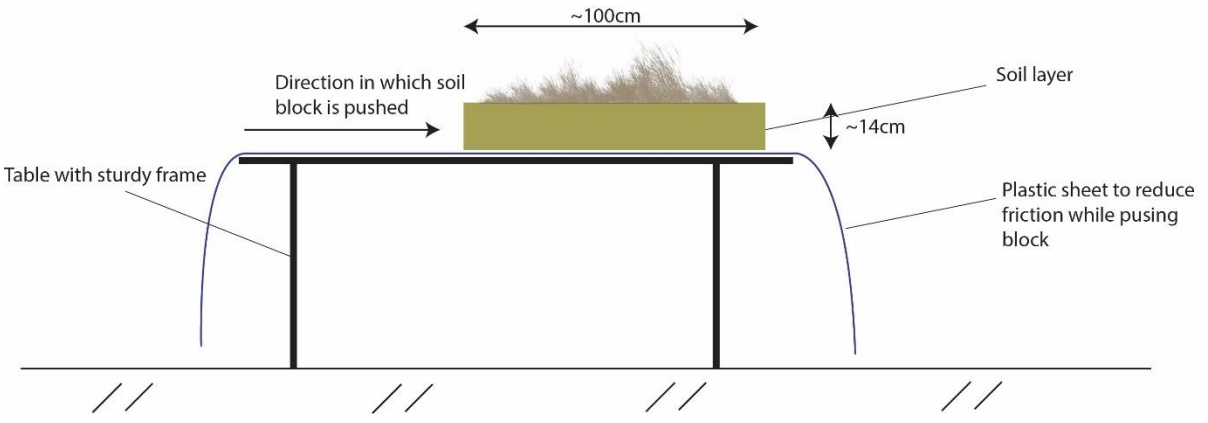

Figure 63: Soil failure experimental setup, side view

The process was captured on video from three angles. A camera was placed in the direction of the movement of the soil block, a second one was placed to the side of the block and a final camera was placed above the block. Additionally, the leftover of the soil block and the broken off part were captured on photo and examined for failure behavior. The soil blocks before and after failure were also measured in size and weight.

Figure 64: Experimental setup soil failure experiment

6.2.2 Results

The goal of the experiment was to observe the qualitive nature of the failure type in the soil layer. Available soil data was limited to bulk density, the observation that the soil consisted of mainly fine sediment and that roots were present. Furthermore, this experiment was performed in absence of hydraulic forces acting on the soil. Given the limitations, the results of this experiments were limited to qualitative observations, which is in line with the goals of the experiments outlined in paragraph 6.2.1.

Failure length

The difference in results between the failure in the two soil blocks was remarkable. The first soil block experienced failure (breaking) after being pushed around 23 centimeters from the edge. The second block experienced failure much later, after being pushed around 83 centimeters. The soil layers were extracted from the same location, the first was the top layer of the foreland, the second the layer directly beneath it.

From observation after the experiments, it was found that the cause of this discrepancy was a system of roots in the second layer preventing the soil from failing. Root systems are generally larger in the lower layers of a soil. It is noteworthy that a relatively small difference in layer depth can lead to such drastically different behavior. In order to accurately model erosion of a foreland, the characteristics of the foreland need to be understood in detail. For more documentation of the results of the experiment, see also Appendix G.

Failure type

The expected failure type for a soil layer consisting of fine sediment is rotational failure (see also chapter 4). This failure type was very clearly observed for both cases. The other possible failure type, associated with coarser sediment, would produce a failure of the sliding type, which was not observed in either soil block. This evidence suggests that the failure type for cohesive soils, hypothesized in chapter 4, is indeed rotational. For a timelapse and documentation of the failure types, see also Appendix G.

Figure 65: Rotational failure observed in the soil layer

6.3 Headcut experiment

A second experiment has been performed in collaboration with the University of Antwerp. This experiment examined the headcut erosion and failure type of a soil layer experiencing undermining. This undermining is caused by a water jet flowing from the top of the soil layer from the upstream direction. As the jet impacts the bed, some of the energy of the impact causes undermining at the base of the soil layer. This experiment closely resembles a foreland during a breaching event.

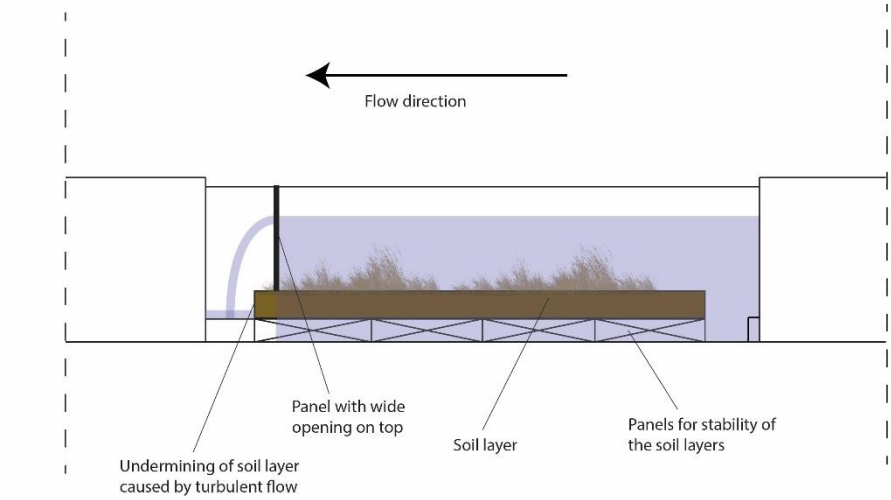

Figure 66: Setup headcut experiment, side view

The soil layers taken for this experiment were taken from a foreland of a dike that surrounds the Hedwige Polder in the south of the Netherlands. The water adjacent to the dike is brackish and the foreland is heavily covered by tall reed. Detailed soil samples were not available, however cohesive material and a strong network of roots was observed over the entire soil layer.

The goals of these experiments are listed below:

- Observe expected undermining in the soil layer caused by the jet flow
- Observe failure type of the expected headcut erosion in the foreland as a result of undermining
- Gain insight in the required forces for undermining and headcut to occur in a realistic soil layer with roots and non-uniform sediment types.

6.3.1 Experimental setup

This experiment was conducted in a flume facility, in which an intact soil layer was taken from the foreland and placed in a large flume. A vertical panel with the width matching the flume width was placed near the downstream end of the soil layer. Close to the top of the panel a rectangular opening was created.

When the flume turned was on, the water level started to rise on the upstream side of the panel. A low backwater downstream of the soil layer was also created. Once the water height reached the rectangular opening, a clear nappe started flowing from the opening. The nappe hit the backwater and turbulence started to occur in the backwater. This turbulence is what causes undermining of the soil layer. Expected subsequent periodic failure of the layer is the headcut behavior sought to be observed from the experiment.

The length of the flume was six meters, the first five meter measured from upstream were covered by the panel. The width of the flume was 80 centimeters. The panel was placed roughly 20 centimeters upstream of the downstream edge of the foreland. The hole in the panel was 70 cm wide, 20 centimeters high and located 72 centimeters above the flume bottom. The width of the soil layer covered the entire 80 centimeter of the flume and was approximately 18 centimeters high. The maximum discharge through the flume was 220L per second. The setup is documented in more detail in Appendix H.

6.3.2 Results

From this experiment several valuable results were obtained. These results were limited to qualitative results. This is due to limitations of the flume compared to a real foreland (limited soil width, soil layer height, flow rates), combined with several factors that could disturb the results such as a minor leakage past the panel. Below the obtained results are presented for each of the three goals of the experiments.

Expected undermining in the soil layer caused by the jet flow

The expected erosion process from chapter 4 describes the water jet flowing from the top of the foreland, causing turbulence in the backwater which will cause an upstream undermining in the foreland. This behavior was very clearly observed and captured on photo and video. See Appendix H for documentation and figures.

Observe failure type of the expected headcut erosion in the foreland as a result of undermining

Similar to the dry soil failure experiment, the failure type in the cohesive soil layer was expected to be rotational. With the hydraulic forces on the soil now being present, the failure type was indeed again of the rotational type. This further supports the hypothesis that real, non-uniform soil layers consisting of mainly fine sediment, experience this failure mode. See Appendix H for documentation and figures.

Gain insight in the required forces for undermining and headcut to occur in a realistic soil layer with roots and non-uniform sediment types

In the experiments, the soil layer and bed downstream of the panel experienced significant amounts of erosion during testing. However, this did require large flow rates and jet dimensions. The most important observations related to erosion are listed below:

- At the locations where roots were present in the soil layer, the erosion was considerably less than in areas without roots
- The closer the impact point of the jet is to the soil layer, the larger the undermining
- All other things equal, higher flow rate caused more undermining of the soil layer
- A higher flow rate, accompanied by a larger distance between the jet impact and the soil layer often led to a reduction of undermining. The distance between the jet impact and the soil layer has a relatively higher impact on undermining than an increased flow rate.
- Lower backwater level caused more undermining in the soil layer
- The water jet falling from a greater altitude caused stronger undermining
- The assumption that when a soil block fails, it is quickly washed away and does not affect the undermining rate for the next soil block, holds for the scale of the model.

Except for the presence of roots in the soil layer, all these observations were tested against the foreland model. The model simulated the same behavior as observed in the experiment. This is evidence the model functions correctly, however more quantitative data is suggested to allow for further testing.

The fourth observation, indicating that a higher flow rate may lead to less undermining is significant is significant, in that it could be seen as counterintuitive. If the flow rate over the foreland decreases, one could expect to observe less undermining. However, if this decreased flow

rate is accompanied by a decreased flow velocity, the impact point of the jet will become closer to the foreland. In many cases this will likely cause more undermining, as the impact of the decreased jet distance is stronger than the decreased flow rate.

6.4 Interpretation of model results and sensitivity analysis.

This paragraph will discuss the results of the different models and scenarios. These scenarios are combination of two variables, whether or not the foreland is cohesive, and whether there is a stable foundation or an erodible foundation.

The sensitivity analysis conducted for the model is limited to computing one scenario at a time and changing a single parameter to see the effect on the output of the model.

6.4.1 Interpretation of the results

Using the data from the Zwin experiment (see chapter 3) as input for the model, a model run was performed using the scenario of a non-cohesive foreland with a stable foundation. Using the results of this computation, Figure 67 presents the value of discharge coefficient m over time. Five distinct stages can be distinguished. At the start of the run the discharge coefficient is constant and equal to one, after which the discharge coefficient starts to rise rapidly in a sawtooth pattern. From there the sawtooth pattern continues but trends downwards, in the fourth phase the downward trend still continues but the sawtooth pattern is no longer present. Lastly, in the final stage the discharge coefficient is constant and roughly equal to 1.13.

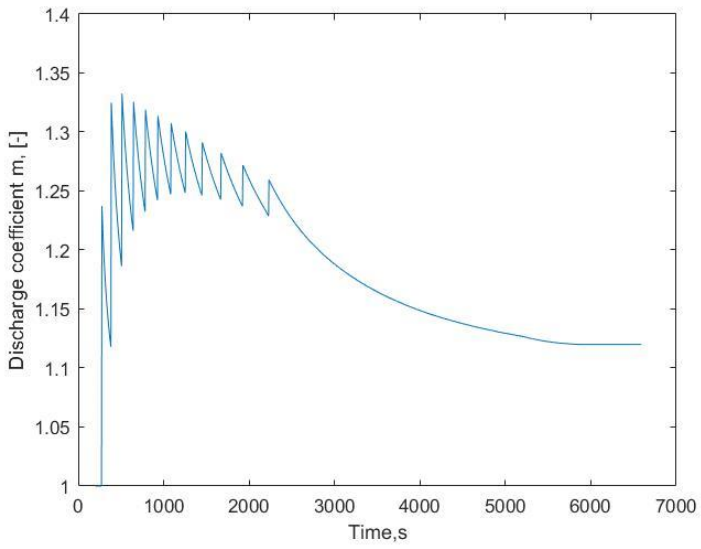

Figure 67: Discharge coefficient over time for the Zwin experiment

The first section in the graph where the discharge coefficient is equal to 1.0, corresponds with stages one through three in the BRES model. During this time the headcut erosion in the foreland is zero, and the elliptical shape is not yet present on the foreland, explaining this value of 1.0.

The second and third section in the graph, the rising and falling sawtooth pattern relate to stage four and the start of phase five in the model. During this time, the foreland experiences periodic headcut erosion. When a soil block fails, the discharge coefficient experiences an instantaneous

increase. After this failure, the breach continuous to grow, and causes the discharge coefficient to decrease until the next soil failure.

The period of time in the graph where the discharge coefficient decreases without the sawtooth pattern corresponds to the second phase of stage five in the model. During this time, the foreland does not experience headcut erosion anymore, but the breach width continuous to grow. This leads to a reduction in the discharge coefficient. The asymptotic behavior is explained by the fact that the flow rate through the breach is solely dictated by the critical water depth on the foreland. Assuming a relatively constant water level on the foreland, the discharge into the breach remains constant, however the water depth in the breach increases as the water level in the polder continuous to rise. This leads to a reduction in the flow velocity in the breach, and subsequently a decrease in the erosion rate on the embankment sides, causing a reduction in lateral breach growth.

The fifth and final section of the graph corresponds with the end of stage five in the BRES model. There is still a flow through the breach, however, the flow velocity through the breach is no longer strong enough to erode the embankment. This causes the discharge coefficient to remain constant. The endpoint of the graph marks the situation where the water level in the polder is equal to outside water level. Figure 68 shows the different stages in the BRES model using different colors.

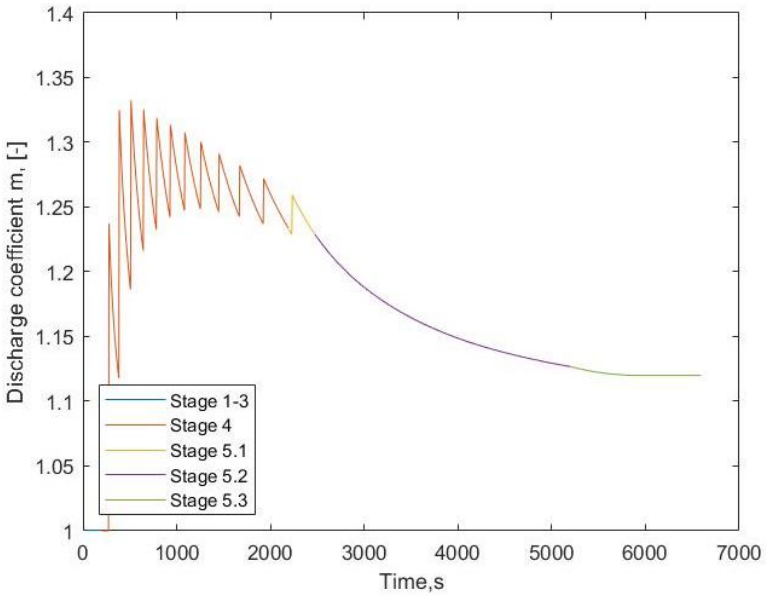

Figure 68: Discharge coefficient over time for the Zwin experiment, colored for different stages of the BRES model

An interesting comparison can be made between the erosion models using a cohesive approach (rotational failure) and the models using a non-cohesive approach (sliding failure). Figure 69 shows the discharge coefficient over time using the rotational failure model with an erodible foundation, using again the data from the Zwin experiment. Comparing the results from Figure 69 to the results from Figure 67, several observations can be made. First, the general behavior is very similar, starting with a constant discharge coefficient, followed by the sawtooth pattern, then a stable reduction and ending again with a constant value. The most striking difference is the number of 'teeth' in the sawtooth pattern. This is due to an increase in failure block length caused by the cohesion. Another effect is that the time-averaged value of the discharge coefficient is lower for the cohesive case. This is explained by the increased resistance to undermining in the foreland in cohesive sediment. Lastly, the total amount of time required for the water level in the polder to become equal to the outside water level is larger than for the case of non-cohesive sediment. This

can be attributed to the fact that the lower value of the discharge coefficient leads to a reduction of the spillway length. The spillway length is directly proportional to the flow rate through the breach, meaning more time is required for the polder to be completely inundated.

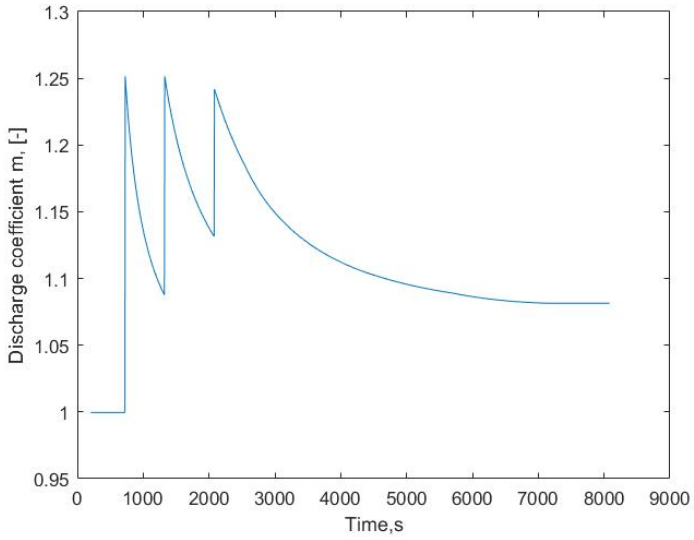

Figure 69: Discharge coefficient over time for the Zwin experiment using the rotational failure model

Two other parameters that are important to consider are the flow velocity and the flow rate over time. These are presented in Figure 70 and Figure 71 using the sliding failure model and a non-erodible foundation with the input of the Zwin experiment.

The shape of the graph for flow velocity resembles the shape of the graph for the discharge coefficient. This is because the flow velocity and the discharge coefficient are both heavily influenced by the breach width. When the breach width increases, the value of both of these parameters is expected to decrease, which is also observed in the figures.

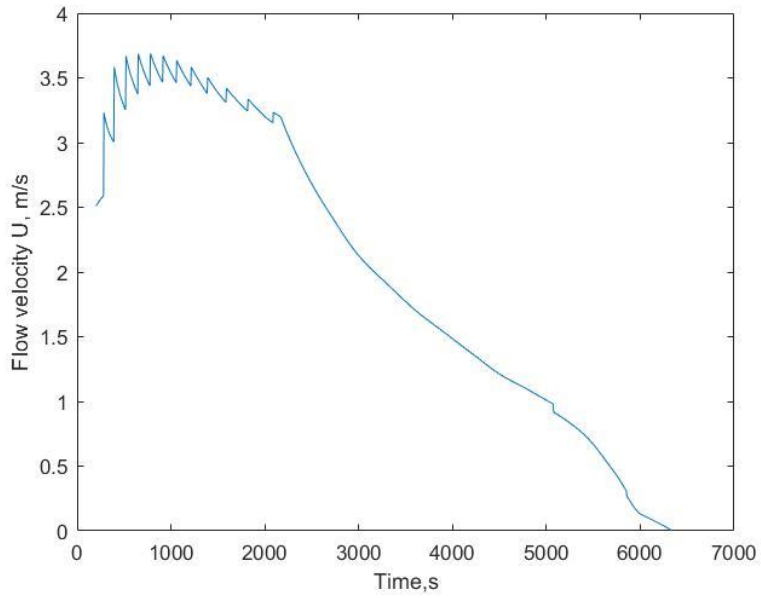

Figure 70: Flow velocity over time for the Zwin experiment using the rotational failure model

An important section to note in Figure 70 is the vertical drop in flow velocity around 5100s. This is a consequence of the approach taken in the original BRES model. The flow rate in stage 4 of the original model is calculated using the critical depth over the elliptical spillway length, whereas stage 5 uses the difference in water level over the embankment. In stage 5 the elliptical shape of the foreland is no longer taken into account, leading to a sudden drop in discharge and subsequent flow velocity. In the modified BRES model made for this study, stage five is split into three different phases to accommodate for the different conditions caused by the foreland. Only in the third (and last) phase of stage 5, the flow rate is calculated using the water level difference over the breach, explaining the drop in flow velocity. Comparing the time of this drop with the initiation of phase 3 observed in Figure 69, it can be seen that they coincide as expected.

In contrast to the flow velocity, the graph for flow rate presents a very different shape. This can be explained by the fact that the flow rate is a multiplication of the flow velocity and the breach width. As the breach width increases, the flow rate continues to increase for a period of time when the flow velocity starts to reduce. Eventually the flow velocity becomes so low that the discharge also reduces.

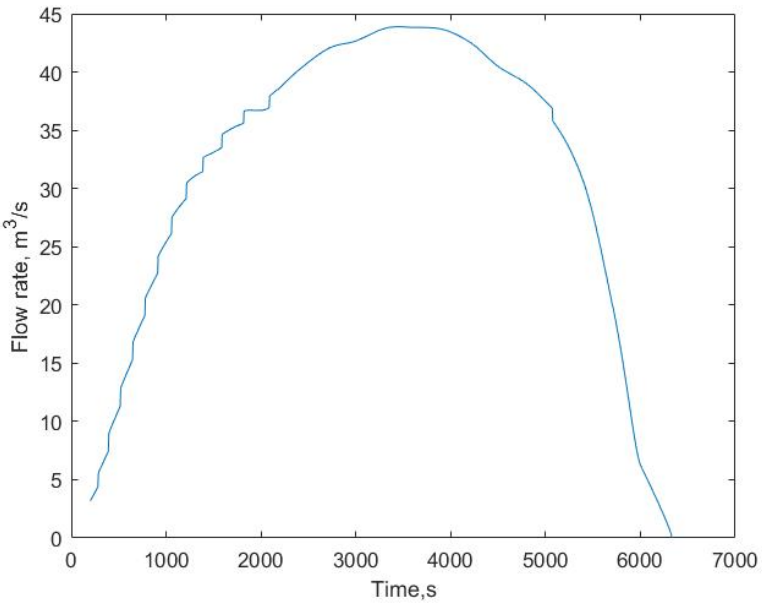

Figure 71: Flow rate over time for the Zwin experiment using the rotational failure model

6.4.2 Sensitivity analysis

The sensitivity analysis was performed by adjusting a single parameter and observing the effect is has on the discharge coefficient. This was chosen because the discharge coefficient quantifies the effects of the foreland erosion shape on the flow rate through the breach in a single parameter and forms the link between the foreland module and the modified BRES model.

The sensitivity analysis has been performed using the sliding failure model with a non-erodible foundation. A total of five parameters will be examined on their relative impact on the discharge coefficient, and also their influence on the total time required for complete inundation of the polder. These five are the most relevant parameters for the elevated foreland functionality in the BRES model. They are outside water level $H_w(m)$, elevation of the foreland $Z_f(m)$, undrained

shear strength $c_u(kPa)$, soil density of the foreland $\gamma_s(kg/m^3)$ and finally embankment elevation $Z_b(m)$.

The initial value of the outside water level is defined by: $H_w = H_{w,Zwin}$, where $H_{w,Zwin}$ is the outside water level from the Zwin experiment, varying from $H_w = 2.7m$ at $t = 0$ until $H_w = 2.11m$ at $t = 6000s$ onwards. The full list of values is presented in table 3. The other initial values for the examined parameters are: $Z_f = 1.5m, c_u = 15000kPa, \gamma_s = 1800kg/m^3$ and $Z_b = 2.5m$.

T	**0**	**300**	**600**	**900**	**1200**	**1500**	**1800**	**2100**	**2400**
H_w	2.70	2.72	2.71	2.68	2.63	2.56	2.51	2.46	2.45
T	**2700**	**3000**	**3300**	**3600**	**3900**	**4200**	**4500**	**4800**	**5100**
H_w	2.44	2.42	2.41	2.39	2.37	2.34	2.30	2.27	2.23
T	**5400**	**5700**	**6000**	**120000**					
H_w	2.19	2.14	2.11	2.08					

Table 4:Outside water level over time for the Zwin experiment

Outside water level

Figure 72 displays three different graphs for varying outside water levels. As the water level increases, the depth on the foreland also increases. Looking at the increased values of the discharge coefficient during phase four of the breaching event, it can be concluded that for a higher critical water depth (and subsequent higher flow velocity and flow rate) at the edge of the foreland more headcut erosion takes place. The higher discharge coefficient further increases the flow rate through the breach due to the increased spillway length. The increased flow rate by these two factors explain the decreasing time period during which the sawtooth pattern is present, the water level in the polder increases faster for a higher outside water level and the state at which the jet from the foreland no longer causes erosion of the foreland is reached more quickly. Finally, a result can be observed related to the total time required for the water level in the polder to become equal to the outside water level. For $H_w = 1.25H_{w,Zwin}$, the effect of the increased flow rate through the breach dominates the increase in polder water level required for complete inundation of the polder, leading to a decrease in total time. For $H_w = 1.5H_{w,Zwin}$, the increase in required polder water level dominates the effect of the increased flow rate, leading to an increase in total time required for complete inundation.

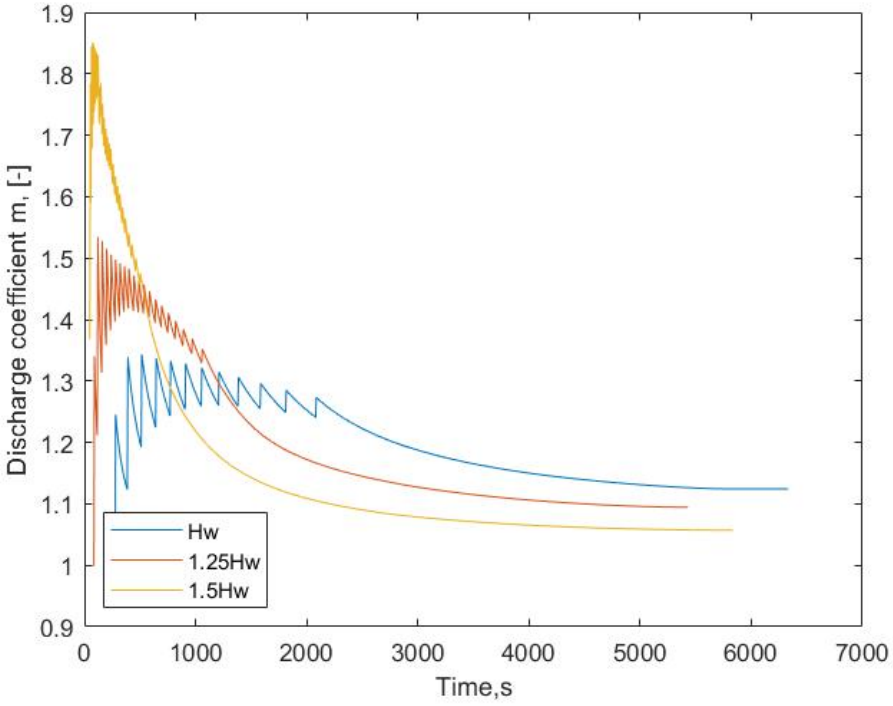

Figure 72: Discharge coefficient over time for different values of Hw

Foreland elevation

From the performed model runs using different foreland elevations it can be seen that for an increasing foreland height the time required for complete inundation sharply increases. This can be understood by considering the decreased water depth over the foreland, leading to an decreased critical depth at the edge of the foreland, limiting flow rate through the breach. Another observation can be made to the value of the discharge coefficient for $Z_f = 1.8m$, where its value surpasses $\frac{\pi}{2}$, meaning the major axis in the elliptical erosion shape in the foreland changes from the direction of the breach width to the direction of the headcut erosion. Lastly it can be seen that for $Z_f = 1.8m$, the discharge coefficient continues to rise until the end of the sawtooth pattern. This means that the headcut erosion dominates the breach growth all the way until the jet falling from the foreland can no longer impact the bed, causing headcut erosion to cease.

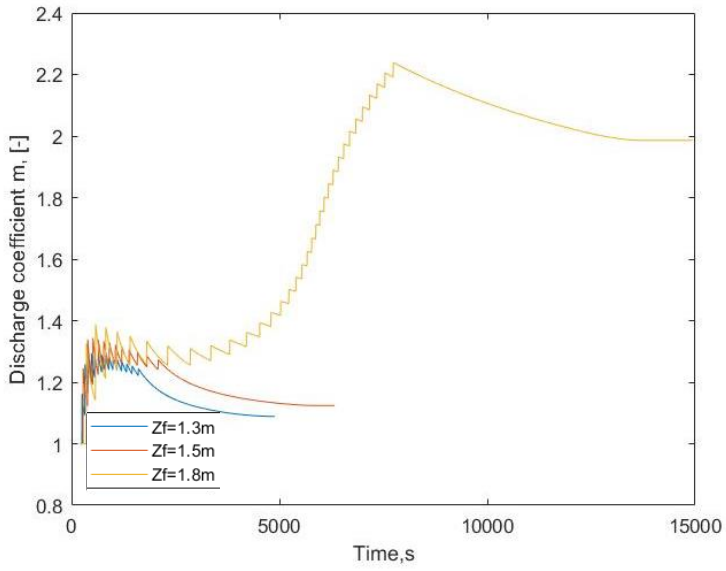

Figure 73:Discharge coefficient over time for different values of Z_f

Undrained shear strength of the foreland

The shear strength of the foreland affects the undermining rate of the foreland. A decrease in shear strength causes an increase in undermining rate, leading to more erosion in the foreland and a subsequently higher discharge coefficient. This increased discharge coefficient causes a longer spillway and therefore a higher flow rate through the breach, leading to a reduction in time of all stages in which headcut erosion occurs.

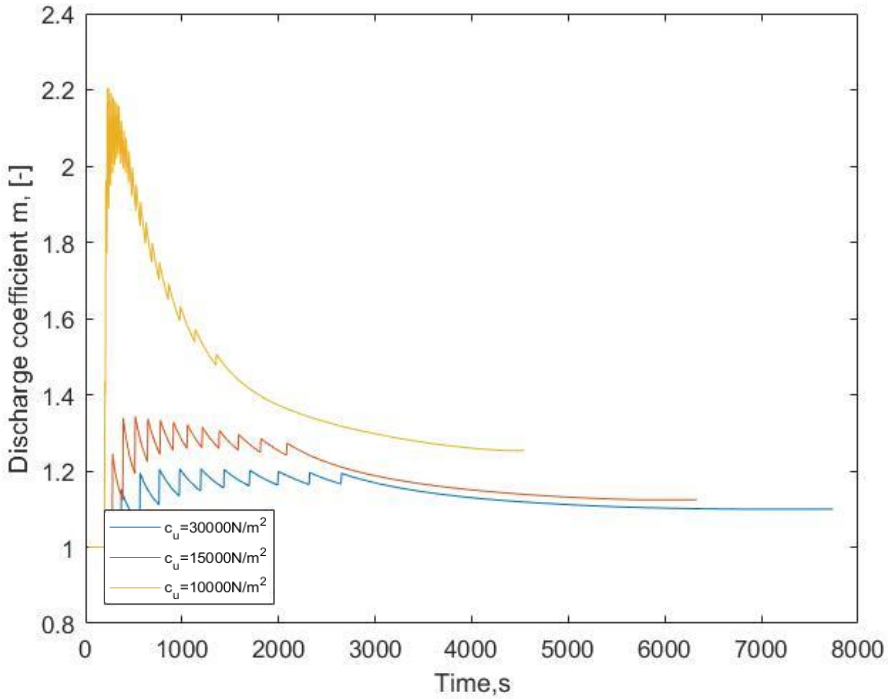

Figure 74: Discharge coefficient over time for different values of c_u

Soil density of the foreland

Figure 75 shows the effect of the soil density on the discharge coefficient. For a higher soil density the discharge coefficient increases and causes stages four and five to become shorter. This can be understood from the force balance equation, where an increase in soil density causes the soil block to become unstable more quickly, increasing the headcut erosion rate in the foreland. The increased discharge coefficient causes an increase in the flow rate through the breach through an increased spillway length, leading to stage four and five becoming shorter.

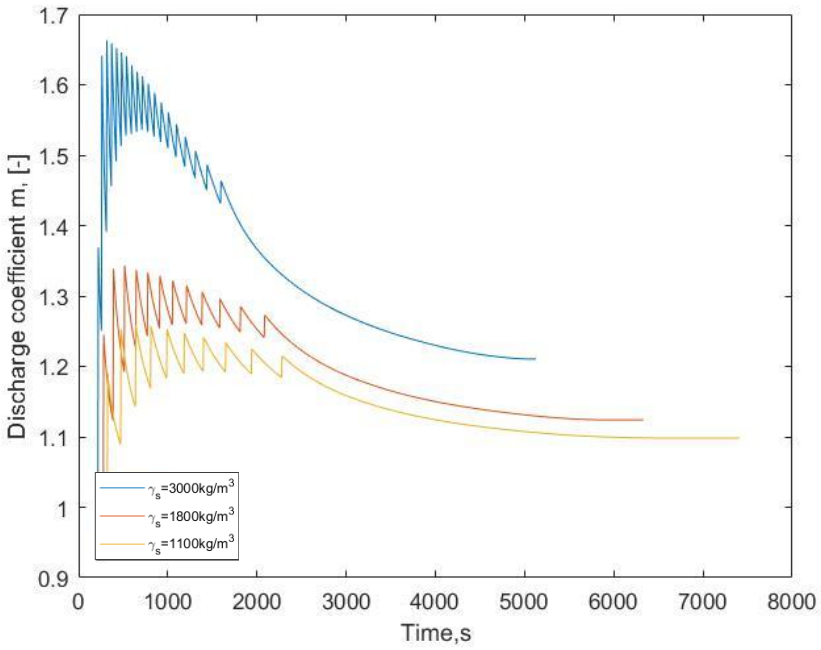

Figure 75: Discharge coefficient over time for different values of the soil density

Embankment height

The effect of the embankment height on the discharge coefficient is very limited, as can be seen from Figure 76. This is because the embankment height is only relevant during stage one through three of the breaching event. This period of time is limited compared to stage four and five, as observed in Figure 68. Another observation to be made is that the increased time period during stage one through three cause an even larger increase in time required for complete inundation. This can be attributed to the fact that when the foreland starts to experience headcut erosion (the embankment level has been reduced to foundation), the water level in the polder is higher for the situation of a high embankment than for the situation of a low embankment. From Figure 55 we can see that for a lower backwater level, headcut erosion is more efficient, causing a longer spillway length and increased flow rate through the breach.

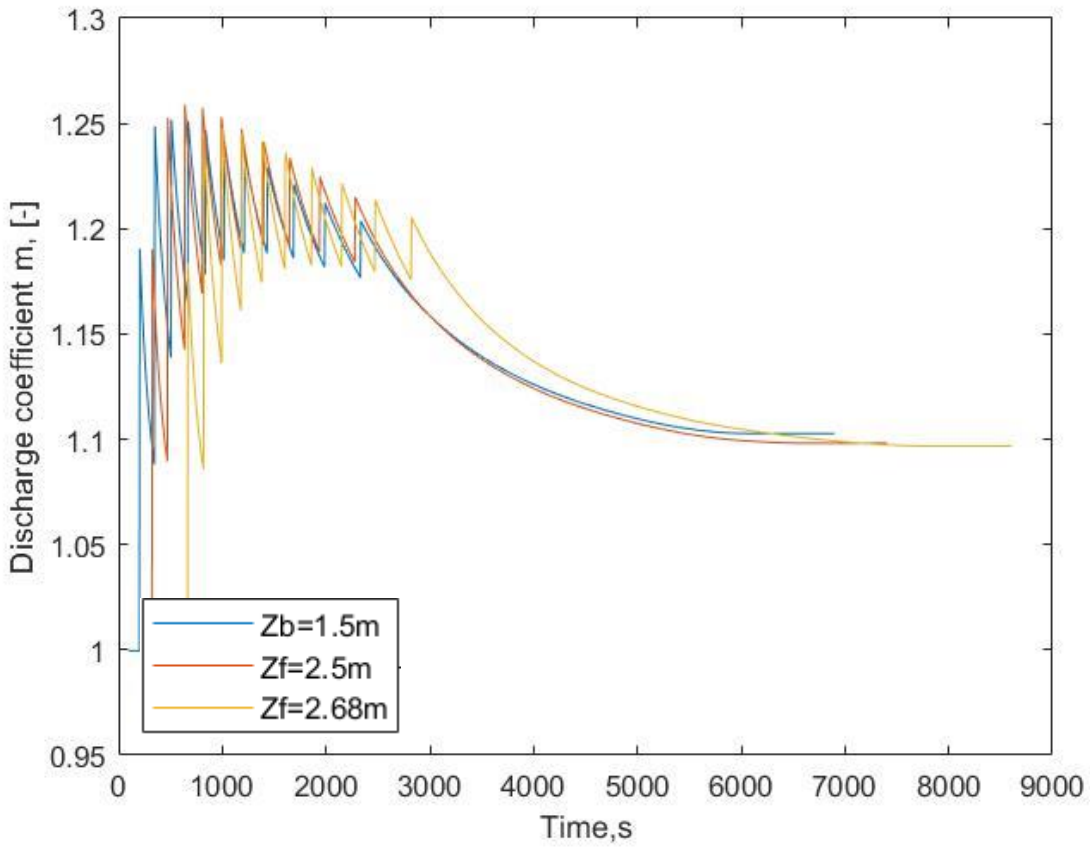

Figure 76: Discharge coefficient over time for different values of the embankment height

Chapter 7. Discussion

The goals of this research were twofold. Firstly, the research focused on understanding and explaining the behavior of a foreland and the consequences it has on the full breaching process of a dike. Different erosion models were used to describe the behavior of coarse (non-cohesive) sediment, and fine (cohesive) sediment. The second goal of the research was to create a module that calculates the effects the presence of a foreland has on the breaching process of an embankment This module was created to fit into an existing 1D breach program called BRES (Visser, 1998). Two experiments were performed to veryify the module and the hypothesized failure modes of forelands. Additionally, the foreland module was tested against experimental data from previous research. Finally, a sensitivity analysis was performed to examine the relative importance of the main parameters.

This chapter evaluates the results of the research and discusses its limitations. The limitations are mainly centered around the accuracy of the foreland module caused by inherent uncertainties when working with building with nature approaches in the field of hydraulic engineering.

7.1 Evaluation of the approach

Dike breaches are highly complex problems with a plethora of different parameters and physical relations involved. When modelling hydraulic problems there are two general approaches that can be taken. The first involves using small timesteps and using detailed equations for every process, leading to results with a relatively high accuracy. The second approach involves using larger timesteps and a reduced level of complexity by using assumptions and approximations for the less significant processes.

Given the duration and the large scale of a breaching event the second approach is the most appropriate for breach models. This is also the approach that Visser took with his BRES model. The largest simplification is that the flow and erosion through the breach is described by 1-D flow and a pick-up equation. A second simplification is that the slopes of the dike erode in a continuous manner as opposed to periodic failure. Since the foreland module is created for the BRES model, the approach taken in BRES is also the framework for the foreland module. The flow equations remain one dimensional and the input flow properties are the same as for the BRES model. Notable erosion of a foreland is not taken as continuous by the model, as opposed to the erosion of dike slopes. Erosion of a foreland is often very limited and follows a clearly observable headcut erosion pattern. In order to realistically model this behavior, the foreland erosion had to be taken as periodic and is calculated by the foreland module.

The results of the conducted experiments show that the hypothesis regarding the expected failure modes were correct. Specifically cohesive sediment experiences rotational failure in both dry and wet situations. From the flume experiment it was also observed that the foreland experiencing headcut erosion caused by undermining of the soil layer. This undermining is caused by the jet flow that falls from the foreland into the backwater of the breach.

The results of the experiments performed for this study are limited to the qualitative description of observed processes, as the setups for both experiments and the available data of the soil did not allow to obtain quantitative results. Fortunately, some experimental headcut erosion data from other research is available and the foreland model was tested against those data sets (Hanson, Robinson, & Cook, 2001). The model performed well for all cases. The experiments performed by others to obtain this data were highly idealized compared to a real foreland situation, mainly by assuming a uniform soil layer and no presence of flora and fauna. From the soil experiment

conducted for this research (see chapter 6) it was observed that especially root systems can cause significant strengthening of the soil layer. Therefore, the assumption that a soil layer is uniform is not realistic for the case of a foreland. However, the dataset from those experiments have been useful to verify behavior of the foreland model. In the absence of a significant amount of detailed and accurate data on headcut erosion in realistic foreland soil layers, this was the most appropriate approach to test the foreland model.

7.2 Limitations of the model

The presented model can predict breaching behavior for a variety of scenarios. Both cohesive and non-cohesive material can be modelled, as well as different foundation types. The model has been tested against various experimental datasets and performed well. There are however limitations to the model. These limitations can be categorized into two groups. Firstly, limitations caused by assumptions and approximations in the model, and secondly the effects of the foreland on breach growth that were not included in the model.

The first category consists of the same limitations as the BRES model, as well as some additional ones specific to the foreland module. For the specific limitations of the BRES model the reader is advised to refer to "*Breach growth in sand-dikes"* (Visser, 1998). Below a list is presented with the limitations of the foreland module.

- Uniformity of the sediment. The presented model assumes a uniform soil layer in the foreland. From the experiments conducted it has been observed that this is not the case in most natural forelands. Especially root systems from plants create a much more erosion resistant soil layer.
- The elliptical shape of the foreland. The presented model follows the initial approach of BRES regarding relatively high forelands by Visser. This approach assumes an erosion pattern in the foreland shaped as half of an ellipse with the major axis coinciding with the dike, see Figure 59 or Figure 47. This stems from the fact that BRES is a 1D model which means the 3D shape of the foreland cannot be fully modelled. Instead, it is assumed that the spillway follows the main direction of the headcut in an elliptical shape. See chapter 5 for a more detailed explanation.
- Erosion of fine sediment is difficult to predict accurately. Various models for fine transport have been created over the past decades, but their results vary greatly. Robinson and Hanson (1996) note that the difference in expected erosion rates by various models can vary up two to three orders of magnitude. Given this inherent insecurity, the user of the model should be wary of possible errors in the results when modelling forelands that consist of fine sediment.
- Effects not considered in the model. The current model considers the effects of a foreland on the flow properties through the breach and subsequent erosion rates, as well as limited inundation of the hinterland due to the height of the foreland. A process not considered in the model is the effect of waves. Waves can lead to increased shear stress on forelands, which could have a significant effect on forelands consisting of non-cohesive sediment. Additionally, a fluctuation in discharge over the spillway caused by the waves could lead to a change in erosion rates.

7.3 Evaluation of the model

The model presented in this study serves as a significant first step towards simulating the effects of a foreland on embankment breaching. Paragraph 6.4.1 showed that the model results are in line with the expected behavior for the different scenarios in terms of cohesivity and foundation type. Additionally, using the input of the Zwin experiment (Visser, Smit, & Snip, 1996), the model predicts a discharge coefficient that fluctuates around 1.2-1.3 (Figure 67). The observations during the Zwin experiment revealed a discharge coefficient of 1.3 (Visser, 1998), which is a promising conclusion.

The model is highly sensitive to uncertainties in input, in particular water level on top of the foreland and soil erodibility coefficient M_f. These parameters affect the flow rate through the breach which, in combination with the water level in the polder, determine the breach growth rate. Remarkably, the initial height of the embankment has little influence on the results. However, the height of the embankment is very relevant during the initiation phase of the breach, which is not considered by the BRES model as it assumes a small initial breach on top of the foreland.

This is the first model of its kind and as discussed in paragraph 7.2 there are limitations to it. Some of these limitations cause the model to be more conservative in the expected erosion of the foreland and are therefore also conservative in the prediction of the breach growth.

- Exclusion of wave energy reduction effect. A high foreland causes waves to break earlier than in the situation where there is no foreland present. The breakage of the waves leads to a signification reduction in wave energy exerted on the dike. Wave effects and wave reduction were not within the scope of this research.
- Exclusion of natural strengthening or weakening of the foreland by flora and fauna. Root systems have been proven with the conducted experiments to make the soil layer much stronger, causing erosion of the foreland to occur much slower. Since the erosion of the foreland has a positive relation with the amount of discharge through the breach, this reduced foreland erosion leads to a reduction of the breaching growth rate.

Two other limitations of the model are not conservative by nature and require additional research or calibration to accurately predict the effect of the foreland on a breach. Firstly, the uncertainty in erosion formulas for cohesive sediment can lead to an overestimation of the soil strength. Secondly, the elliptical shape assumed in the foreland will be much more irregular in nature, which can lead to a spillway length that is larger than predicted.

In conclusion, the model can be used to gain insight in a relatively untouched phenomenon within the field of embankment breaching, however the user should be aware of the limitations of the model and use their expert judgement to interpret the model results.

Chapter 8. Conclusions

This chapter will present the main conclusions of the research. The research questions will be repeated and discussed.

Main research question:

"How can we incorporate the effects of forelands on embankment breaching in an existing breach development model?"

The presented foreland model is a module for the existing breach development model BRES. The module is a combination of several headcut erosion models, developed for different bed types and soil properties. The key parameter used to determine the effects of the foreland on breach growth is the flow rate through the breach. The overarching concepts in the model are a reduction in discharge caused by the elevated foreland and an increase in discharge caused by an elliptical spillway in the foreland due to headcut erosion. The elliptical shape of the spillway is based on observations in the field and is captured in the non-dimensional discharge coefficient m. The foreland model is limited to this approach due to the 1D nature of the BRES model. Furthermore, many of the concepts and assumptions used in BRES are also used for the foreland model, most importantly the uniformity of the soil and the 5 stages in embankment failure.

Research sub-questions:

- *"What processes related to a breaching event are affected by the presence of a foreland?"*

The key processes caused by the presence of a foreland during an embankment breach are:

- Reduced of water level, flow rate and flow velocity through the breach caused by the height of the foreland compared to the situation in which a foreland was not present.
- Increased discharge through the breach compared to the situation in which a foreland is not present, caused by the elliptical erosion pattern in the foreland. The increased discharge is captured in the non-dimensional constant m. This effect is often secondary to the reduced flow rate caused by the height of the foreland.
- Limited inundation as the foreland effectively functions as the new embankment when a storm subsides and the outside water level drops below the elevation of the foreland (usually situated around mean high water level).

- *"How can the relevant effects of a foreland on the breaching process be modelled?"*

The presented model uses a combination of several headcut erosion models for different soil and foundation types. Combining the headcut model with the elliptical erosion pattern in the foreland and the height of the foreland provides the hydraulic parameters required for BRES to model the breach development.

- *"Which existing breaching model is best suited for the incorporation of a foreland erosion module?"*

The model chosen for this study is the BRES model by Visser (1998). The 1D nature of the BRES model allowed for optimal integration of the 1D headcut models, which serve as the backbone of the foreland module. Additionally, the complexity level, availability of the code and elliptical foreland concept for non-elevated forelands made this the best choice.

- *"What is the sensitivity of the developed model to uncertainties in input?"*

The model is highly sensitive to uncertainties in input, especially foreland elevation, water level on top of the foreland and soil erodibility coefficient M_f. These inputs heavily influence the flow rate through the breach, which is the parameter that determines the effect of a foreland on breach growth. Interestingly, the initial height of the embankment has very little influence on the results. However, the height of the embankment is very relevant during the initiation phase of the breach, which is not considered by the BRES model as it assumes a small initial breach on top of the foreland.

- *"How can the proposed model be used in a flood defense framework?"*

The presented model can be used during assessments of existing flood defense plans, as well as for the design of new structures. More accurate predictions can be made on potential breaches, and there is an additional benefit during risk analyses. Risk can be defined as probability of an event multiplied by the damages caused by this event. As the potential damages can be decreased when a foreland is present, the risk will also decrease accordingly.

Chapter 9. Recommendations

This final chapter contains the recommendations following the research laid out in this thesis. Some recommendations are related to further studies into the effects of forelands during breaching events, other recommendations consider the implementation of forelands in flood defense programs.

Several of the assumptions used in the model affect its accuracy. The most important one is that the sediment type in the foreland is uniform, consists of a single particle size and no other elements are present in the soil that change the erosion properties. In reality, forelands are often highly fertile and root systems can cause significant local strengthening of the soil. The uniform soil layer is a conservative approach as it assumes the situation leading to the most erosion, however a better understanding of the influence of root systems could provide more accurate results. Given the unpredictability of natural processes like plant growth, the expected results of study into the effect of root systems are limited. In addition, the proverb "a chain is only as strong as its weakest link" serves as a cause of warning when looking at the strength of forelands, as a local weakening of the soil is normative for failure of an entire layer.

The uncertainties in the model are not limited to the physical assumptions made for the model. One of the largest uncertainties of the model comes from the limited amount of verification data. Therefore, it is recommended that more quantitative experimental data is collected to further verify the model and reduce the level of uncertainty. Ir. v.d. Berg, TU Delft, is planning a large-scale experiment involving the breaching of a full-scale dike that has a foreland. The main goal of this experiment is to collect data of the erosion that will occur in the foreland. This experiment is expected to provide a lot of useful data for further verification of the model presented in this thesis.

Finally, two recommendations are given for the implementation of forelands in flood defense programs. The first recommendation is to perform additional research into wave energy reduction caused by a foreland. This reduction stems from the limited water depth on the foreland. The presence of a foreland severely limits the water depth, causing waves to break and wave energy on the embankment to be highly reduced. This means that if a foreland is present, construction of an embankment further inland will be beneficial in reducing the risk of a breach occurring.

The second recommendation is to use the breach growth reducing effect of forelands in risk analyses. Presently Rijkswaterstaat (the executive agency of the Ministry of Infrastructure and Water Management for the Netherlands) and other institutions do not consider the effects of a foreland on breaching events (personal communications P.J. Visser, TU-Delft). This can be explained by the fact that the Rijkswaterstaat wants to prevent embankment breaches and the most notable effects of a foreland, limited inundation and reduction of breach growth rate, are only observed after the adjacent embankment has reduced to its foundation level, meaning a dike has completely failed. These effects caused by foreland are highly beneficial in reducing damage, but do not contribute to the prevention of embankment breaching. Nevertheless, insight in the effects of forelands on flood can be valuable during the risk analysis of a flood defense program. Since risk is defined as the possibility of an event occurring multiplied by the ensuing damages, the risk of an embankment breach in absence of a foreland could be much greater than the case where a foreland is present. The presented model would therefore be a valuable addition during risk analyses for both existing and new flood protection measures.

Bibliography

Bennet, J., Alonso, V., Prasad, S., & Romkens, S. (2000). Experiments on headcut growth and migration in concentrated flows typical of upland areas. *Water resources research, vol. 36, No.7* , 1911-1922.

Cristofano, E. (1965). *Method of computing erosion rate for failure of earthfill dams.* Denver, Colo.: U.S. Bureau of Reclamation, Engineering and Research Center.

Fagherazzi, S., Mariotti, G., Leonardi, N., Canestrelli, A., Nardin, W., & Kearney, W. (2020). Salt Marsh Dynamics in a Period of Accelerated Sea Level Rise. *Journal of Geophysical Research: Earth Surface, 125*.

Foortse, B., Visser, P., Bisschop, R., & van Rhee, C. (2019). *Experimental investigation into the reduction of erosion of sand at high flow velocities.* Delft: Proceedings of the Institution of Civil Engineers: Maritime Engineering.

Fread, D. (1988). *BREACH: An erosion model for earthen dam failures.* Silver Spring, Maryland: Hydrologic Research Laboratory, National Weather Service, NOAA.

Hanson, G., Robinson, M., & Cook, R. (2001). Prediction of headcut migration using a deterministic appraoch. *Transactions of the ASAE, 44*, 525.

King, S., & Lester, J. (1995). The value of salt marsh as a sea defence. *Marine Pollution Bulletin, 30*, 180-189.

Marin-Diaz, B., Bouma, T., & Infantes, E. (2020). Role of eelgrass on bed-load transport and sediment resuspension under oscillatory flow. *Limnology and Oceanography, 65*, 426-436.

Masson-Delmotte, V., Zhai, P., A., P., Connors, S., Péan, C., Berger, S., . . . (eds.), B. Z. (2021). *IPCC, 2021: Climate Change 2021: The Physical Science Basis. Contribution of Working Group I to the Sixth Assessment Report of the Intergovernmental Panel on Climate Change.* Cambridge: Cambridge University Press.

Möller, I. (2019). Applying Uncertain Science to Nature-Based Coastal Protection: Lessons From Shallow Wetland-Dominated Shores. *Frontiers in Environmental Science, 7*, 49.

Morris, J., Sundberg, K., & Hopkinson, C. (2013, September). Salt Marsh Primary Production and Its Responses to Relative Sea Level and Nutrients in Estuaries at Plum Island, Massachusetts, and North Inlet, South Carolina, USA. *Oceanography, 26*, 78-84.

Nagy, L. (2006). Estimating Dike Breach Length from Historical Data. *Periodica Polytechnica-civil Engineering, 50*, 125-138.

Peeters, P., Heredia Gómez, M., Van Damme, M., & Visser, P. (2016, January). Unveiling the consequences of your breach growth model choice. *E3S Web of Conferences, 7*, 3005.

Pietrzak, J. (2020). *An Introduction to Stratified Flows for Civil and Offshore Engineers, From Shelf to Shore.* Delft Technical University.

Rijkswaterstaat. (1961). *Verslag over de stormvloed van 1953.* Staatsdrukkerij- en uitgeversbedrijf.

Robinson, K. (1996). *Gully erosion and headcut advance.* Oklahoma, US: Doctoral dissertation, Oklahoma State University.

Robinson, M. K., & Hanson, G. (1996). Gully Headcut Advance. *Transactions of the ASAE, 39*, 33–38.

Robinson, M., & Hanson, G. (1994). A Deterministic Headcut Advance Model. *Transactions of the ASAE, 37*, 1437–1443.

Robinson, M., Hanson, G., & Hassan, M. (2008, October). Improving the accuracy of breach modelling: Why are we not progressing faster? *Journal of Flood Risk Management, 1*, 150-161.

Schiereck, G. J. (2003). Introduction to Bed, Bank and Shore Protection. Delft: Delft university press.

Taylor, B., Paterson, D., & Baxter, J. (2019). Sediment Dynamics of Natural and Restored Bolboschoenus maritimus Saltmarsh. *Frontiers in Ecology and Evolution, 7*, 237.

Temple, D. M., Hanson, G. J., Neilsen, M., & Cook, K. R. (2005, January). Simplified breach analysis model for homogeneous embankments: Part I, Background and model components. *Proceedings of the 2005 U.S. Society on Dams Annual Meeting and Conference*, 151-161.

van Prooijen, B. (2019). *Sediment Dynamics: Sediment Classes and Bed Composition.* Technical University Delft.

Visser, P. (1998). *Breach growth in sand-dikes.* Delft: Technical University Delft.

Visser, P. (2021). *Documentation of 1953 breaches, unpublished.*

Visser, P., Smit, M., & Snip, D. (1996). *Zwin '94 experiment: Meetopstelling en overzicht van alle meetresultaten.* Delft: TU Delft, Department Hydraulic Engineering.

Vrijling, J., Schweckendiek, T., & Kanning, W. (2011, June). Safety standards of flood defenses. *International Symposium for Geotechnical Safety and Risk*.

Vuik, V., Borsje, B., Willemsen, P., & Jonkman, S. N. (2019, April). Salt marshes for flood risk reduction: Quantifying long-term effectiveness and life-cycle costs. *Ocean and Coastal Management, 171*, 96-110.

Wahl, T. (2010). Dam breach modeling, an overview of analysis methods. *2nd Joint Federal Interagency Conference, La.* Las Vegas, USA.

Wurbs, R. (1987). Dam-breach flood wave models. *Journal of Hydraulic Engineering, 113*, 29-46.

Zedler, J. B., Bonin, C. L., Larkin, D. J., & Varty, A. (2008). Salt Marshes. In S. E. Jørgensen, & B. D. Fath (Eds.), *Encyclopedia of Ecology* (pp. 3132-3141). Oxford: Academic Press.

Zhu, Y. (2006, September). *Breach growth in clay-dikes.* Delft: Technical University Delft.

Zhu, Y. H., Visser, P. J., & Vrijling, J. K. (2004). Review on embankment dam breach modeling. *New Developments in Dam Engineering, Taylor & Francis Group, London, UK*, 1189–1196.

Zhu, Z., Vuik, V., Visser P.J., S. T., van Wesenbeeck, B., van de Koppel, J., Jonkman, S., . . . Bouma, T. (2020). Historic storms and the hidden value of coastal. *Nature sustainability (3)*, 853-862.

Appendix A. Adaptation length

The adaption length l_n can be approximated by taking the difference between the outside water level H_w and the height of the breach bottom Z_{br} and dividing the result by the friction coefficient of the soil, C_f:

$$l_n = \frac{H_w - Z_{br}}{C_f}$$

This equation can again be reduced if the difference between the water level on the sea-side and the height of the dike H_d can be assumed small compared to the difference between the sea-side water level and the height of the breach bottom:

$$|H_w - H_d| \ll H_w - Z_{br}$$

This is a reasonable assumption given the failure mode of dike is related to overtopping. Using this, we can approximate the depth of the breach, h:

$$h = H_d - Z_{br} \approx H_w - Z_{br}$$

Combining the above equations the final equation for adaptation length is obtained:

$$l_n = \frac{h}{C_f}$$

Appendix B. Input and output BRES model

Input

Presented below is a list of all the input parameters and adjustable model functions for the BRES model.

Model functions

- Erosion functions: allows the user to choose an erosion function per stage of the breaching process.
- Breach type: requires the user to select the breach type to be modelled. In case of breach type B a value for discharge coefficient m is also required. The discharge coefficient is dimensionless.
- Inclusion of a flow slope: calculates the quantities that determine the erosion of the inner slope, u, d and C_f during phase one through three. Can be toggled on or off.
- Timesteps: requires the user to set the timestep to be used during calculations for stages three through five.
- Saving results: Gives the user the option to save the results in Matlab or export them to Microsoft Excel.

Water parameters

- ρ, the density of the water $\left[\frac{kg}{m^3}\right]$
- T, temperate of the water $[°C]$
- H_p, water level in the polder above Z=0 where Z=0 is the reference line$[m]$
- H_w, outside water level above Z=0 $[m]$
- H_{ww}, outside water level above Z=0 in time, requires water level for different timestamps $[m]$

Dike body parameters

- Z_p, polder level above Z=0 $[m]$
- Z_{br}, breach height above Z=0, requires initial value $[m]$
- Z_w, height of the watercourse bottom above Z=0 $[m]$
- H_d, height of the dike above Z=0 $[m]$
- W_d, width of the dike crest $[m]$
- b, width of the breach at breach bottom, requires initial value $[m]$
- α, inclination angle of the outer slope in degrees
- β_0, inclination angle of the inner slope in degrees
- β_1, critical value of inclination angle of the inner slope in degrees
- γ, inclination angle of the side slopes in degrees

Sediment parameters

- ρ_s, sediment density $\left[\frac{kg}{m^3}\right]$
- D_{10}, the particle size for which the portion of particles with diameters smaller than this value is 10% $[m]$

- D_{50}, the particle size for which the portion of particles with diameters smaller than this value is 50% $[m]$
- D_{90}, the particle size for which the portion of particles with diameters smaller than this value is 90% $[m]$
- p, bed porosity $[-]$
- $\ni$, porosity of sheared layer $[-]$
- ϕ_d, angle of repose of the bed layer in degrees
- κ, Von Karman constant $[-]$
- C_f, friction coefficient $[-]$

Additional parameters

- g, gravitational constant $\left[\frac{m^2}{s}\right]$

Output

Below is a list of all the output parameters of the BRES model.

Parameters given as a function of the computed timestep

- B_t, breach width at the top of the dike $[m]$
- B_w, breach width at the water line $[m]$
- B, depth averaged breach width (over water depth d) $[m]$
- b, breach width at breach bottom $[m]$
- Q_{br}, breach inflow rate $\left[\frac{m^3}{s}\right]$
- U, depth average flow velocity $\left[\frac{m}{s}\right]$
- d, water depth above breach bottom $[m]$
- H_w, outside water level above Z=0 $[m]$
- H_p, water level in the polder above Z=0 $[m]$
- Z_{br}, breach height above Z=0 $[m]$

Additional parameters

- Time t, for which the previous phase ends and the next one begins $[s]$.

Appendix C. Calculating ellipse circumference

For the calculations of the elliptical erosion shape in the foreland, five different methods were examined. Three approximations and two series. First the exact equation is presented which cannot be directly implemented in a mathematical model. Then the three approximations will be presented and followed by the two the mathematical series examined. Finally a table is presented with performance results of the methods.

Perfect formula

$$p = 4a \int_0^{\frac{\pi}{2}} \sqrt{(1 - e^2 \sin^2 \theta)} d\theta$$

with:

$$eccentricity, e = \frac{\sqrt{a^2 - b^2}}{a}$$

Where a is the radius of the major axis of the ellipse and b the radius of the minor axis.

Approximation 1

$$p \approx 2\pi \sqrt{\frac{a^2 + b^2}{2}}$$

Where p is the circumference of the ellipse, a is the length of the major axis and b is the length of the minor axis.

Approximation 2

$$p = \pi[3(a + b) - \sqrt{(3a + b)(a + 3b)}$$

Where again p is the circumference of the ellipse, a is the length of the major axis and b is the length of the minor axis.

Approximation 3

$$p \approx \pi(a + b)(1 + \left(\frac{3h}{10 + \sqrt{4 - 3h}}\right)$$

Where

$$h = \frac{(a - b)^2}{(a + b)^2}$$

Mathematical series 1

$$p = 2a\pi \left(1 - \sum \frac{(2i)!^2 \, e^{2i}}{(2^i i!)^4 (2i - 1)}\right)$$

Where

$$e = \frac{\sqrt{a^2 - b^2}}{a}$$

Mathematical series 2

$$p = \pi(a + b) \sum_{n=0} \binom{0.5}{n}^2 h^n$$

Where

$$h = \frac{(a - b)^2}{(a + b)^2}$$

Below the results for the different approaches are presented for different values of a/b. Additionally an almost perfect value is obtained by using the second series with 1000 terms. This however is not feasible for the breaching model due to required computational power, especially during the sensitivity analysis.

Method	a/b = 1	a/b=2	a/b=4	a/b=10	a/b=100	a/b=1000
Approximation 1	6.2831	4.9672	4.5796	4.4650	4.4431	4.4428
Approximation 2	6.2831	4.8442	4.2887	4.0605	3.9874	3.9837
Approximation 3	6.2831	4.8442	4.2892	4.0639	4.0001	3.9985
Series 1 (100 terms)	6.2831	4.8442	4.2892	4.0655	4.0107	4.0101
Series 2 (7 terms)	6.2831	4.8442	4.2892	4.0638	3.9990	3.9969
"Perfect" value (Series 2 with 1000 terms)	**6.2831**	**4.8442**	**4.2892**	**4.0640**	**4.0011**	**4.0000**

Table 5: Performance of methods for different values of a/b

Appendix D. Validation sliding failure model

The model was validated using the approach laid out in paragraph 6.3.3.1. Figure 77 shows two graphs where the migration rate is plotted against the undrained shear strength. Using the experimental parameters as input for the sliding failure model, the shear strength can be obtained. For Figure 77(a), the changing variable is the headcut failure block, T. It should be noted that this parameter does not depend on the effective shear stress. This means that the shear strength obtained from an arbitrary ratio of failure block length over foreland height, $\frac{T}{H}$, the shear strength can be used for all other ratios of $\frac{T}{H}$. The parameters used in the experiment are used as input parameters for the sliding failure model and are as follows: $H = 1.2m$, $\frac{T}{H} = 0.5$, $\frac{B_w}{H} = 0.0$, $\frac{d_a}{H} = 0.2$, $\gamma_s = 0.2\frac{Mg}{m^3}$, $k_d = \frac{7.0cm^3}{Ns}$ and $\tau_c = 0.1\ Pa$. Where H is the foreland elevation, d_a approach flow depth on the foreland, γ_s the unit weight of the soil, k_d the erodibility coefficient and finally τ_c critical shear stress.

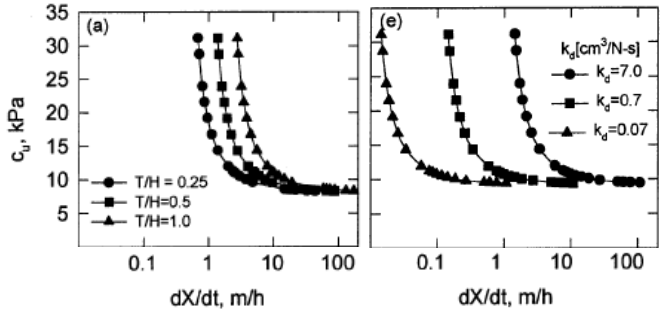

Figure 77: Results of flume test by Hanson, Robinson and Cook, migration rate dX/dt versus undrained shear strength
Note: reprinted from: "Prediction of Headcut Migration using a deterministic approach", Hanson, Robinson &Cook, 2001

In Figure 78, the results of the model are compared to the results of the model by Hanson, Robinson and Cook(2001) for the different values of $\frac{T}{H}$. These results are almost identical. The value of the shear strength used as input for the model has been obtained from observed values of Figure 77, therefore a slight discrepancy can in part be attributed to an error related to reading the values from the graphs.

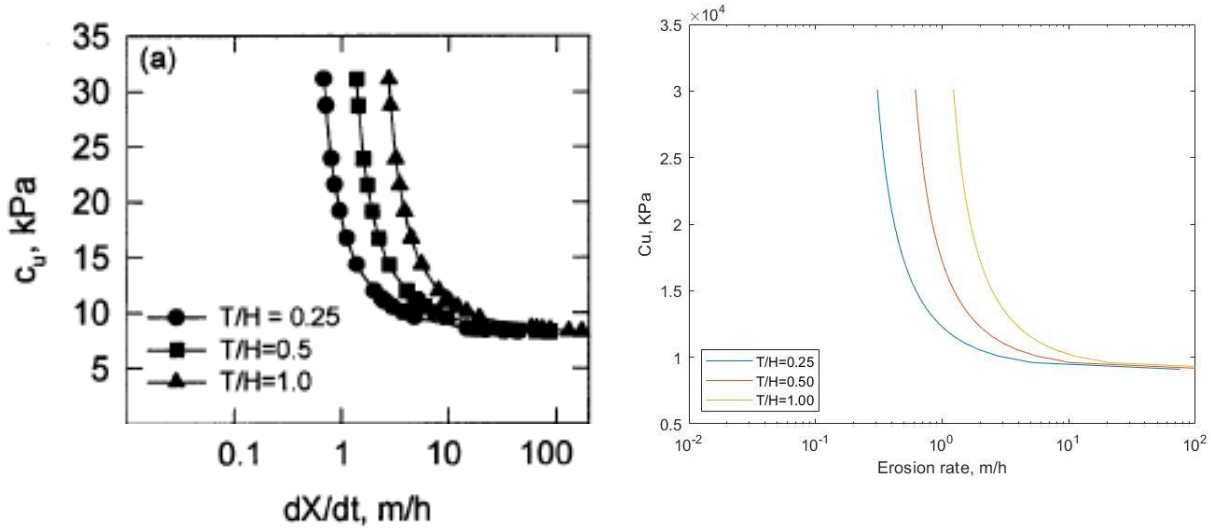

Figure 78: Comparison erosion rate versus undrained strength, left: model results by Hanson, Robinson and Cook., right: model results sliding failure model
Note: reprinted from: "Prediction of Headcut Migration using a deterministic approach", Hanson, Robinson &Cook, 2001

Another important parameter is the erosion coefficient. The sliding failure has been tested by again using the parameters from the flume experiments as input for the model. The results of the sliding failure model are almost identical to the results of the model by Hanson, Robinson and Cook and are presented in Figure 79. The observed behavior in terms of erosion rate can be attributed to the erosion rate formula, presented below. The erodibility coefficient does not depend on the effective shear stress and thus the effective shear stress is constant for all values of k_d. A perturbation in the erodibility coefficient leads to a linear change in the headcut erosion rate, as can be understood from the equation.

$$\varepsilon = k_d(\tau_e - \tau_c)$$

Where $k_d$is the erodibility coefficient and $\tau_e$and τ_c are the effective and critical shear stresses.

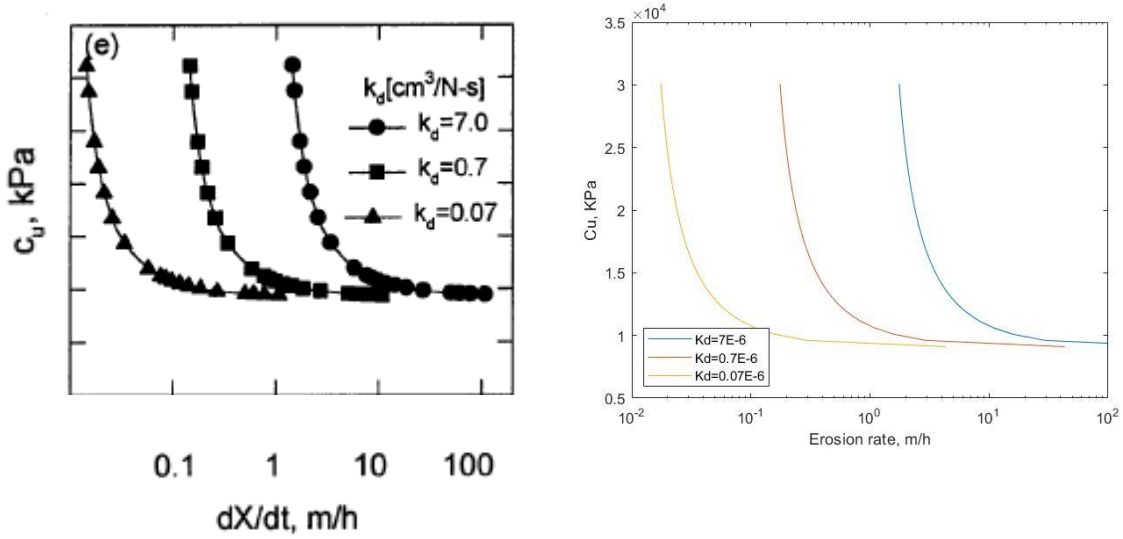

Figure 79: Comparison erosion rate versus undrained strength left: model results by Hanson, Robinson and Cook., right: model results sliding failure model
Note: reprinted from: "Prediction of Headcut Migration using a deterministic approach", Hanson, Robinson &Cook, 2001

As mentioned in chapter 6, the effective shear stress in the experimental results can be found using Figure 55. In order to verify the values obtained from the graphs, the equation for effective shear stress by Robinson (1996) can be used, repeated below for convenience. Using the values read from Figure 78 and Figure 79, the failure model computed an effective shear stress of around $15 - 20Pa$. The shear stress equation below resulted in a value of $16.5Pa$.

$$\pi_1 = 0.025\pi_2^{-1.295}\pi_3^{0.026}\pi_4^{0.221}\pi_5^{-1.062}$$

With

$$\pi_1 = \frac{\tau_e}{\rho g D_a}$$

$$\pi_2 = \frac{q^2}{g D_a^3}$$

$$\pi_3 = \frac{H}{D_a}$$

$$\pi_4 = \frac{B_w}{D_a}$$

Appendix E. Verification rotational failure model

In order to verify the rotational headcut failure model, a set of experiments by Bennet et al. was used. The experiment was conducted in a $5.5m$ long flume in which a clayey soil bed with a length of $2.0m$ was placed with water flowing over it. The flow over the soil layer is caused by a head level difference between the inflow and the outflow locations, additionally, a rainfall simulator was placed above the soil bed increasing the discharge over the bed. The rainfall simulator was necessary for the study by Bennet et al., however in this study is plays no role and does no influence the headcut erosion behavior. An aluminum frame was placed in the soil bed to limit the flow width to $0.165m$. An initial step in the level of the bed was created $1.52m$ downstream of the beginning of the soil layer. This step was a drop of $2.5cm$ in downstream direction. A water jet appears over the initial step and causes a scour hole to form, see also Figure 58.

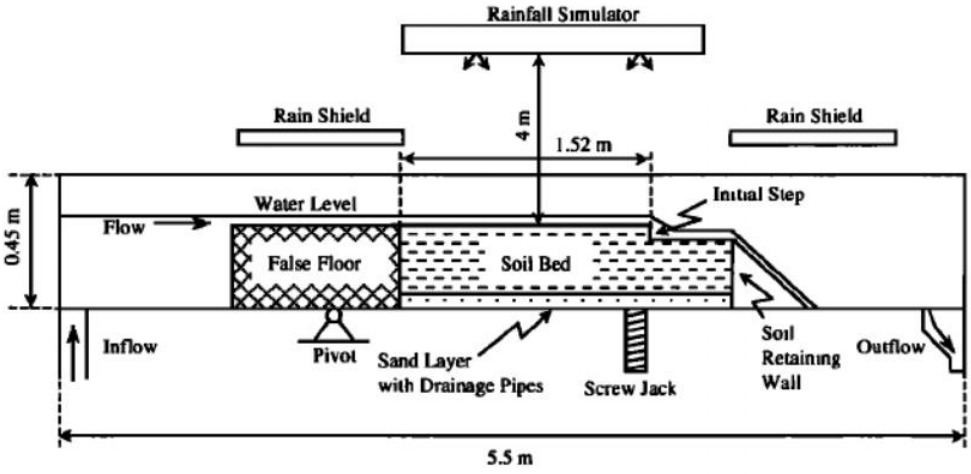

Figure 80: Experimental setup for headcut erosion tests
Note: reprinted from "Experiments on headcut growth and migration in concentrated flows typical of upland areas.", Bennet et al., 2000.

Below a selection of the most important values used in the experiments is presented. Additionally, the observed migration rate and the migration rate computed by the rotational failure model are presented.

Test run number	Flow rate $(10^{-3}\frac{m^3}{s})$	Flow velocity upstream of headcut $(\frac{m}{s})$	Water depth directly upstream of headcut (m)	Water depth directly downstream of headcut(m)	Scour hole ratio[1]	Calculated migration rate (mm/s)	Migration rate from experiments (mm/s)	Error $(\%)$
1	0.545	0.367	0.009	0.008	1.2-1.7	1.7	1.8	5.8
2	0.665	0.504	0.008	0.007	1.0-1.4	1.9	1.7	10.5
3	0.692	0.500	0.008	0.008	1.1-2.1	1.9	2.0	5.3
4	0.890	0.450	0.012	0.011	1.2-2.6[2]	1.6	1.4	12.6
5	1.058	0.495	0.013	0.012	0.9-1.6	1.6	1.6	0.0
6	1.1366	0.561	0.012	0.012	1.2-1.7	1.7	1.9	11.7

Table 6: Values used for most important parameters in headcut experiment, calculated migration rate and predicted migration rate

[1] defined by the ratio between the horizontal distance from the scour hole bottom to the headcut plane and the scour hole depth. Varies up to 100% during the duration of the test runs.

[2] 2.6 was an anomaly within the test run, the rest of the run was between 1.2-21.

Appendix F. Documented foreland erosion shapes

This appendix contains documentation of the elliptical erosion patterns observed in forelands after the 1953 floods in the Netherlands. Due to the absence of experimental and historic data regarding foreland erosion during breaching events, photographs taken by the ministry of infrastructure and water management after the floods, supply valuable insight in the erosion shape. The images were all retrieved from "Verslag over de stormvloed van 1953" (Rijkswaterstaat, 1961). It should be noted that no differently shaped erosion patterns in forelands were found in any of the figures from the report, further substantiating the hypothesis of elliptical erosion patterns.

The below figure shows repair measures taken in the southern part of the province of South-Holland in the Netherlands. In location 3 and 4 in the figure, a foreland was present. It can be seen that repairs were conducted in the foreland in the form of an ellipse. This contributes to the notion that foreland erodes in this pattern.

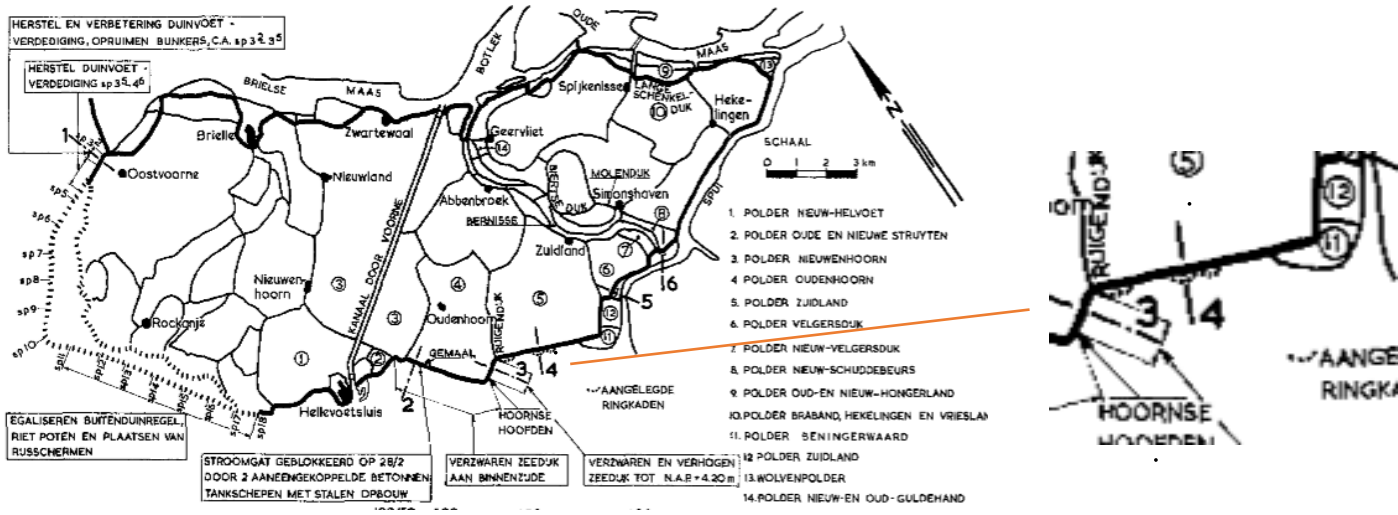

Figure 81: Elliptical erosion observed in South-Holland after the 1953 floods
Note: reprinted from: "Verslag over de stormvloed", Rijkswaterstaat, 1961.

Additionally, the profile of the repairs conducted in location 4 show seawards headcut erosion. In the figure below the soil layers with slanted lines and dots show the repair measures, where the sea is on the left and the polder on the right of the figure. After the dike had been breached, seawards headcut erosion took place at approximately constant depth. The small dike on the left of the image is an emergency embankment, a similar embankment is shown in Figure 84.

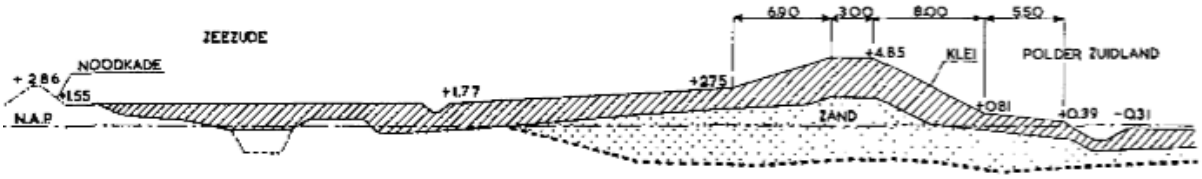

Figure 82: repair measures conducted on the foreland
Note: reprinted from: "Verslag over de stormvloed", Rijkswaterstaat, 1961.

The figure below shows another dike breach from the 1953 floods where a foreland was present. This one occurred in the Gouweveer polder, located in Zealand, in the south of the Netherlands. On the sea side of the two breaches in the figure, clear elliptical erosion pattern can be observed. They can be distinguished by the dark color of the water.

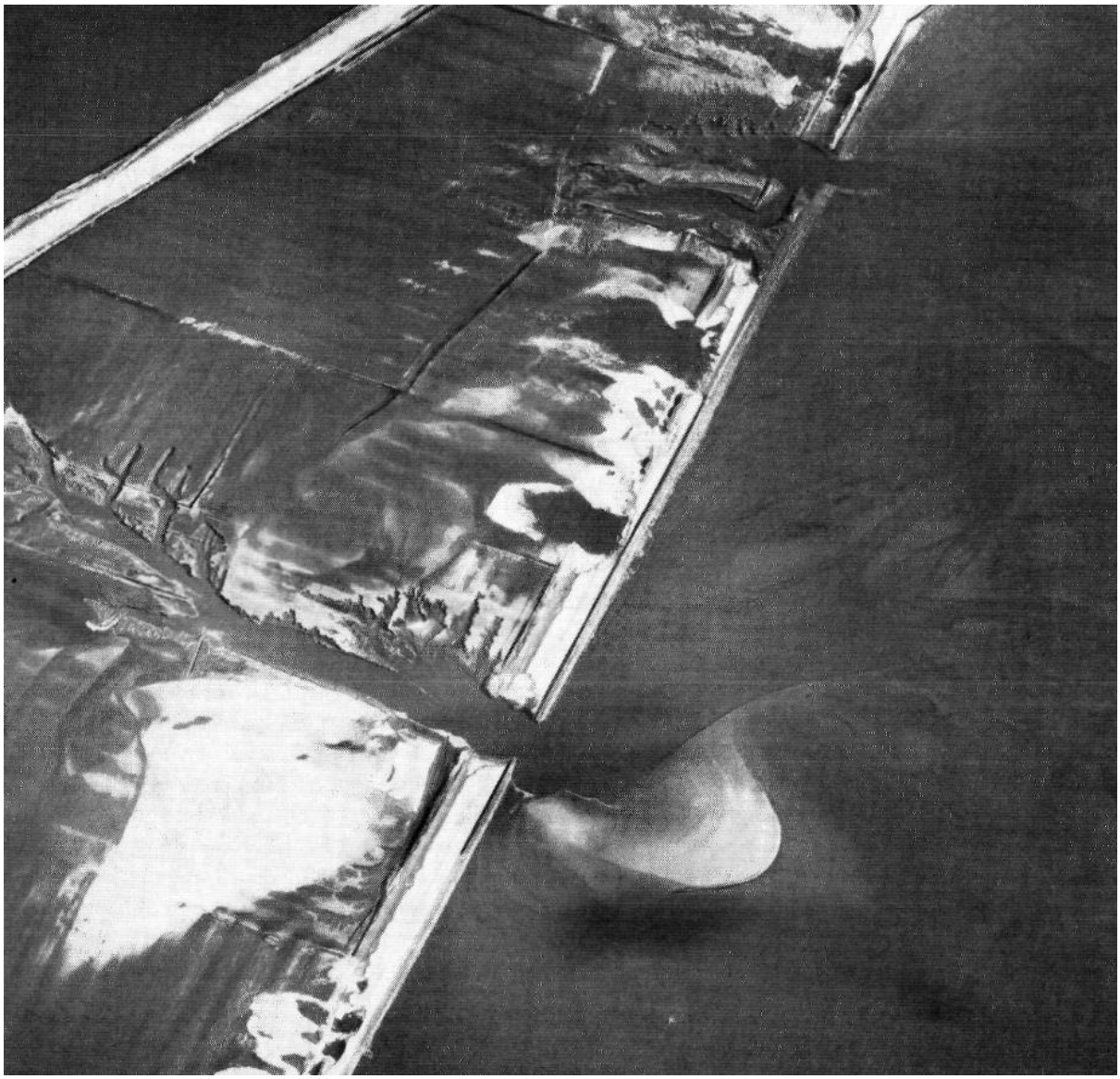

Figure 83: Elliptical erosion on the foreland next to the Gouweveer polder
Note: reprinted from: "Verslag over de stormvloed", Rijkswaterstaat, 1961.

A final figure from the report showing elliptical erosion of the foreland is presented below. This figure also clearly shows the unpredictability of natural sediment layers. The elliptical shape can be observed, however it is far from a perfect ellipse. This can be attributed to local differences in soil strength.

Figure 84: Elliptical erosion pattern in foreland after dike breach
Note: reprinted from: "Verslag over de stormvloed", Rijkswaterstaat, 1961.

Appendix G. Soil failure experiment

The distance required for failure of the soil blocks is highly different. A timelapse for both soil blocks is presented from initiation until failure. The first sample failed after 83 centimeters, the second after 23 centimeters. Below the timelapse for the second sample is presented, where failure occurred after 83 centimeters.

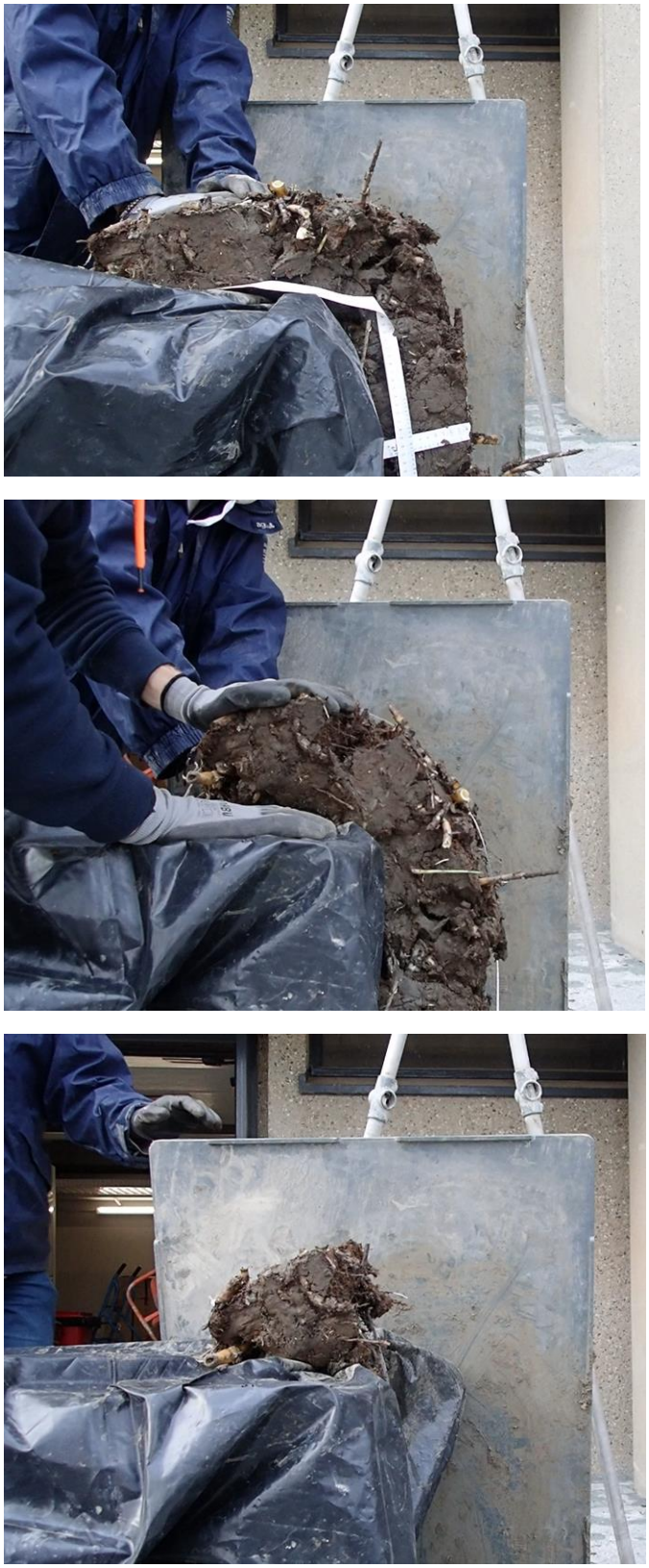

Figure 85: Soil failure timelapse for first sample

Below the timelapse for the second sample is presented, failure occurred after 23 centimeters.

Figure 86: Soil failure timelapse for second sample

The expected failure type for this cohesive sediment type was rotational. From the experiment it can be clearly observed that the failure type was indeed rotational, concluding that the hypothesis was correct.

Figure 87: Clear rotational failure observed during the experiment

From the experiment it was observed that the strength of the root system was normative for the soil layer strength. The figure below shows a large crack in the sediment, however the soil block does not fail due to some large roots.

Figure 88: Normative strength in soil caused by root systems

The roots in the first sample were much thicker than the second. This can be explained by the fact that the second sample was taken directly from the ground level and the first was located directly below it. The sample with the thicker roots was much stronger than the sample with smaller roots. This can be seen from the figures below

Figure 89: Vegetation on top of the foreland and large roots in the soil increase the strength of the soil layer, bottom picture show the sample that was located lower in the foreland.

The soil in a foreland is highly fertile. This is evidenced by the tall reed on top of the samples which continued heavy growth even after the sample had been removed from the foreland.

Figure 90: Continued reed growth, reed was cut in top figure for the experiment

Appendix H. Headcut experiment

This appendix shows the experimental setup and results of the flume experiment conducted in collaboration with the University of Antwerp. Firstly, the setup and the dimensions of the experiment will be presented. After that the results are shown and discussed.

Experimental setup

The length of the flume was six meters, the first five meter measured from upstream were covered by the panel. The width of the flume was 80 centimeters. The panel was placed roughly 20 centimeters upstream of the downstream edge of the foreland. The hole in the panel was 70 centimeters wide, 20 centimeters high and located 72 centimeters above the flume bottom. The width of the soil layer covered the entire 80 centimeter of the flume and was approximately 18 centimeters high. The maximum discharge through the flume was 220 Liters per second.

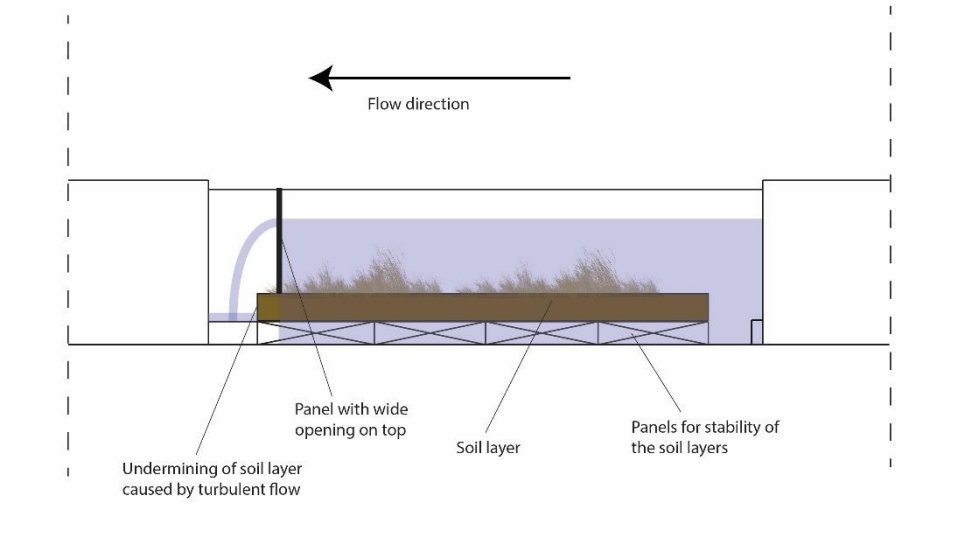

Figure 91: Experimental setup flume experiment, side view

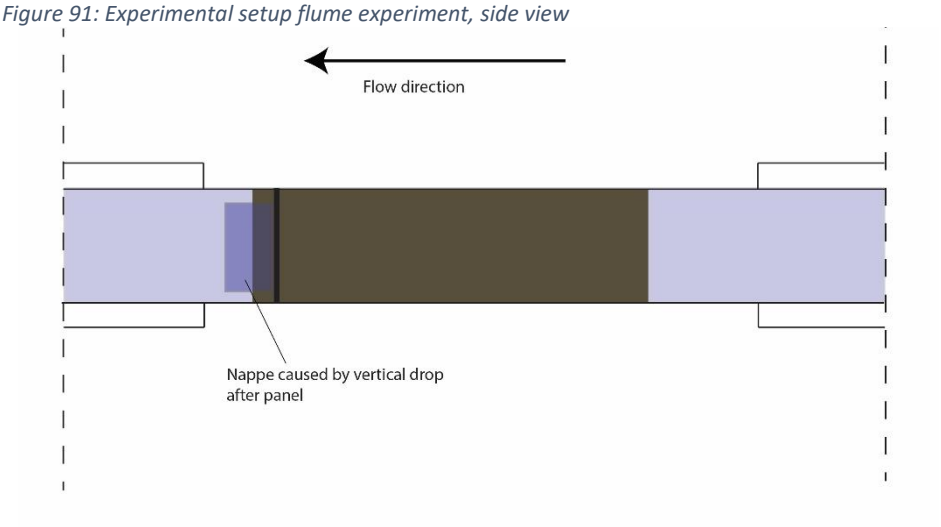

Figure 92: Experimental setup flume experiment, top view

Figure 93: Impression of experimental setup

Figure 94: Impression of experimental setup, nappe profile

Model results

Presented below are the results of the conducted experiment.

Firstly, the divergence of the jet was observed as well as the expected turbulence and subsequent undermining. Comparing this to Figure 28 (repeated below for convenience, Figure 96), an almost identical situation is observed.

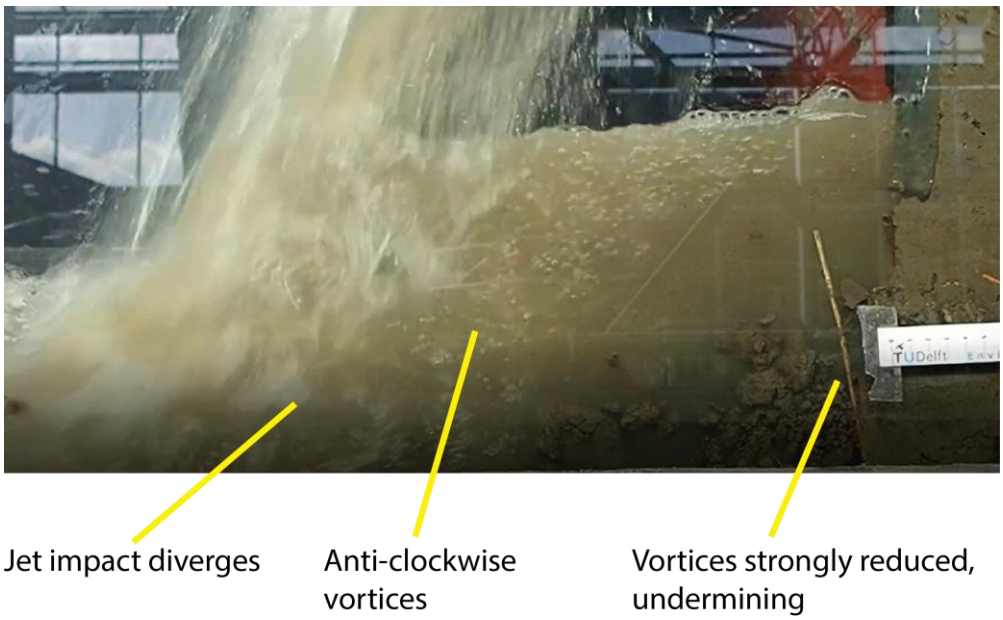

Figure 95: Undermining of foreland, flow rate in flow 160L/s

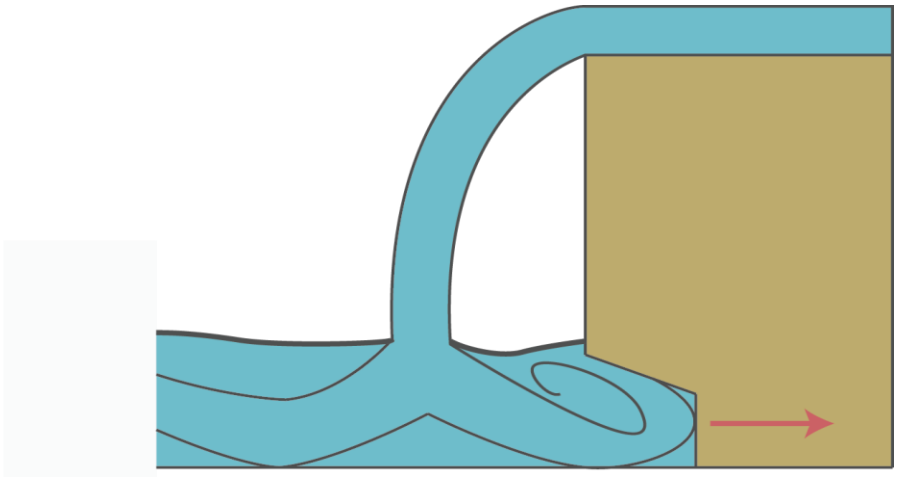

Figure 96: Undermining caused by plunging jet

A second important result from the flume experiment was the failure type experienced by the foreland under realistic circumstances. The soil failure experiment was performed dry, whereas in the flume hydraulic effects were also present.

The expected failure type for this cohesive soil layer was rotational. From the figures below it can be clearly observed that the failure type was indeed rotational, showing the hypothesis was correct.

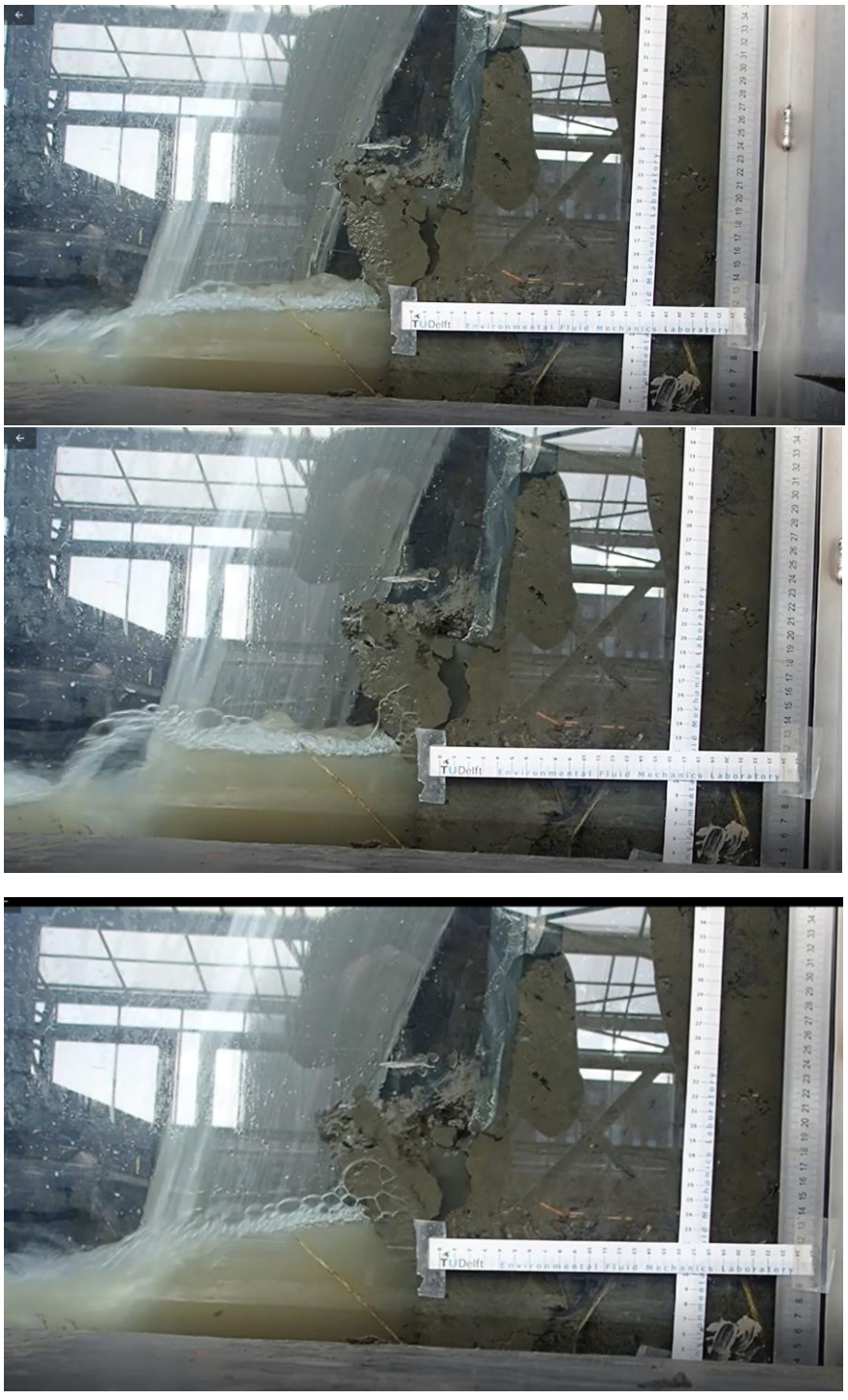

Figure 97:Rotational failure experienced at the edge of the foreland

One of the key assumptions for the headcut models was that when a soil block fails and lands in the backwater, the block is quickly washed away and does not affect the undermining of the newly exposed soil layer. This assumption holds for the scale of this experiment. Below three figures are presented, the first shows the soil block right after failure. The second shows the soil block toppling over, and finally the third shows the soil block being washed away. The duration between soil failure and the block toppling over was approximately 23 seconds, the washing away downstream after this accord was almost instantaneously.

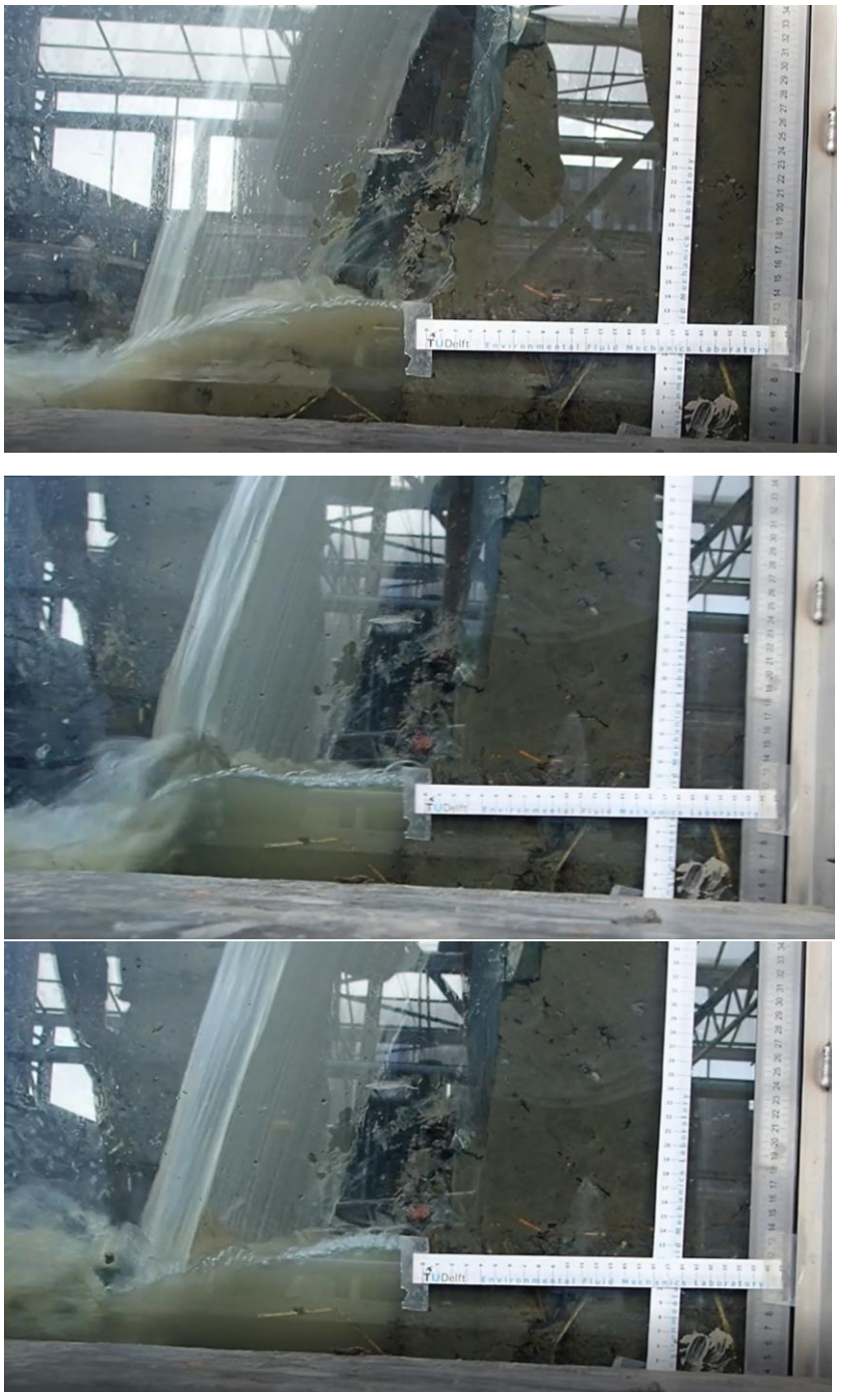

Figure 98: Soil block washed away quickly